COMBUSTION DEVELOPMENT OF A HIGH LOAD HIGH-EFFICIENCY MICRO-PILOT DIESEL NATURAL GAS ENGINE

By

Vinicius Bonfochi Vinhaes

A DISSERTATION

Submitted in partial fulfillment of the requirements for the degree of

DOCTOR OF PHILOSOPHY

In Mechanical Engineering-Engineering Mechanics

MICHIGAN TECHNOLOGICAL UNIVERSITY

2022

This dissertation has been approved in partial fulfillment of the requirements for the Degree of DOCTOR OF PHILOSOPHY in Mechanical Engineering-Engineering Mechanics.

Department of Mechanical Engineering-Engineering Mechanics

Dissertation Co-Advisor:	*Dr. Jeffrey D. Naber*
Dissertation Co-Advisor:	*Dr. Mahdi Shahbakhti*
Committee Member:	*Dr. Gordon McTaggart-Cowan*
Committee Member:	*Dr. Brian J. Eggart*
Department Chair:	*Dr. William Predebom*

Table of Contents

List of Figures

List of Tables

"Science is not only a disciple of reason but also one of romance and passion."

– Stephen Hawking

Author Contribution Statement

This project developed solutions to the barriers to diesel micro-pilot combustion in a stoichiometric natural gas engine in collaboration with Westport Fuel Systems Inc. and the U.S. Department of Energy. A coordinated and integrated effort in experimental engine investigation and fundamental injection and ignition studies supported the modeling and simulation work.

This dissertation contains the manuscripts published and submitted to scientific journals as a result of the collaborative work. I am the first author of all publications included here as chapters and the main person who has conducted the engine setup and commissioning, experimental investigation, 1-D simulation, and data processing. Credit for the key personnel that supported these tasks is given as follows:

1. Engine Setup & Commissioning
    a. Westport Fuel Systems Inc.: Gordon McTaggart-Cowan, Ashish Singh, and Alejandro Buse
    b. APS Labs Staff: Paul Dice, Joel Duncan, William Hansley, and Brian Eggart
    c. MTU Graduate Students: Jithin Joseph, Akash Modi, and Hakan Uras
2. Engine Experimental Investigation
    a. APS Labs Staff: Paul Dice, William Hansley, and Brian Eggart
    b. MTU Graduate Students: Sai Sharath Gorthy, Akash Modi, Xuebin Yang, Vikram Deshmukh, and Hakan Uras
3. 1-D Engine Simulation
    a. Westport Fuel Systems Inc.: Gordon McTaggart-Cowan, Alejandro Buse, and Marco Turcios
    b. MTU Graduate Students: Sai Sharath Gorthy and Devika Mandge
4. Data Processing was conducted by me with inputs and feedback from the research team

All the work, including this dissertation, is done under the guidance and supervision of Dr. Jeffrey D. Naber and Dr. Mahdi Shahbakhti.

Papers that are part of the dissertation:

1. Bonfochi Vinhaes V, Yang X, McTaggart-Cowan G, Munshi S, Shahbakhti M, Naber JD. “Development of a medium-duty stoichiometric diesel micro-pilot natural gas engine.” International Journal of Engine Research. April 2022. DOI: https://doi.org/10.1177/14680874221087954

   This paper focused on demonstrating the micro-pilot concept and presenting the limitations for ignition and combustion. The first author conducted experiments with the assistance of the second author. The first author completed the test data analysis while review inputs and feedback were given by the remaining authors.

2. Bonfochi Vinhaes, V., Yang, X., McTaggart-Cowan, G., Eggart, B., Munshi, S., Naber, J.D., Shahbakhti, M. “Multi-Variable Sensitivity Analysis and Ranking of Control Factors Impact in a Stoichiometric Micro-Pilot Natural Gas Engine at Medium Loads". SAE Technical Paper 2022-01-0463, 2022. DOI: https://doi.org/10.4271/2022-01-0463.

   This work focused on systematically studying, quantifying, and ranking the controlling factors for the combustion and performance of a diesel micro-pilot natural gas engine operating at a mid-load condition. The first author conducted experiments with the assistance of the second author. The first author completed the test data analysis, while review inputs and feedback were given by the remaining authors.

3. Bonfochi Vinhaes, V.; McTaggart-Cowan, G.; Munshi, S.; Shahbakhti, M.; Naber, J.D. “Experimental Studies of Low-Load Limit in a Stoichiometric Micro-Pilot

Diesel Natural Gas Engine.", Energies, 2022, 15, 728. DOI: https://doi.org/10.3390/en15030728.

This work focused on studying the limits of the low-load operation of a micro-pilot diesel natural gas engine and the effect of controlling parameters with the goal of reaching the minimum load limit. The first author conducted experiments. The first author completed the test data analysis, while review inputs and feedback were given by the remaining authors.

Acknowledgments

Every accomplishment begins with the decision to try, and I feel extremely fortunate for the path I went through since I decided to embark on my Ph.D. journey. What once began as a dream has become an unforgettable and invaluable life experience.

First and foremost, I would like to express my sincere gratitude to my advisors and mentors, Dr. Jeffrey Naber and Dr. Mahdi Shahbakhti. Their support and guidance have been nothing short of constant encouragement and inspiration to me. They have strongly influenced whom I became as a person and as a professional, and they will always be my role models for their exceptional knowledge and passion for research.

I want to thank my committee members, Dr. Gordon McTaggart-Cowan and Dr. Brian Eggart, for their guidance, carefully reviewing and providing insightful discussions throughout my research. I am grateful for all the weekly and bi-weekly meetings we spent having technical discussions, especially for our "off-line" conversations that have pushed me to strive for continuous growth.

This dissertation would not have been possible without the financial support from the Office of Efficiency and Renewable Energy, National Energy Tech Lab (NETL), a subunit of the U.S. Department of Energy, and Westport Fuel Systems Inc., an important industry partner in this research. I want to give special thanks to Westport Fuel Systems Inc. team members Dr. Sandeep Munshi, Marco Turcios, Ashish Singh, and Alejandro Buse. I would also like to express gratitude to ACAT/UMICORE for providing the catalyst aftertreatment.

I have been more than fortunate to collaborate with many talented and inspiring individuals at Michigan Tech and the APS Labs. I would like to give special thanks to the extraordinary staff members that have been part of this journey, including Paul Dice, Joel Duncan, William Hansley, and Tucker Alsup, for their support during engine development and experimental studies; Tina Sarazin, Alex Normand, Julie Hendrickson, and Marlene

Lappeus, for their support with the administrative work; Henry Schmidt, and William Atkinson for their support during experimental studies in the combustion vessel lab. I have learned a lot from each of them, and I am forever grateful for them making me feel part of the team.

I want to thank the Michigan Tech students and alumni that participated in this research for their impactful contributions, including Jithin Joseph, Akash Modi, Devika Mandge, and Vikram Deshmukh. I owe special thanks to Sai Sharath Gorthy and my research partner Xuebin Yang, the countless hours we spent in the lab are unforgettable, and I am grateful for our exceptional collaboration.

Throughout this experience, I have made friends that will have a long-lasting impact on my life. To my friends, Roger, Neil, Nick, Matt, Sid, Sterling, Niranjan, Tyler, Nicolas, Amir, Behrouz, Stas, Zhuyong, Ehsan, Magdalena, Zak, Shane, and many others, it was an honor meeting you, and I am grateful for the support you provided through all the adversities of the last six years. I owe special thanks to Tania Demonte for her incredible support through this journey.

No words can express my gratitude to Dennis and Illa Garver for embracing me as part of their family. I will forever be grateful for their support and for making me feel at home. The love I received from them feels like the love from my grandparents, and for that, I will always keep them in my heart.

Lastly, and most importantly, my deepest and heartfelt thanks to my parents, Maury Silva Vinhaes and Elida Souza Bonfochi Vinhaes. I would not be where I am today if it was not for their love, encouragement, and sacrifices. Words are insufficient to describe how grateful I am. Finally, to my sister Vivian Bonfochi Vinhaes for her support during this journey's challenging but rewarding moments.

Vinicius Bonfochi Vinhaes

List of Abbreviations

AFR	Air to Fuel Ratio	**LCFS**	Low Carbon Fuel Standard
AEO	Annual Energy Outlook	**LHV**	Lower Heating Value
AHR	Apparent Heat Release	**LLC**	Low Load Cycle
BMEP	Brake Mean Effective Pressure	**LTC**	Low-Temperature Combustion
BTE	Brake Thermal Efficiency	**IMEP**	Indicated Mean Effective Pressure
BSFC	Brake Specific Fuel Consumption	$\dot{m}$	Mass flowrate
BSNOx	Brake Specific NOx	**MAP**	Manifold Air Pressure
BSUHC	Brake Specific UHC	**MBT**	Maximum Brake Torque
CA	Crank Angle	**MHC**	Methane Hydrocarbons
CAD	Crank Angle Degree	**MOC**	Methane Oxidation Catalyst
CA50	Crank Angle position at which 50% of the heat from combustion has been released	**NG**	Natural Gas
CARB	California Air Resources Board	**NMEP**	Net Mean Effective Pressure
CI	Compression Ignition	**NOx**	Oxides of Nitrogen
CO	Carbon Monoxide	**NTE**	Not to Exceed
CO_2	Carbon Dioxide	**P**	Pressure
COV	Coefficient of Variance	**P-ECU**	Prototype Engine Control Unit
CR	Compression Ratio	**PDF**	Power Distribution Function
DOC	Diesel Oxidation Catalyst	**PM**	Particulate Matter
DPF	Diesel Particulate Filter	**SET**	Supplemental Emissions Test
DSR	Diesel Substitution Ratio	**SI**	Spark-Ignition
EES	Engineering Equation Solver	**SCR**	Selective Catalyst Reduction
EIA	Energy Information Administration		
EGR	Exhaust Gas Recirculation	**SOC**	Start of Combustion
EGT	Exhaust Gas Temperature	**SOI**	Start of Injection

EPA	Environmental Protection Agency	**T**	Temperature
EQR	Equivalence Ratio	**TDC**	Top Dead Center
FS	Full Scale	**TWC**	Three-Way-Catalyst
FTP	Federal Test Procedure	**UHC**	Unburned Hydrocarbons
GHG	Green House Gases	**ULSD**	Ultra-Low Sulfur Diesel
HP	High Pressure	**VGT**	Variable Geometry Turbocharger
HPDI	High Pressure Direct Injection	**VVA**	Variable Valve Actuation
ICE	Internal Combustion Engine		
IMAT	Intake Manifold Air Temperature		
Kpp	Knock peak-to-peak		

Abstract

The conventional internal combustion engine will continue to exist for a long time. Likewise, demand for higher output efficiencies, higher specific power output, increased reliability, and lower emissions will continue to grow. There is also a growing requirement to run on various gaseous fuels and natural gas, whether for environmental, economic, or resource conservation reasons.

This dissertation investigates a 6.7L diesel engine converted to run stoichiometric diesel micro-pilot / natural gas premix combustion with a maximum diesel contribution target of 5% of the total fuel energy with a three-way catalyst aftertreatment. The research centers on investigating the dominant factors and their impact on the critical barriers of this technology, including the positive and negative impact on combustion stability at low loads, the most influential factors and their impact on maximizing thermal efficiency at medium loads, the controlling parameters at preventing combustion knock at high-loads, and the ability of the three-way catalyst to minimize emissions.

A diesel-like efficiency of 41% brake thermal efficiency was achieved with a high load output of 23 bar brake mean effective pressure when operating in the micro-pilot mode. This operating condition reduced up to 25% brake-specific CO_2 emissions compared to diesel-only. Low loads can be achieved by delaying combustion phasing, reducing the injection pressure, adding exhaust gas to the intake, and increasing the total diesel pilot quantity. Maintaining stable ignition of the diesel pilot becomes a challenge at low loads, as the intake pressure is reduced; the chamber pressure at diesel injection decreases, and the presence of a near-stoichiometric mixture of NG will act to inhibit the diesel ignition. As such, maintaining the stoichiometric combustion resulted in a minimum load output of 5 bar BMEP. The pilot injection pressure reduction improved combustion stability at lower loads. While lean operation enabled further load reduction, it precludes using a three-way catalyst to control NOx emissions. At medium loads, a design of experiments investigation revealed that, when the equivalence ratio is constrained at stoichiometric, exhaust gas recirculation and pilot injection timing are the most influential factors in controlling combustion and performance metrics. In contrast, intake air temperature and pilot injection pressure showed the least sensitivity. While it was possible to achieve 25 bar BMEP for high loads, such operation was limited by pre-ignition. Exhaust gas recirculation and pilot injection timing can mitigate abnormal combustion effectively. At a steady-state, near stoichiometric condition, it was observed that the catalyst operates efficiently, consistent with a three-way catalyst operation with very low NOx and unburned methane emissions.

Overall, this dissertation demonstrates that diesel-like performance can be achieved with the stoichiometric micro-pilot concept and provides an understanding of the primary controlling factors and their limitations.

Keywords: Diesel, Micro-Pilot, Natural Gas, Stoichiometric, Performance, High-Efficiency, High-Load

1 INTRODUCTION

1.1 The U.S. Energy Consumption Trend

Transportation is essential in modern society, and due to the abundant supply, convenience, and affordability of oil-based fossil fuels, the transportation sector is almost entirely powered by traditional internal combustion engines (ICEs). In addition, stationary combustion engines for power generation (i.e., generators) are required in medical facilities, industry, and other critical services [1].

The demand for high-efficiency engines with high specific power production, low greenhouse gas (GHG) emissions, and low pollutant emissions is predicted to increase in the future[2, 3]. Figure 1-1 shows the recent assessment from the 2022 Annual Energy Outlook (AEO) [4] by the U.S. Energy Information Administration (EIA), petroleum and natural gas (NG) will continue to be the most widely used energy sources in the United States through 2050.

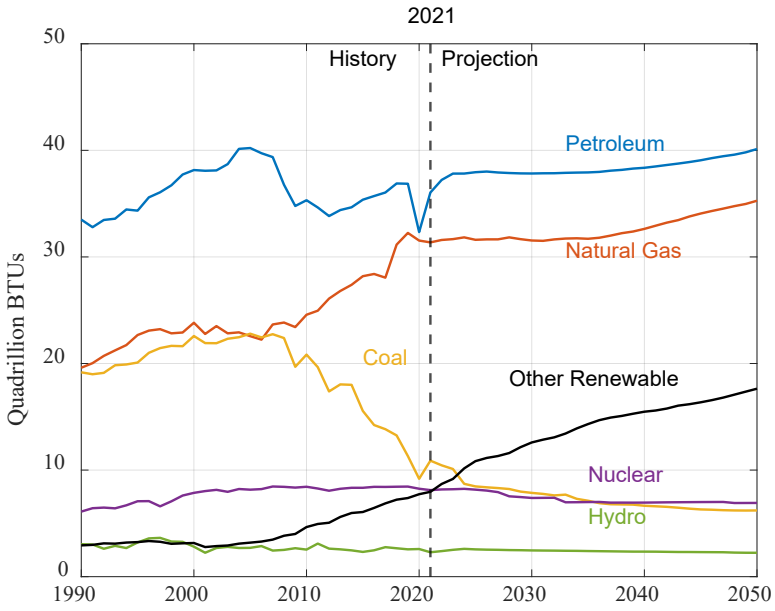

Figure 1-1. Energy consumption in the U.S. by fuel. Figure created by the author with data from the 2022 AEO [4].

Natural Gas is a remarkable resource. It has the lowest carbon intensity of all fossil fuels, emitting 10%-20% lower GHG compared to gasoline [5]. It burns efficiently and cleanly, producing relatively few non-carbon pollutants [6]. Moreover, in the world transportation sector, an annual growth of 5-7% in NG-fueled heavy-duty vehicles is expected from 2022 to 2032[7, 8]. Because of its high potential to reduce CO_2 and nitrogen oxide (NOx) emissions, low cost, and availability, NG as an alternative fuel offers an attractive near-term opportunity in ICE [9].

1.2 Motivation

Due to increased emissions restrictions from all vehicle applications, alternative fuels with comparable performance and lower GHG emissions potential became possible candidates for use as substitutes in both short and long-term plans [10]. While the future of transportation is moving toward electric vehicles, a large and immediate shift seems unlikely due to the existing infrastructure and resources. Therefore, there is a need for a new transitional fuel that can help achieve the objective of low-carbon emissions. Furthermore, the low cost of NG is another aspect that is attracting more NG applications [11, 12]. As a result, NG has emerged as the front-runner to fill the void left by recent developments [13].

According to the EIA, NG fuel consumption in the U.S. transportation sector (shown in Figure 1-2) will continue to see a significant increase in demand, with an expected increase of 40% by 2050[4].

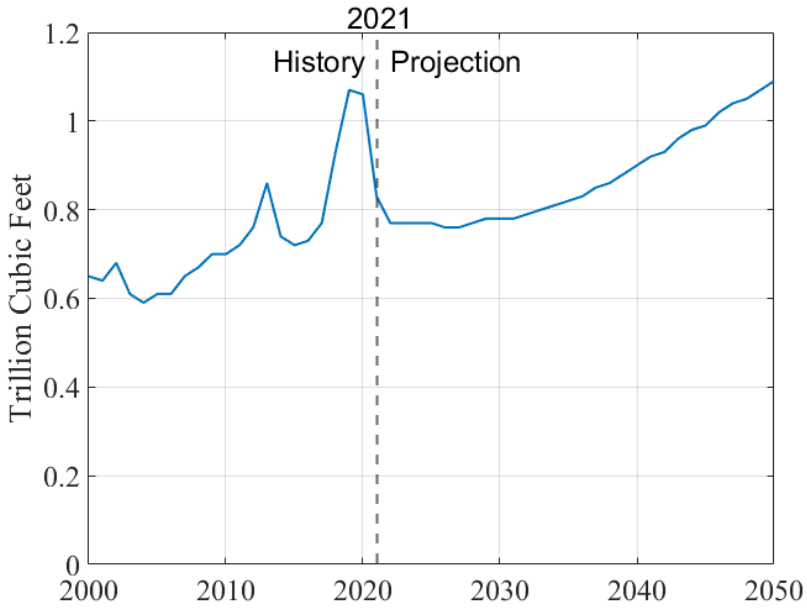

Figure 1-2. U.S. Transportation sector NG consumption. Figure created by the author with data from the 2022 AEO [4].

Moreover, when bio-produced (e.g., anaerobic digestion and anaerobic fermentation [14, 15]), NG is the most carbon negative of all fuels, according to the California Low Carbon Fuel Standards (LCFS), when compared to gasoline and diesel [16].

1.3 Emissions Regulatory Standards

1.3.1 Criteria Pollutant Standards for CO, UHC, NOx, and PM

The U.S. Environmental Protection Agency (EPA) sets the federal emissions standards for heavy-duty engines, and the California Air Resources Board (CARB) sets the California standards. The emissions standards presented in this chapter apply to on-road heavy-duty vehicles (e.g., trucks and buses) that operate on diesel or compression ignition engines that utilize natural gas or other alternative fuel. Regulatory emissions testing includes the transient Federal Test Procedure (FTP) cycle, the Supplemental Emissions Test (SET), and the Not-to-Exceed (NTE) testing.

Historically, both EPA and CARB standards have agreed in the heavy-duty engine sector. However, starting from 2024, the CARB Ultra-Low NOx emissions standard will make California standards more stringent. The new CARB standard will be implemented in two main stages:

1. For model years from 2024 to 2026, engine manufacturers are allowed to meet less stringent standards.
2. For models year 2027 and later, engine manufacturers will have to meet the final Ultra-Low NOx standard.

For the federal standards, the EPA proposed a new set of rules implemented in two stages starting from 2027 to 2030. For model years 2031 and later, the EPA will implement the Ultra-Low NOx regulation with stringent targets for CO emissions. Table 1-1 shows the current and the future EPA & California Ultra-Low NOx emissions limits for heavy-duty engines. Additionally, a Low Load Cycle (LLC) testing has been added to the Ultra-Low NOx test requirements.

Table 1-1. U.S. EPA and CARB emissions standards for heavy-duty engines

	Test	**CO**	**UHC**	**NOx**	**PM**
	-	**g/bhp.hr**	**g/bhp.hr**	**g/bhp.hr**	**g/bhp.hr**
Current (EPA & CARB)	FTP+SET	15.5	0.14	0.20	0.01
Future (2027 - CARB)	FTP+SET	15.5	0.14	0.02	0.005
	LLC	15.5	0.14	0.05	0.005
Future (2031 - EPA)	FTP+SET	6.0	0.40	0.02	0.005
	LLC	6.0	0.60	0.05	0.005

1.3.2 Greenhouse Gas Standards for CO_2, CH_4, and N_2O

This section describes the greenhouse gas standards, including CO_2, CH_4, and N_2O. For CO_2, the emissions standard testing differs depending on the engine's family and intended

service class. For medium heavy-duty engines and heavy heavy-duty engines to be certified as tractor engines and other line-haul applications, certification is done using the SET test cycle. If such engines are to be certified both as tractor and vocational engines, the certification requires testing both SET and FTP test cycles. Certification requires using the FTP test cycle for all other engines, including SI heavy duty engines.

Table 1-2 shows the CO_2 emissions standards according to the latest Federal Register /Vol.87, NO. 59, proposed on March 28th, 2022, for compression ignition engines from light heavy-duty to heavy heavy-duty applications.

Table 1-2. CI Engine CO_2 emission standards in g/bhp.hr

Model Year	Light heavy-duty	Medium heavy-duty vocational	Heavy heavy-duty vocational	Medium heavy-duty tractor	Heavy heavy-duty tractor
2014-2016	600	600	567	502	475
2017-2020	576	576	555	487	460
2021-2023	563	545	513	473	447
2024-2026	555	538	506	461	436
2027 - later	552	535	503	457	432

The CH_4 emissions standard began in 2014 for CI engines and 2016 for SI engines and is 0.10 g/bhp.hr measured using the transient FTP. For N_2O, the emissions standard is the same, 0.1 g/bhp.hr, and follows the same testing method.

1.4 Natural Gas Engines Application and Limitations

Natural gas has been used to generate heat and electricity since the 1940s. It has also been utilized in the transportation sector for decades [17]. This section discusses the spark ignited and compression ignition engine types that use natural gas as a fuel source and their limitations.

1.4.1 Natural Gas in Spark-Ignition Engines

Natural gas is mainly used in spark-ignition (SI) applications because of its high autoignition temperature, requiring high ignition energy that is provided through a spark. The current NG-SI technology consists of spark-ignition with lean and stoichiometric air-fuel ratio and cooled exhaust gas recirculation (EGR). In the combustion of an SI engine, the start and formation of a self-sustaining flame kernel are complex processes with several stages. The stages are divided into three categories: pre-breakdown, plasma, and initial combustion [18-20]. The ignition system is required to create a large enough ignition kernel and a long enough voltage release time [18]. The needed minimum ignition energy varies based on the fuel type and the local equivalency ratio [21]; for instance, the minimum ignition energy in the air for natural gas is 15% higher than gasoline[13]. Therefore, NG-SI systems require a more complex, higher-energy spark ignition system than that of gasoline engines.

Despite its higher-octane number when compared to gasoline (120 for methane versus 91-99 for Gasoline) [18], the NG-SI engine's performance is still limited by combustion knock due to the slower flame propagation from its single ignition point [22-25]. Increased CO and unburned hydrocarbons have also been reported by Hassan, M.H., et al. [23], especially at low speeds and low-load operating conditions [26].

1.4.2 Natural Gas in Compression-Ignition Engines

Compression ignition (CI) engine types that burn a premixed gas-air lean mixture with a considerable quantity of pilot injection (in the order of 20-40%) as the combustion pilot are often described as dual-fuel engines [27]. In dual-fuel engines, two distinct fuels in

different mixture quantities are burned; a high reactive fuel is used as the ignition source of the low reactivity primary fuel. As the primary constituent of NG, methane is the cleanest fuel with the lowest particulate matter (PM) formation due to its high hydrogen to carbon ratio [28]. Therefore, methane is the most popular pre-mixed gas fuel used in dual-fuel engines as it provides a significant PM emissions reduction and anti-knocking properties due to its high octane number [29]. In such engines, diesel-like fuel conversion efficiencies and low NOx emissions have been observed. However, low combustion efficiency, limited diesel replacement, and significant unburned methane emissions have restricted system development and on-road vehicle adoption [30, 31]. As a result, lean-burn dual-fuel engines have failed to capture a significant portion of the on-road vehicle market.

1.5 Introduction to the Diesel Micro-Pilot Natural Gas Engine

This dissertation describes the development and experimental investigation of a combustion method that combines an overall stoichiometric fuel-air mixture with a small diesel pilot injection ("micro-pilot"). The concept combines the benefits of both dedicated NG-SI and lean-burn diesel dual-fuel technology (shown in Table 1-3), such as using a diesel pilot for improved ignition quality, de-throttling via EGR for reduced pumping losses, maintaining diesel-like compression ratio (CR) for improved efficiency, and operating at the stoichiometric air-fuel condition for the use of a three-way-catalyst (TWC) to obtain very low NOx, Carbon Monoxide (CO) and unburned hydrocarbon (UHC) emissions. This novel combination of strategies offers the potential to achieve diesel-like fuel conversion efficiency and GHG emissions reduction at medium and high load operations by keeping diesel-like CR paired with a low-carbon fuel. The utilization of a low-cost TWC enabled by maintaining a globally stoichiometric fuel-air ratio is a substantial simplification and potential cost reduction compared to the multi-element aftertreatment systems required to meet emissions limits in modern diesel engines.

Table 1-3. Natural Gas engine technologies comparison. Data reported in the literature [13, 22, 32-37].

	Dedicated SI NG	**Lean-burn diesel dual-fuel**	**Stoichiometric Micro-Pilot NG (This work)**
Ignition source	Spark Plug	Diesel Pilot	Diesel Pilot
Piston	Optimized	Not DF Optimized	Can be optimized for NG operation
Compression ratio	Low (11 - 13)	High (16 – 19)	High (15 – 17)
Diesel pilot contribution	0%	20%-40%	1%-10%
Brake thermal efficiency	29-37%	35-43%	29-43%
Peak BMEP	17 bar - Limited by knock	24.5 bar - Limited by knock	24 bar - Limited by knock**and by Pre-Ignition
Throttling losses	Yes	No	Minimized***
Combustion	Stoichiometric	Lean	Stoichiometric
Exhaust aftertreatment requirement	TWC	MOC + DOC + DPF + SCR *	TWC + DPF ****
Heat transfer losses	High	Low	High
Variable Valve Actuation (VVA)	On certain models	No	Can be added

*MOC: Methane Oxidation Catalyst; DOC: Diesel Oxidation Catalyst; DPF: Diesel Particulate Filter; SCR: Selective Catalytic Reduction

** Can be mitigated by VVA and extended dilution limit

*** Using EGR due to the extended dilution limit; Can benefit from VVA operation

**** May require Lean NOx Trap/SCR

In lean-burn applications, particulate matter emissions can benefit from minimizing diesel fuel consumption. However, the stoichiometric operation concept discussed in this dissertation is expected to be a challenge as the lower air-fuel ratio increases PM formation.

Particulate matter emission was outside of the scope of this work and is not included in this dissertation.

Current NG fueled on-road engine products for the medium-duty market (9-12L) employ stoichiometric combustion with EGR and a spark plug to provide ignition. Instead of a spark plug, the ignition source in the micro-pilot approach is a small quantity of diesel pilot (1-10% of the total fuel energy). This method provides a more robust ignition when compared to an SI engine, premixed turbulent flame combustion, and shorter distances for the flame to propagate across the combustion chamber, thanks to higher ignition energy and a more distributed ignition source for the premixed mixture. Compared to premixed SI systems, these effects are expected to reduce the potential for combustion knock, allowing for higher thermal efficiency through higher compression ratios, better combustion timing, better combustion stability, and shorter combustion duration.

However, five key barriers can limit the successful employment of such a strategy:

1. Maintaining stable ignition at low loads
2. Throttling losses at medium loads
3. Combustion knock and pre-ignition
4. Increased unburned methane emissions
5. Increased particulate matter emissions (not part of the scope of this dissertation)

It is critical for the assessment, evaluation, and future development of the micro-pilot engine concept that an in-depth understanding of the engine's operational benefits and limitations be determined.

1.6 Goals / Objectives

The goal of this research was to develop a micro-pilot diesel with a stoichiometric NG premixed charge engine aiming at a low diesel pilot contribution of 1-5%, high BMEP of 25 bar, and high brake thermal efficiency (BTE) of up to 44%. This combustion system

was used to evaluate and develop solutions to the barriers to micro-pilot combustion in a stoichiometric natural gas engine.

The specific objectives of this dissertation are as follows:

1. Identify the dominant factors and their impact on maximizing the thermal efficiency at medium loads. This provides the basis for understanding the primary factors that control engine performance and a path forward for developing a high-efficiency engine with an optimized fuel and air handling system.

2. Determine the factors that positively and negatively impact combustion stability at low load. The results provide a quantitative assessment of the individual factors and their impact on combustion stability. This investigation also provides insights on how to best overcome the limitations of this operating condition.

3. Specify the positive and negative factors for reducing combustion knock impact via a medium load sensitivity study. As discussed later in this dissertation, pre-ignition and high injector tip temperatures due to the reduced diesel flow are limiting factors for high load operation. However, understanding the impact of the controlling factors that can be used towards minimizing combustion knock occurrence is critical. The results obtained in the medium load investigation provided insights for achieving high load output at the limit of combustion knock.

4. Investigate the ability of a TWC to effectively minimize emissions (i.e., UHC, CO, NOx) and its sensitivity to equivalence ratio. This helps determine if the application of a TWC is feasible and provides a path forward to optimize the design of components (i.e., piston).

1.7 Dissertation Outline

The study of the micro-pilot engine involved the development of the engine testbed, including the conversion of a commercially available diesel engine for micro-pilot diesel

natural gas operation, instrumentation, and the installation of the TWC aftertreatment. The combustion development was comprised of an extensive experimental investigation and data analysis that has been organized into five chapters.

Chapter 2 reviews the existing literature and current state of the art on diesel pilot natural gas engines, including the significant findings from previous works and a discussion concerning the gaps in the current knowledge describing how this research contributes to it.

Chapter 3 discusses the research methodology with a detailed description of the development of the micro-pilot engine testbed. Further explanation of each experimental approach is given in Chapters 4, 5, and 6.

Chapter 4 includes the manuscript approved for publication in the International Journal of Engine Research, focused on understanding the limitations for ignition and combustion of the micro-pilot concept at low, medium, and high load, including the aftertreatment sensitivity to equivalence ratio and insights into the technology placement amongst the SI and Diesel counterparts.

Chapter 5 includes the 2022 SAE World Congress Experience publication, focused on quantifying and ranking the combustion control parameters for medium load operation.

Chapter 6 includes the publication in MPDI Energies Journal, which focused on studying the limits of low load operation and combustion control parameters' effect on finding the lowest load operating condition.

Chapter 7, a summary of the conclusions from this dissertation is presented.

Chapter 8 lists the recommendations from this dissertation and the scope for future work.

2 LITERATURE REVIEW

Although diesel fuel has been commonly employed for medium- heavy-duty CI engines, it has been recently linked to environmental concerns. Several technology advancements have been applied (e.g., turbochargers, advanced combustion control, aftertreatment devices) to meet stringent emissions regulations. However, such approaches come at an increased cost [38]. Therefore, the application of alternative fuels for ICEs has become an attractive field of research to reduce diesel emissions environmental issues and establish an improved combustion strategy. Because of its great potential to reduce GHG and NOx emissions, low cost, and availability, NG as a diesel substitution is an alternative fuel and a promising subject of research in the application of CI-ICE in a dual-fueling mode.

There are different strategies for dual-fuel operation, including reactivity-controlled low-temperature combustion (LTC) and pilot-ignited combustion. The scope of this dissertation is limited to the diesel pilot ignition of a natural gas engine, and this chapter identifies the gaps in recent literature that employs such a strategy.

2.1 Diesel Pilot Ignition Natural Gas Engines

The gaseous fuel combustion makes up most of the energy in the diesel pilot-ignition natural gas engine, while the diesel liquid fuel is used for ignition via controlled in-cylinder diesel injection. In an ideal scenario, there would be optimal variation in liquid fuel quality and injection timing in relation to the gaseous fuel delivery to provide the highest performance for any given engine over the whole load range [39]. This concept has the potential to achieve operational characteristics that are comparable to or better than those of traditional diesel or spark ignition engines [30].

Depending on how the gaseous fuel is introduced, there are two types of dual-fuel strategies, shown in Figure 2-1. In the first strategy (Figure 2-1(a)), the gaseous fuel is direct injected at a high pressure into the cylinder during the compression stroke after the

injection and ignition of the liquid diesel fuel. This strategy is known as high-pressure direct injection (HPDI) [40]. In NG HPDI operation, over 90% of the diesel substitution ratio (DSR) can be achieved with diesel-like thermal efficiency and power [41, 42]. Current drawbacks of the HPDI technology include the PM formation due to its non-premixed combustion and the complexity and cost of engine modifications (i.e., high pressure gaseous and liquid fuel injector) required for the fuel system [33, 43]. The HPDI strategy is outside the scope of this dissertation.

The second strategy (Figure 2-1(b)) consists of the gaseous fuel injection upstream of the intake port and premixed with the intake air. The NG-air mixture is inducted into the cylinder, compressed, and then ignited by direct injection of a liquid pilot fuel near the top dead center (TDC). This strategy is termed premixed pilot ignition [27]. Conventionally, the premixed pilot ignition operates with a large amount of diesel fuel (20-40% of the total fuel energy) injected into a lean premixed NG-air mixture to be used as the ignition source. Typically, the pilot injection occurs 5-20° before the TDC of the compression stroke.

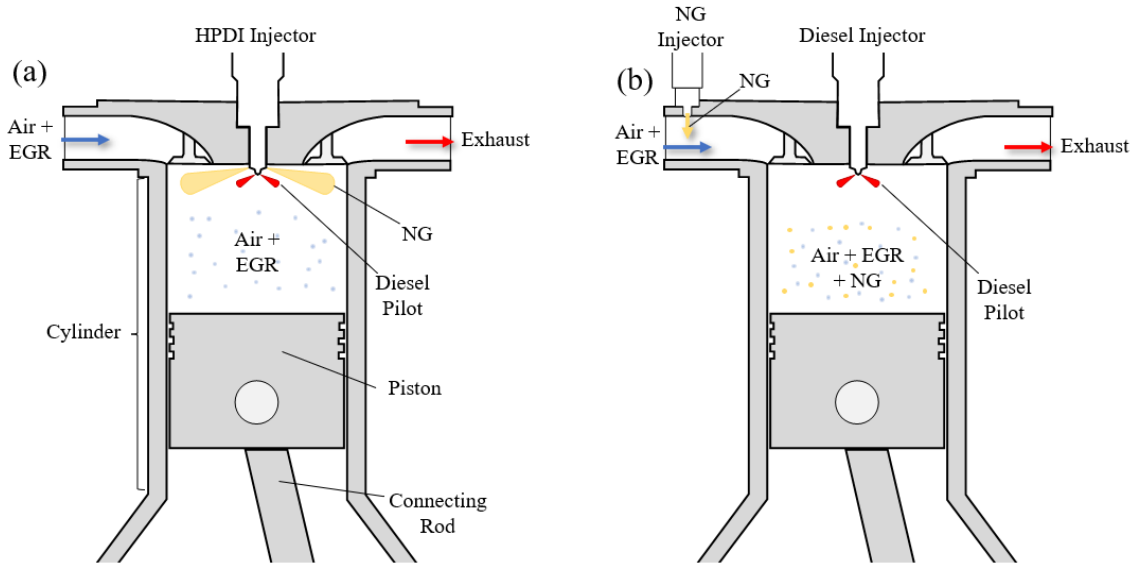

Figure 2-1. Natural Gas Ignition Strategies. (a) HPDI; (b) Premixed Pilot Ignition

Three phases of energy heat release were observed in the diesel pilot-ignition NG engine, including the premixed combustion of the diesel fuel, the combustion of the NG in the

vicinity of the diesel spray, and the propagation of the NG flame within the NG-air mixture [30].

Compared to base diesel engines, this technique is advantageous in preserving diesel-like performance and the potential for reducing PM and NOx emissions [44-47]. Uma et al. [48] and Liu et al. [49] have shown a considerable increase in CO and UHC emissions under low load, agreeing with Gebert et al. [50]. The main causes of this increase are excess air, which is common in unthrottled engines, large crevice volumes caused by the large distance between the piston top surface and the first piston ring, and the long valve overlap found in diesel engines, which helps scavenge the cylinder and increases UHC emissions due to premix escaping through the exhaust valves.

2.2 Recent Diesel Pilot-Ignition NG Engines Studies

The diesel pilot-ignition NG engine has a wide range of uses. They have been used in fleet vehicles, heavy-duty trucks, buses, railroad locomotives, maritime vessels, and construction and agricultural field applications. Engine electric power generators, pumps, and cogeneration units have been used in stationary applications. Although many engines are currently being used, there is still room for reducing cost and improving performance [51]. Recent studies that focused on pilot-ignited NG engines can be divided into three groups: HPDI, Micro-Pilot, and Conventional, as shown in Figure 2-2.

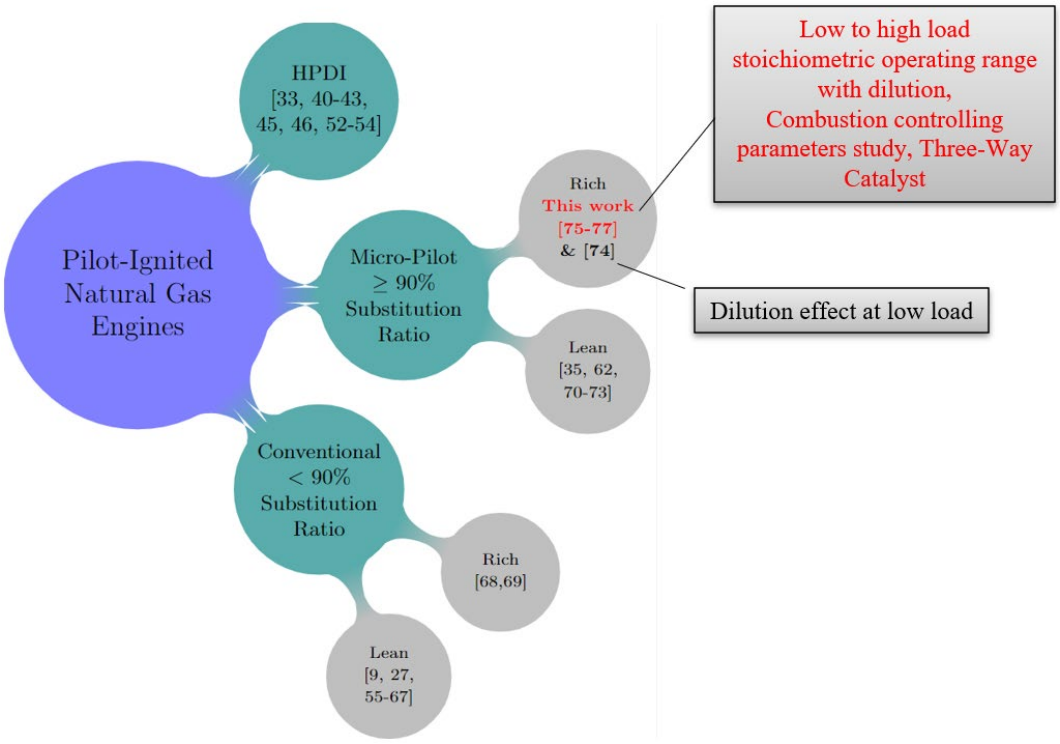

Figure 2-2. Recent Diesel Pilot-Ignition NG engine research and contribution of this work compared to the state-of-the-art. [33, 40-43, 45, 46, 52-54], [9, 27, 55-67], [68, 69],[35, 62, 70-73], [74],[75-77]

2.2.1 Conventional Diesel Pilot-Ignition NG Engine

The performance and emissions of conventional diesel pilot-ignition operation have been the focus of several studies, including the effects of intake manifold air temperature (IMAT) and intake manifold air pressure (MAP), different substitution ratios, EGR, equivalence ratio (EQR), and injection timing. The recent studies relevant to this dissertation are discussed in this section.

Zheng et al. [55] investigated the influence of EQR in premixed lean-burn diesel pilot ignition engines. According to their findings, increasing the EQR increases the heat release rate and exhaust gas temperature, resulting in increased thermal efficiency and fewer methane emissions. However, because of the high temperatures caused by the increase in EQR, NOx emissions increase if no dilution is utilized.

Yousefi et al. [56] and Zhou et al. [57] investigated the effect of diesel pilot start of injection (SOI) in a range of operating conditions varying from low to high loads and speeds. Both studies agree that the pilot diesel SOI advance increases peak cylinder pressure, thermal efficiency, and undesired NOx emissions due to high in-cylinder temperatures caused by the higher pressure for all engine load-speed conditions investigated. Advancing the pilot SOI greatly reduced unburned methane and CO emissions under low load-low speed and medium load-high speed conditions. Their findings also show that the central part of the combustion chamber is the primary source of unburned methane emissions under low load-low speed and medium load-high speed conditions and that advancing diesel pilot SOI significantly improves premixed mixture combustion in this region of the combustion chamber.

According to Papagiannakis [59], fuel consumption during dual-fuel operation is comparable to that of standard diesel operation at high loads but is inferior when operating partial loads. Guo et al. [61] looked at how the diesel pilot-ignition NG engines performed in terms of combustion and emissions over a wide range of loads and speeds. A pilot injection timing investigation was performed at different NG substitution ratios. They stated that a maximum of 50% NG fraction was achieved at low load, while at medium load, a maximum of 70% NG fraction was achieved. In their analysis, the diesel substitution ratio limiting factor was the minimum pilot quantity of their diesel injection system. At constant pilot injection timing, the increase in NG fraction resulted in delayed combustion phasing, and brake thermal efficiency dropped dramatically at low loads. The NG substitution increased methane emissions while reducing CO_2 emissions. CO emissions increased at low loads due to lower combustion efficiency. This observation is consistent with other research [60, 62, 69].

In a lean, naturally aspirated diesel pilot natural gas engine, Rochussen et al.[63] investigated the effects of fueling control parameters. Their research centered on substitution ratio, diesel pilot SOI, diesel pilot injection pressure, and equivalence ratio. They observed a two-stage apparent heat release curve, with stage 1 exhibiting behavior consistent with auto-ignition of diesel, gas, and air premix mixture. Stage 2 of the heat

release curve started right after stage 1, with gaseous fuel EQR greater than 0.4 showing a strong association with turbulent flame propagation. Below 0.4, the fuel seems to be converted via an unknown mechanism. In stage 1, the diesel injection parameters (e.g., quantity and pressure) significantly impacted combustion

Azimov et al. [64] studied the sensitivity of a supercharged dual-fuel engine running on different Syngas fuel mixtures. Their research introduced the combustion mode termed Premixed Mixture Ignition in the End-gas Region (PREMIER). A two-stage heat release is observed in this mode. The first stage is the propagation of the gaseous fuel flame, and the second stage is the auto-ignition of the end-gas mixture. The pilot fuel SOI, gas EQR, and EGR were the key controllers of the second stage. As the hydrogen content in the syngas increased, so did the mass fraction burn in the second stage, suggesting an increase in combustion temperature, mean effective pressure, thermal efficiency, and a significant increase in NOx emissions. Furthermore, it was also observed that with an increase in the Syngas CO_2 content, the pressure rise rate, combustion temperature, thermal efficiency, and NOx decreased, despite increasing the mass fraction burned in the second stage of the combustion heat release.

The effect of intake manifold conditions when operating a light-duty diesel pilot NG engine at low loads is shown in Valladolid and Tunestal's study [65]. The findings reveal that the intake manifold air temperature is critical for flame propagation under high dilution conditions and that an increased air temperature lowers UHC emissions. Throttling significantly reduced emissions and increased fuel conversion efficiency under high dilution due to a richer premixed NG-air mixture. It is expected to be possible to achieve unburned hydrocarbons levels below the legislated limit and exhaust gas temperatures high enough to allow methane oxidation in the aftertreatment when the engine is operated above 5 bar indicated mean effective pressure (IMEP). Their work suggested that the stoichiometric operation may be used to enable the application of a TWC. However, this strategy imposes a penalty on energy efficiency.

2.2.2 Diesel Micro-Pilot Ignition NG Engines

In this section, the literature on diesel micro-pilot injection is reviewed. Figure 2-2 shows the micro-pilot ignition with a diesel substitution ratio greater than 90%. This distinction is used in this dissertation because conventional diesel injection systems degrade the spray quality for the pilot quantities of less than 10% of the full load quantity; therefore, a dedicated micro-pilot injection, while not essential, is recommended to achieve very low injection quantities with a fully developed spray. Lowering the injection pressures or shortening the injection durations are two options for achieving micro-pilot injection amounts with an injector sized for full diesel operation. Low injection pressures lead to poor spray development and large fuel droplets, as Wang et al. [78] reported. Spray breakup and the subsequent mixing process are negatively affected when pilot injection pressures are less than 300 bar. Very short injection durations are necessary for more conventional injection pressures (>600 bar), especially for partial load. Yang, X. et al. [70] found that a fully developed spray could be achieved for diesel injection quantities as low as 2% of total fuel energy at full load for the same injector used in this dissertation; this agrees with comparable findings from Zirngibl, S. [71].

Due to very small injection quantities and short injection durations, maintaining a low diesel energy ratio at low loads is a significant challenge. The short injection durations have an influence on injectors because the needle never fully opens and is always in the opening or closing phase. This considerably increases performance variability, both between injectors and within a single injector as a function of operating temperature. It also ensures that the fuel in the injector sac is never at full pressure, limiting spray atomization and resulting in broad spray penetration variations. A dedicated injector designed for micro-pilot fuel quantities would allow longer injection durations at higher injection pressures, resulting in more stable and repeatable injection events. Furthermore, injector tip temperature management becomes a concern due to the low fuel flow, as addressed later in Chapter 4.4. An optimized micro-pilot injection system, acting only as an ignition source with better cooling, is usually recommended [30]. Additionally, conventional diesel pilot

ignition natural gas engines can run under pure diesel over a great range of the operating map.

While several studies have recently focused on pilot-ignited natural gas engines operated at low loads, only a few focused on micro-pilot ignition [62, 79, 80]. Jamrozik et al. [73] and Choi et al. [72] work focused on the effect of methane substitution ratio from 0% to 98.7%. They reported that the increase in NG substitution ratio increases the ignition delay of the diesel pilot and shortens the overall combustion duration. While operating lean, the micro-pilot strategy reduced NOx emissions by about 90%. However, UHC emissions doubled. By observing the combustion through an optical engine, they reported that the cycle-to-cycle variation is attributed to the turbulent flow and the changes in the location of the ignition sites.

Umierski et al. [35] demonstrated that for a micro-pilot six-cylinder lean-burn supercharged natural gas engine utilizing only 1% to 5% total diesel energy contribution, a load output of up to 22 bar BMEP with a CR of 14.5 is possible. They reported the absence of particulate matter and NOx emissions below EURO V standards. The unburned hydrocarbons have shown to be higher than a similar SI engine, and fuel consumption was increased by 7% compared to the diesel counterpart, resulting in a CO_2 reduction of 18%. Furthermore, a custom cooling device added to the cylinder head allowed full load operation without signs of injector overheating (e.g., coking).

Only one study was found that paired the micro-pilot ignition in a globally stoichiometric mixture. The dilution effect of inert gases (Ar, N_2, and CO_2) at low load stoichiometric conditions on a 6-cylinder turbocharged engine is discussed by You et al. [74]. As the dilution ratio was increased, Ar and N_2 were observed to increase engine power. CO_2 (usually supplied through exhaust gas recirculation systems), on the other hand, deteriorated the combustion process, including heat release rate, cylinder peak pressure, and combustion phasing. Of the three gases tested, CO_2 dilution resulted in the lowest NOx emissions due to the lower cylinder temperature, while Ar produced the highest NOx emissions.

2.3 Novelty of this research

Several research works have recently investigated the conventional diesel pilot ignition natural gas engine operation and performance, with few studies under the micro-pilot strategy. However, the investigations conducted so far have not provided a comprehensive overview of the micro-pilot strategy operating with a stoichiometric NG-air premixed mixture and the application of a TWC for emissions controls. Therefore, the overall viability of the stoichiometric micro-pilot engine remains in question, and this includes investigating its operational limits. This research aims to address that gap and develop an understanding of the stoichiometric micro-pilot engine holistically considering experimental investigations. The novelty of the research is outlined below:

- A comprehensive insight into the challenges of the combustion development of an NG stoichiometric premixed charge ignited by a micro-pilot injection.
- A systematic study determining factors that impact low load stability, medium load strategy targeting maximizing BTE, and maximum load knock limit.
- Tailpipe emissions control ability through a TWC and its sensitivity to EQR.
- Comparison of the stoichiometric micro-pilot engine performance at low and high load to its SI-NG and CI-diesel counterparts.

3 METHODOLOGY

The methodology to develop the engine incorporates a combination of engine technologies integrated on a medium-duty diesel engine platform. The development and specifications of the primary systems are presented in this chapter. These include combustion system, charge handling system, fuel system, aftertreatment, control system, and instrumentation

3.1 Overview of the Micro-Pilot Diesel Natural Gas Engine

A Cummins ISB 6.7L engine was converted from its stock configuration to the final micro-pilot operating design throughout this dissertation. Table 3-1 summarizes the engine's final specifications.

Table 3-1.Micro-Pilot Engine Specifications

Base Engine Model	Cummins ISB6.7 CM2250
Cylinders	6
Bore & Stroke	107 x 124mm
Connecting Rod Length	192 mm
Displacement	6.7 L
Compression Ratio	15.0: 1
Aspiration	Turbocharged (Wastegate) + Charge Air Cooler + HP EGR + Throttle Valve
Diesel Micro Pilot Injection System	Stock Injector 8 holes (168 microns diameter)
Natural Gas Fueling System	6 CNG injectors (Westport AEC 8 g/s)
Rated Power	231 kW (310 HP) @ 1800 RPM

Rated Torque	1230 Nm @ 1620 RPM
Peak BMEP	24 bar
Boost pressure at Peak BMEP	247 kPa
Minimum Throttling Pressure	70 kPa
Exhaust Temperature Limit	350 to 870 °C
Peak Cylinder Pressure at Peak BMEP	<150 bar
Aftertreatment	ACAT/Umicore TWC Herringbone metallic substrate

The estimated torque curve for the presented micro-pilot engine is shown in Figure 3-1.

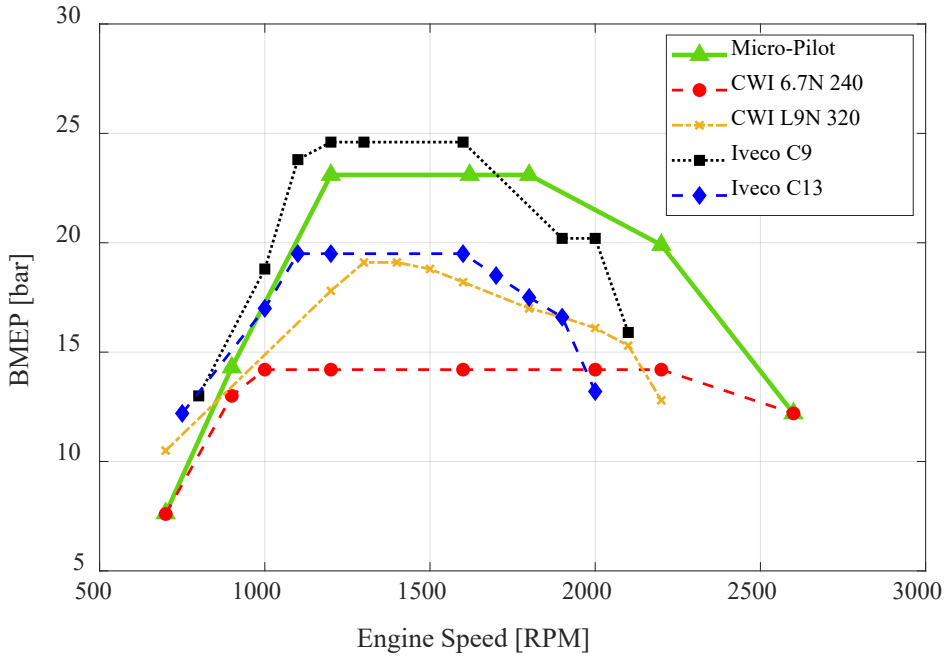

Figure 3-1. Micro-Pilot engine torque curve compared with other commercially available engines

Figure 3-2 shows an overview of the engine testbed schematics with the key modifications to convert the base engine to micro-pilot operation highlighted. Each modification is discussed later in this chapter.

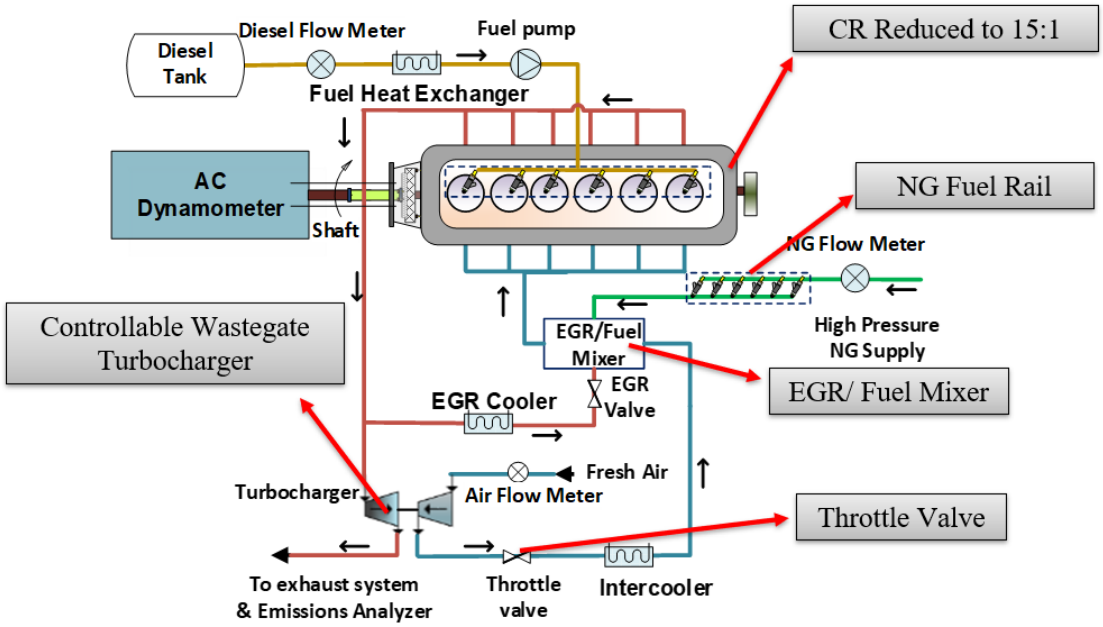

Figure 3-2. Micro-Pilot engine testbed schematics

Figure 3-3 shows the engine's final configuration with the TWC aftertreatment in the APS Labs heavy-duty test cell. The engine was built on an in-house fabricated cart that enables exchange in the test cell with other engines in 40 mins. Custom cart parts fabricated incudes the cart framework, mounting brackets, flywheel housing, pivoting wire tray, aluminum panel housing, and wiring harness.

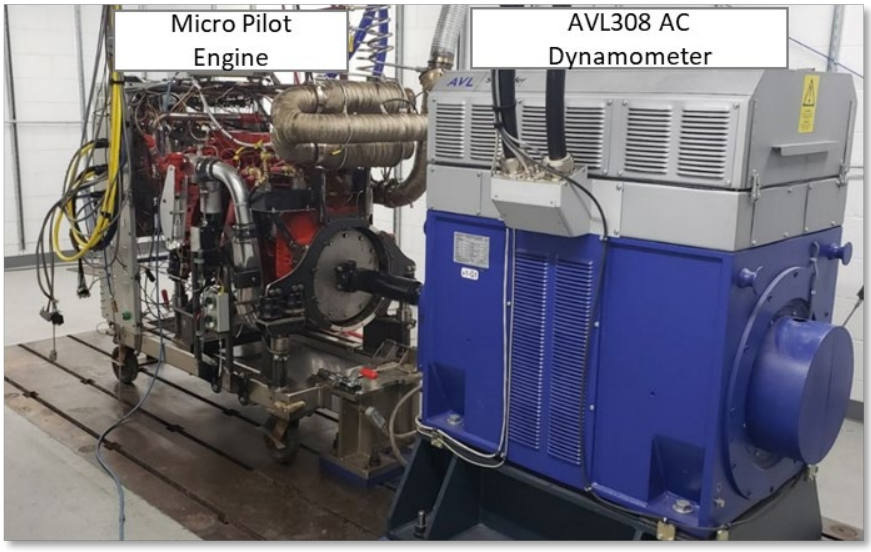

Figure 3-3. Micro-Pilot Engine test bed in the Heavy-Duty Dyno Test Cell

The complete list of parts, including engine control, engine mounting, engine instrumentation, engine cooling, fuel delivery, torque delivery, intake plenum, exhaust collection, and performance system procured to convert the base engine to the micro-pilot operation is provided in Appendix 9B.

3.2 Combustion System

The Cummins ISB 6.7 L engine is converted to run stoichiometric and diesel micro-pilot / NG combustion. The original CR of 17.3 was reduced to 15.0 to reduce the combustion knock propensity at high loads. A detailed description of the CR reduction is presented in section 3.2.1. Although the combustion chamber design is likely not optimal for the premixed combustion of the NG, the optimization of the combustion chamber geometry apart from the CR was outside the scope of this dissertation.

The ability of the diesel injector used in this project to deliver a micro-pilot injection as low as 2% of total energy contribution was reported by Yang, X. et al.[70]. The diesel fuel is injected by a direct-injection, high pressure (common-rail) injection system with six medium-duty 8-hole diesel injectors with 168 µm diameter and 150° included angle (see section 3.4.2).

The NG fuel is delivered at a single point upstream of the intake manifold through an EGR-air-Fuel mixer described in sections 3.3.3 and 3.4.1.

3.2.1 Compression Ratio Reduction

The stock CR of 17.3:1 from the base engine was decreased to 15:1 to prevent combustion knock and pre-ignition at high loads while also considering the efficiency loss and combustion stability reduction at low loads caused by the lower compression ratio.

The target CR15:1 was achieved by combining two techniques. First, a thicker head gasket similar to that used in the marine Cummins QSB variant was employed to reduce the CR to 16.5:1. Modified pistons from the marine Cummins QSB variant were added to reduce the CR further. These pistons were chosen because of their proven production performance in a 30 bar BMEP version of the engine. The pistons were modified by milling a 1.7mm deep chamfer at a 45° angle on the periphery and milling the top face of the crown to a depth of 2.8mm, as shown in Figure 3-4. The final compression ratio was determined by the milling and chamfer depths chosen because the volume of material removed from the piston crown increased the clearance volume.

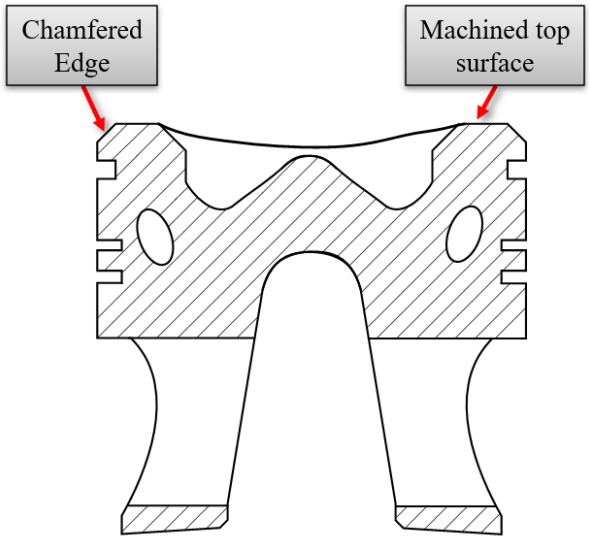

Figure 3-4. OEM piston cross-section representation. Machining operations overview to reduce the CR.

The compression ratio impact at a high load operating condition (20 bar BMEP) is shown in Table 3-2. The diesel pilot SOI is one crank angle degree (CAD) advanced in the reduced CR 15.0 due to exhaust temperature limitation of 800°C for the stock variable geometry turbocharger. Combustion phasing was within one CAD. It is noted that the combustion knock level, as indicated by the 95th percentile of peak-to-peak pressure, was lower with a reduced compression ratio (10.4 bar compared to 4.30 bar) with additional detail given in Figure 3-5. Additionally, the peak cylinder pressure was lowered by 32 bar (156 in comparison to 124 bar).

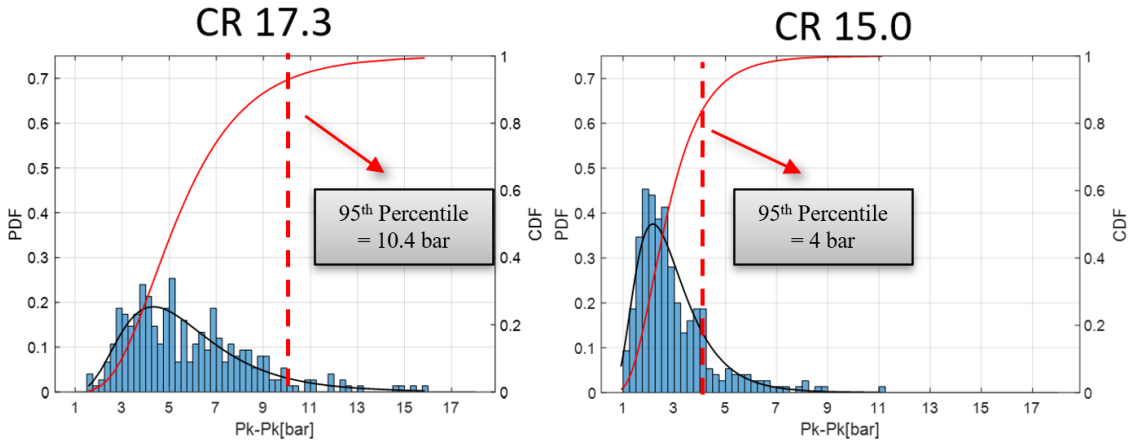

Figure 3-5. Combustion knock peak-peak power distribution function comparison (95th percentiles being 10.4 and 4.3 bar respectively for the CR 17:3 and CR 15.0:1). Engine operating conditions are shown in Table 3-2.

Table 3-2. Compression ratio impact at high loads

Compression Ratio	**17.3**	**15.0**
BMEP [bar]	20.0	20.0
SOI [° bTDC]	2.00	3.00
$IMEP_{COV}$ [%]	3.0	2.7
Pilot Inj. Pres. [bar]	1000	1000
MAP [kPa]	191	191
Diesel Fuel Flow [g/s]	0.35	0.35
CNG Fuel Flow [g/s]	8.50	8.30
Lambda [-]	1.00	1.03

EGR [%]	0.00	0.00
ISFC [g/kWh]	167	164
PCP [bar]	156	124
Knock 95th Percentile [bar]	10.4	4.3
CA50 [°aTDC]	13.0	14.0
EGT [°C]	740	780

The compression ratio change was observed to have a small impact on the base combustion (phasing and duration) but significantly impacted the combustion knock propensity, as desired.

Figure 3-6 shows the Log(P) - Log(V) diagram and the apparent heat release (AHR) of the original CR of 17.3:1 and the reduced CR of 15:1 at the condition described in Table 3-2. A two-stage heat release curve is observed at the CR15.0 condition. As discussed in Chapter 4, it is expected that his secondary peak is attributed to the flame propagation transitioning from inside the piston bowl to the squish region.

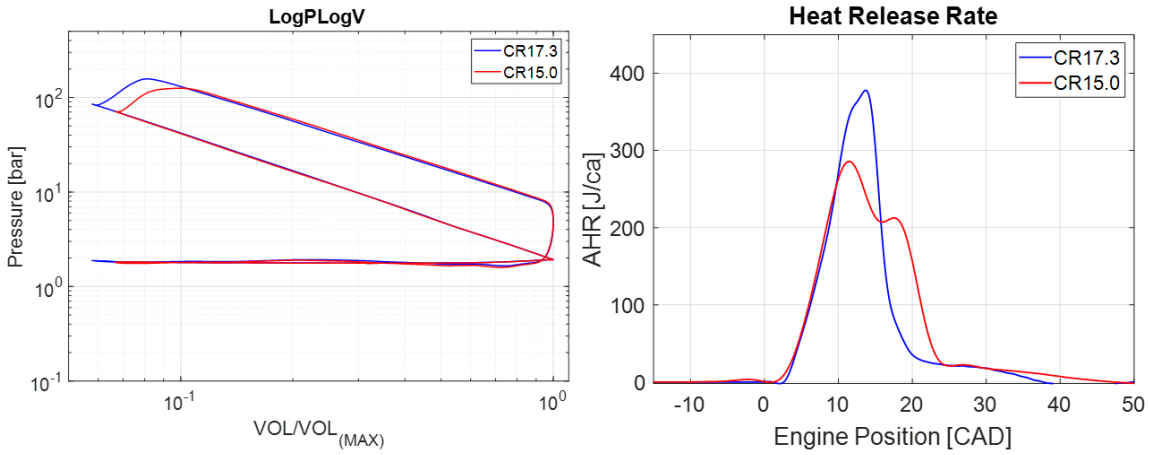

Figure 3-6. Log(P)-Log(V) and Apparent Heat Release (AHR) comparison of the high-load operating condition at the different compression ratios. Engine operating conditions are shown in Table 3-2.

For the low load operation, the lower compression ratio resulted in a longer ignition delay and later CA50, leading to an exhaust gas temperature (EGT) increase of 50°C. The higher EGT can be considered a benefit as an enabler for using the three-way catalyst; however, this is at the cost of higher indicated specific fuel consumption. Additional results and discussion about the compression ratio impact at low loads can be found in chapter 4 of this dissertation.

3.3 Air Handling System

The transition to stoichiometric operation alters the air handling system's requirements significantly. Therefore, the base engine's original air handling system was modified based on the recommendations of the research team through experimental and simulation data analysis. Figure 3-7 shows a diagram of the engine testbed with the air handling system key components highlighted.

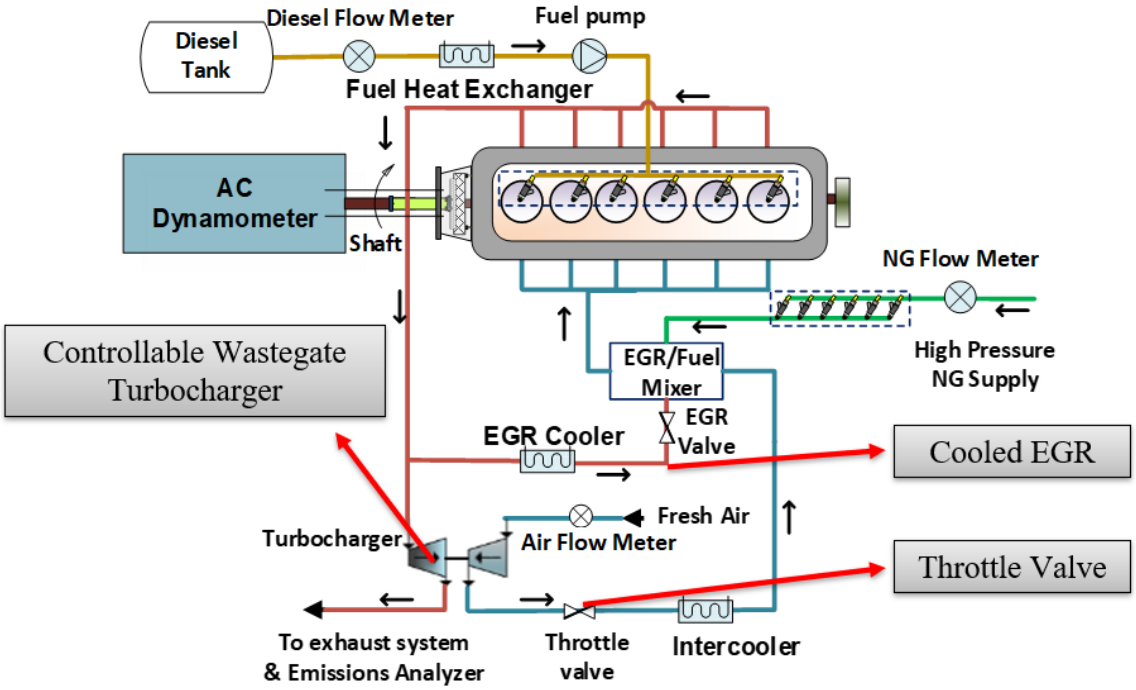

Figure 3-7. Air handling system overview

A throttle was added upstream of the intake manifold to adjust the airflow rate and maintain a stoichiometric mixture ratio at part load. This allows for advanced engine load and EGR management, particularly for low-load control during stoichiometric combustion. The EGR loop was modified to accommodate the EGR/Fuel Mixer located downstream of the throttle valve to ensure a positive pressure difference between the exhaust and intake manifold. Additionally, to achieve the target high-load BMEP (i.e., 25 bar) output and avoid damage due to high exhaust temperature expected at stoichiometric operations, a high-boost turbocharger with controllable wastegate was installed in place of the original.

This section detailed all the individual systems shown in Figure 3-7.

3.3.1 Throttle Valve

A throttle valve body was installed downstream of the compressor outlet. This enabled advanced control of engine load and EGR, specifically for low load control and stoichiometric conditions. The valve control was incorporated into the engine controller custom strategy discussed in chapter 3.5.

3.3.2 Controllable Wastegate Turbocharger

The constraints of the engine's original variable geometry turbocharger (VGT) were investigated using 1-D Engine Simulation in GT Suite, as well as the benefits of a smaller compressor. The 1-D model was insensitive to small inaccuracies in turbine modeling, although large errors were immediately detectable. As a result of the positive results of the compressor scaling analysis and the potential for compressor surge, it was concluded that the original turbocharger would need to be replaced to meet the project's objectives.

To assist in the turbocharger selection, publicly accessible data (i.e., aftermarket turbocharge catalogs) was evaluated, as well as existing Westport Fuel Systems Inc. in-house data from past projects. Through extensive 1-D modeling, in collaboration with Westport Fuel Systems Inc., the research team selected a pre-production Turbonetics high-boost turbocharger shown in Figure 3-8. This unit features a fixed geometry with a smaller compressor and turbine wheels to satisfy the low flow requirements for stoichiometric

combustion. Because the exhaust temperatures are high in the stoichiometric operation and lower levels of EGR are required, this turbocharger uses a wastegate to manage boost pressure rather than a VGT.

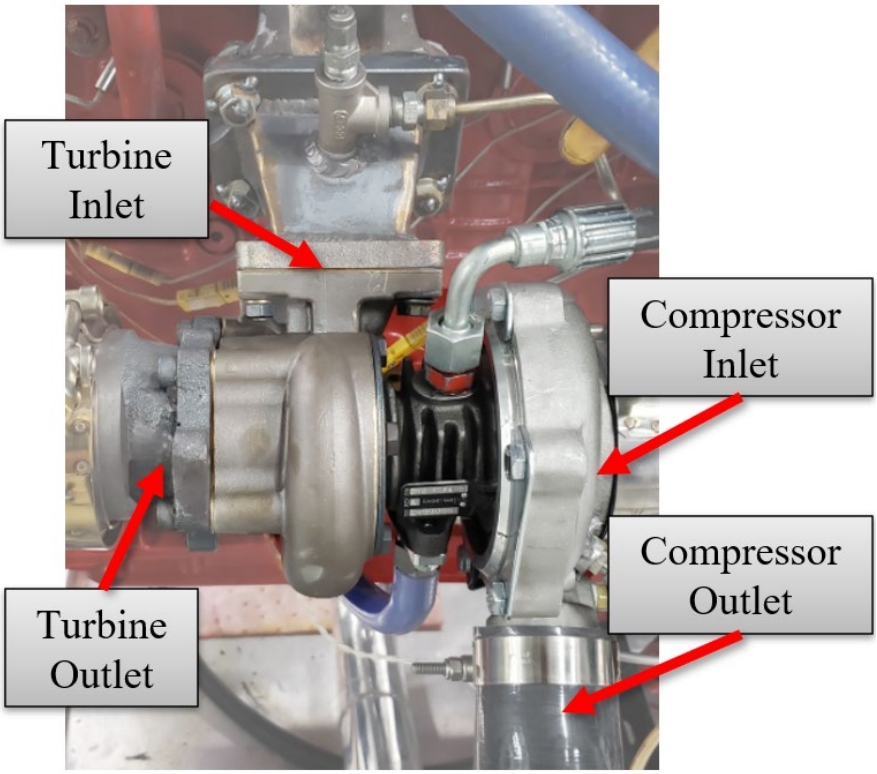

Figure 3-8. Controllable Wastegate Turbocharger installed on the Micro-Pilot engine

The 1-D engine simulation model was optimized by Westport Fuel Systems Inc. based on experimental data with the wastegate turbocharger. The optimized simulation model was then used to assess the new turbocharger's ability to achieve 25 bar BMEP at various speeds. The results showed that the new turbocharger matched the target operating condition requirements. Details are presented in the publication in chapter 4.3.

The wastegate valve positioning control was implemented in the engine test cell's control software to allow the user to command the desired boost pressure. The closed-loop controller enabled the throttle losses to be minimized to only the low-load operating condition, where the intake pressure is below barometric pressure (i.e., 80 kPa).

3.3.3 Cooled EGR

Westport Fuel Systems Inc. designed the custom EGR/Fuel mixer shown in Figure 3-9 to allow a stable operation of the Micro-Pilot engine. The mixer includes a cross-flow EGR mixer with a larger flow area than the NG fuel to minimize pressure loss.

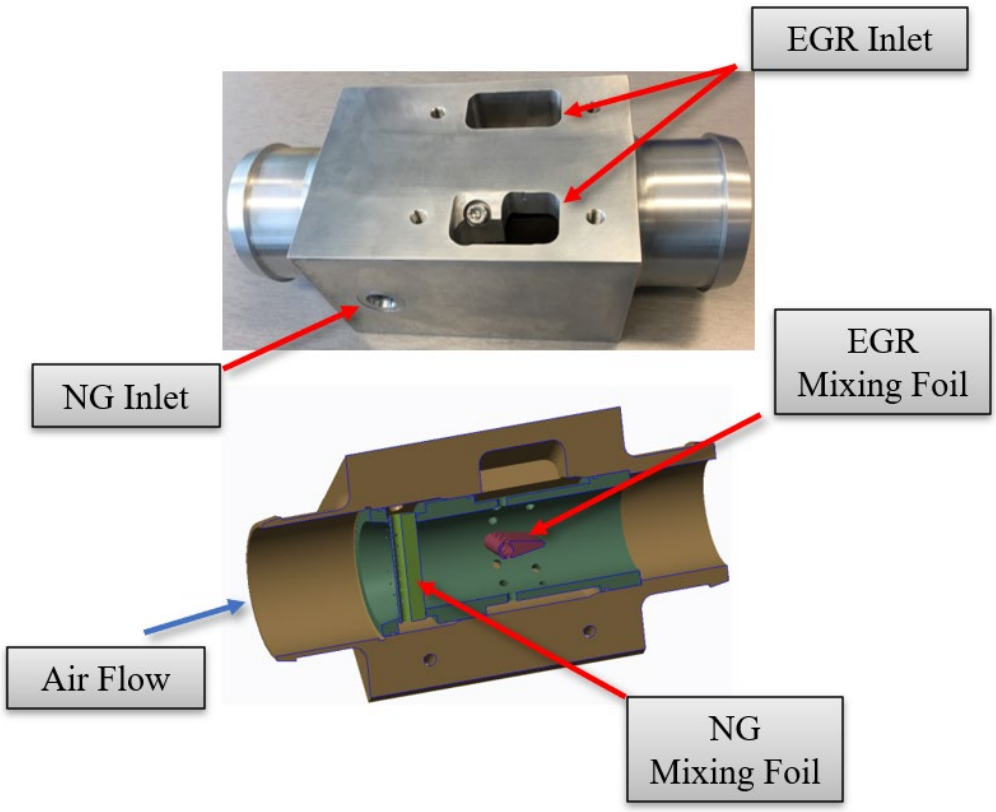

Figure 3-9. EGR/Fuel Mixer

A study that investigates the cooled EGR impact on combustion and emissions of the micro-pilot engine operated at medium loads can be found in Appendix 9C. For the EGR tolerance and impact when operating at low loads, the reader can refer to Chapter 6. Additional investigation is required for the EGR impact when the engine operates at high loads. However, Appendix 9A presents how the addition of EGR enabled a knock-free operation at high loads and describes this operating condition's challenges that require further work.

3.4 Fuel System

The NG port fueling system and the micro-pilot diesel injection system described in this chapter make up the micro-pilot engine fuel system.

The NG fuel is injected through a set of Westport AEC injectors at 8 bar injection pressure into an NG fuel manifold connected to the EGR/Fuel mixer described in chapter 3.3.3 and upstream of the intake manifold.

The micro-pilot diesel injection system is comprised of a common-rail high-pressure system. The injector is side-fed with diesel and is centrally mounted in the combustion chamber.

3.4.1 Natural Gas Port Fueling System

The NG is provided to the engine by six high-flow port fuel NG injectors (Westport AEC 8g/s rating) installed in the custom-designed fuel rail shown in Figure 3-10 (a). The custom control strategy was configured to balance the injections from the NG fuel system to maintain a constant fuel pressure downstream of the NG manifold.

The NG fuel rail outlet is connected to the EGR/Fuel mixer inlet shown in Figure 3-10 (b). The mixer is composed of an airfoil installed across the throat of a mixing venturi with a series of small-diameter holes designed to provide an appropriate pressure drop. The EGR/Fuel mixer is located downstream of the throttle valve but upstream of the intake manifold in the air handling system to provide adequate mixing time before the fuel-air combination is introduced into the engine.

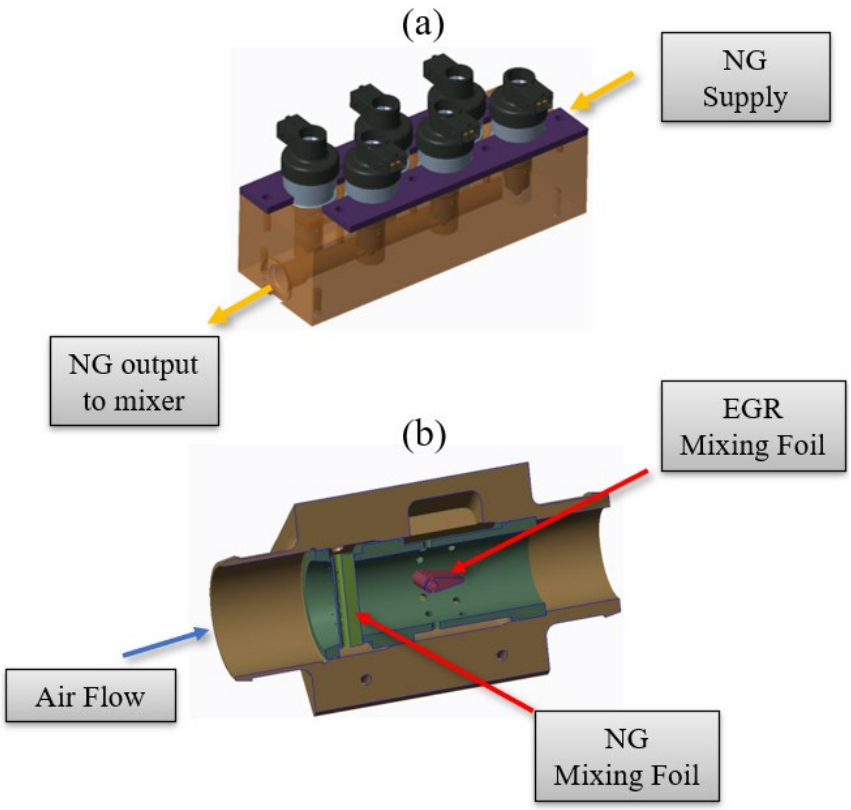

Figure 3-10. (a) NG Fuel Rail; (b) EGR/Fuel Mixer

3.4.2 Micro-Pilot Diesel Injection System

The micro-pilot diesel injection system is comprised of a high-pressure common rail system, including the original heavy-duty diesel injectors shown in Figure 3-11.

Figure 3-11. Original diesel injector

The 8-hole (168 µm diameter / 150° included angle) diesel injectors were sized to operate the base engine in its Diesel-only mode. These injectors are capable of delivering micro-

pilot injection quantities of as little as 2% of the total diesel energy at full load with a fully developed spray. The high-pressure common rail system can inject repeatable sprays from 600 to 2000 bar, and the injectors are centrally mounted on each cylinder and are controlled by the custom control strategy and actuated by a custom injector driver.

3.5 Control System

To allow complete control of all engine actuators, a standalone MotoHawk-based prototype engine control unit (P-ECU) was chosen. A custom engine strategy was developed using the Simulink-based Motohawk programming language. The software was developed in two parts: the first portion involved programming the engine's strategy for running in diesel-only mode, and the second part involved integrating the natural gas injectors for dual fuel mode.

The P-ECU's diesel-only control strategy allowed the engine to run entirely on diesel, emulating operation with the factory ECU. The baseline operational points were checked and compared using this system; the custom strategy was verified by replicating steady-state points even though the factory calibration maps were not accessible in the factory ECU. The confirmed diesel controller was then used as the foundation for converting to a dual-fuel approach. Figure 3-12 shows a block diagram of the diesel-only control strategy.

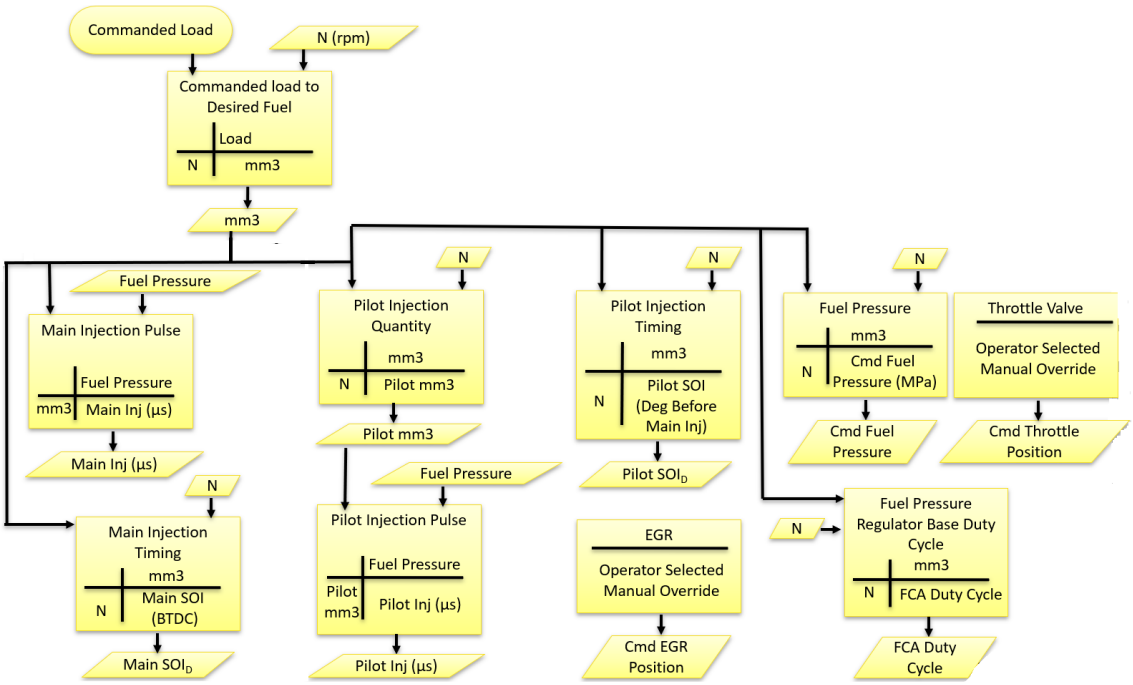

Figure 3-12. Diesel-Only Control Strategy

The load and RPM are the model's two main inputs. In the calibration software, the load is specified as a requested percentage, and the engine RPM is determined using the crankshaft position sensor. The camshaft sensor is used to determine the phase of the engine. A calibration table is used to compute the required fuel quantity value (Figure 3-12 as mm^3), the engine's load parameter, based on engine speed and requested load. The Main Injection Pulse and Timing, Pilot Injection Pulse and Timing, desired fuel rail pressure, and fuel control actuator base duty cycle is calculated using the mm^3 value and engine speed. As shown in Figure 3-12, calibration tables are used to determine these characteristics. The EGR is regulated by a set point specified by the user, and the EGR valve is actuated by an external linear actuator. The boost pressure is controlled by the user's required boost level, and the wastegate position is controlled by an external controller to obtain the desired boost.

As a modified strategy for the diesel-only operation, the micro-pilot feature was implemented. This option disables diesel split injection and reduces the pilot injection

quantity to the required micro-pilot operation condition. Figure 3-13 shows the block diagram implemented for the micro-pilot control model.

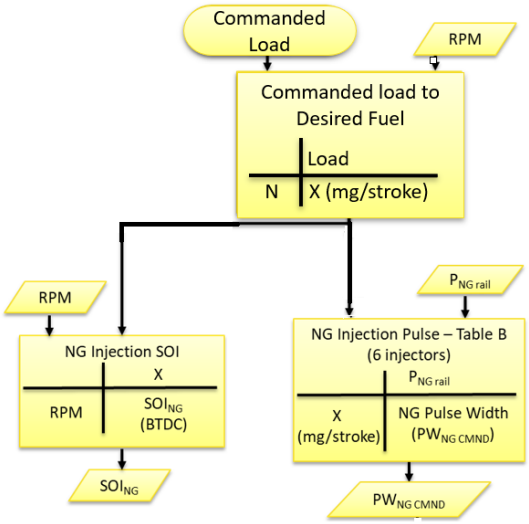

Figure 3-13. Micro-Pilot Mode Control Strategy

As seen in Figure 3-13, the amount of natural gas fuel injected is determined by the engine speed and the commanded load inputs. The injectors are fired sequentially in the mixing block after the start of injection (SOI) is selected from a table. A calibration table establishes the injector pulse width using an 8 bar natural gas rail pressure and the required fuel mass.

Overrides have been added to the model's parameters to the real-time modifications during testing, giving the operator complete control over all systems, including diesel injection timing, diesel injection pressure, diesel injection quantity, global equivalency ratio, and intake manifold conditions, thanks to the control system (wastegate, charge air cooling, dilution).

Limiters and protection are employed in the control strategy to prevent the standalone controller from performing any operations that could harm the engine hardware. The limiters used in the model include:

1. Oil pressure: The oil pressure protection is provided by a mechanical switch that closes when the oil pressure rises above a certain threshold. When the switch closes, the controller detects it and authorizes fuel injection. If oil pressure goes below this level, the fuel supply is terminated.

2. Coolant temperature: If the coolant temperature increases beyond the predetermined limit, the limiter switches off the fuel injection.

3. Maximum fuel quantity: The maximum injection duration is limited so that excessive fuel volumes cannot be demanded due to an incorrect calculation or a miskeyed override.

4. Injection timing limiter: The injection SOI is limited so that it does not perform the main injection or pilot injection at a region that could be hazardous to the engine hardware.

5. Maximum fuel pressure: To keep rail pressure within safe design limits, a fuel pressure limiter is included. As the top limit approaches, the control model reduces the drive output to the fuel control actuator.

6. Maximum engine speed: The limiter switches off the injection when the engine speed goes beyond the set limit.

A custom slave diesel injector driver, shown in Figure 3-14, was developed, allowing complete control of the diesel injector's driving signal.

Figure 3-14. Custom slave diesel injector driver

3.6 Aftertreatment System

ACAT/Umicore provided twin TWCs with a unique herringbone metallic substrate. Each unit features a wash-coat technology with 5.65 g/m3 precious metal loading and a 0.144 m diameter by 0.156 m flow length. To increase the exhaust temperature and improve catalyst performance, all exhaust ducting from the turbine output to the catalyst outlet was insulated. Figure 3-15 depicts the aftertreatment system.

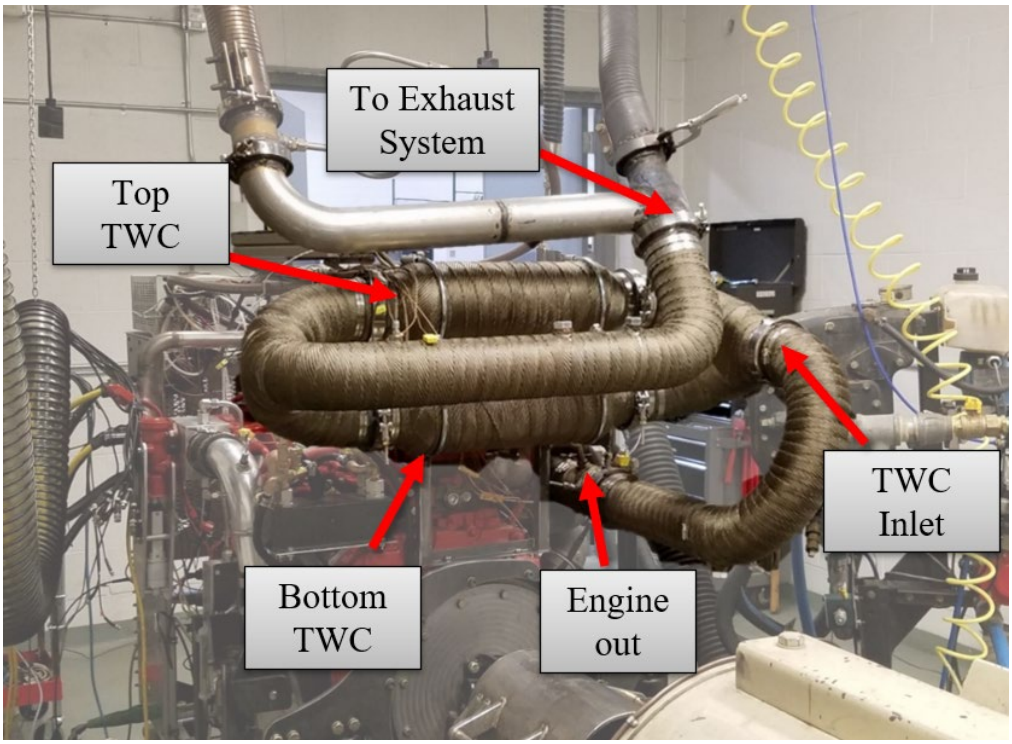

Figure 3-15. Aftertreatment System

While redesigning the exhaust system to include the TWCs, special attention was given to ensuring that the exhaust system could be simply modified to remove the TWCs. TWCs are frequently removed from the exhaust system because certain development processes (such as combustion development) do not require aftertreatment.

3.7 Engine Instrumentation & Measurement Uncertainty

Six in-cylinder pressure transducers (AVL GH series piezoelectric) feed the test unit's real-time combustion analyzer system. A BEI encoder series H25D with 360 pulses per revolution measures the crank angle position, while an AVL A/C Dynoroad 308/4 SX controls the load and speed.

High-speed data acquisition of 300 cycles in an A&D CAS system with a high-speed sampling multiplier provided a crank angle resolution of 0.167 for the combustion analysis

(6 samples per degree). A NI PCIe chassis with appropriate modules for thermocouples and 0-10V analog inputs are used for the low-speed data acquisition system.

The fuel flow rates are measured using two Micro Motion Coriolis Meters ELITE CMFS010P, one for liquid diesel and the other for compressed natural gas. Type K thermocouples are used to measure temperature in areas such as the intake, exhaust manifold, and engine coolant. The Omega Absolute Pressure Transducer MMA050V5P4D1T3A5CE measures the intake and exhaust pressures. The Omega Gage Pressure Transducer GP50 measures other pressures (oil pressure and fuel inlet).

The intake and exhaust CO_2 ratio is used to compute the EGR percentage. CO2 Meter K33 series sensors were used to make the measurements. CO2 concentrations were continuously measured using sample ports fitted in the exhaust and intake manifolds. The sensor's output is relayed to the prototype ECU, allowing for real-time EGR assessment.

A Horiba MEXA 1600 emissions bench is used to monitor gaseous emissions. Engine out or tailpipe emissions were measured using a single analyzer. A 3-way valve was used to choose the sample line from either engine out or tailpipe when the system was in steady-state operation.

Sensor accuracy and systematic error owing to electrical noise, signal conditioning, signal transmission, and hysteresis are examples of measurement errors. Several control points, as well as test repetitions, are taken during engine testing to offset these issues.

The major engine sensors' accuracy and uncertainties for the independent variables are shown in Table 3-3.

Table 3-3.Independent measurement variables accuracy and uncertainty

Measurement	Accuracy	Full scale	Uncertainty (absolute)	Unit
In-Cylinder Pressure transducer	±0.30%FS	0-250	± 0.75	bar
Engine crank angle degree (Encoder)	±1.00	360:1	± 1.00	Deg
Fuel flow rate (Diesel & NG)	±0.05 FS	0-30	± 0.015	g/s
Temperature measurement	±2.20	0-800	± 2.20	°C
Intake/Exhaust Manifold Pressure Transducer	±0.08%FS	0-6.89	± 0.0055	bar
Other pressure measurements	±0.50%FS	0-7 / 0-2	±0.035 / 0.010	bar
Torque measurement	±0.05%FS	0 – 5000	±2.50	Nm
CO2 Analyzer	±1.00%FS	0 – 16	±0.16	%
NOx Analyzer	±1.00%FS	0 – 5000	±50.0	ppm
UHC Analyzer	±1.00%FS	0 – 10000	±100.0	ppm

The uncertainty of the dependent variables in Table 3-4 is estimated using the uncertainty propagation analysis described in Taylor B.N and Kuyatt's NIST Technical Report 1297 (Eq.3-1).

$$U_Y = \sqrt{\sum \left(\frac{\partial Y}{\partial X_i}\right)^2 U_x^2} \qquad \text{(Eq. 3-1)}$$

Where Y is the estimated quantity's value, U is the uncertainty of the variable, and X is the measured variable.

Table 3-4. Dependent variables accuracy and uncertainty

Measurement	Range	Uncertainty (absolute)	Unit
NMEP	4.70 – 8.00	± 0.15	Bar
BSFC	215 – 305	± 3.80	g/kWh
DSR	93 - 97	± 0.50	%
Ignition Delay	1.70 – 4.60	± 0.08	ms
EGR	0.00 - 12.0	± 0.20	%
EQR	0.80 – 1.10	± 0.01	-
CA50	12.0 – 32.0	± 0.60	°aTDC
BSNOx	0.20 - 133	± 34.1	g/kWh
BSUHC	2.10 - 37.0	± 5.00	g/kWh
BSCO2	374 - 680	± 11.8	g/kWh

3.8 Fuels

Table 3-5 shows the properties of the fuels utilized in the engine development. The CNG fuel composition is provided by the local supplier in daily reports. The experimental investigation took a total of fifteen months, out of which the local supplier was able to provide reports for the first ten months. The analysis presented in Chapters 4, 5, and 6 uses the averaged values of the CNG properties seen in Table 3-5. The reader can refer to Appendix 9B for the detailed CNG composition analysis of the fuel used during the experimental investigation. Additional investigation to assess the impact of fuel composition is not the scope of this dissertation and is part of future work (see Chapter 8). A third-party laboratory tested the ULSD #2 fuel properties.

Table 3-5.Properties of liquid and gaseous fuels

Diesel (ULSD)	Density (kg/m^3) @ 15.6°C, 1 atm	Heating value (MJ/kg)	AFR	H/C	Cetane Number
	851.6	42.8	14.60	1.85	51.7
CNG	Density (kg/m^3) @ 20°C, 1 atm	Heating value (MJ/kg)	AFR	H/C	*Methane Number
	0.727	47.5	16.30	3.80	83.0

**Wärtsilä Methane Number [81]*

During this project, the Diesel Substitution Ratio (DSR) is given on an energy basis as described in Eq.3-2.

$$DSR = \frac{\dot{m}_{CNG} \cdot Q_{LHV,CNG}}{\dot{m}_{CNG} \cdot Q_{LHV,CNG} + \dot{m}_{Diesel} \cdot Q_{LHV,Diesel}} \qquad \text{(Eq. 3-2)}$$

Where, $\dot{m}$ is the mass flow rate in kilograms per second (kg/s), and Q_{LHV} is the lower heating value in MJ/kg, as seen in Table 3-5.

The Equivalence Ratio (φ) is determined as shown in Eq. 3-3.

$$\varphi = \frac{\dot{m}_{CNG} \cdot AFR_{stoich,CNG} + \dot{m}_{Diesel} \cdot AFR_{stoich,Diesel}}{\dot{m}_{air}} \qquad \text{(Eq. 3-3)}$$

Where AFR is the stoichiometric mass air to fuel ratio described in Table 3-5.

4 DEVELOPMENT OF A MEDIUM DUTY STOICHIOMETRIC DIESEL MICRO-PILOT NATURAL GAS ENGINE

This article was published in the International Journal of Engine Research, 2022.

Bonfochi Vinhaes, V., Yang, X., Naber, J.D.

Michigan Technological University

Gordon McTaggart-Cowan

Simon Fraser University

Mahdi Shahbakhti

University of Alberta

Sandeep Munshi

Westport Fuel Systems Inc.

Michigan Technological University

Department of Mechanical Engineering-Engineering Mechanics

1400 Townsend Drive, Houghton, Michigan, USA 49931

Email: vbvinhae@mtu.edu, jnaber@mtu.edu

4.1 Abstract

Fueling a compression-ignition engine with premixed natural gas offers the potential to combine a clean-burning, low-carbon fuel with a high compression ratio, high-efficiency engine. This work describes the development of a multicylinder 6.7 L diesel engine converted to run stoichiometric diesel micro-pilot/ natural gas premix combustion with a maximum diesel contribution target of 5% of the total fuel energy and a three-way catalyst aftertreatment system. Results are given by comparing the stoichiometric combustion to the diesel baseline operation, showing combustion characteristics differences, including the rapid two-stage heat release. A high load output of 23 bar brake mean effective pressure was obtained with diesel-like brake thermal efficiency of 41%. This operating condition enabled a brake-specific CO_2 emissions reduction of up to 25% when compared to diesel. It was observed that the low load output is limited by combustion stability when operated at stoichiometric conditions. The three-way catalyst is observed to run at peak efficiency with an equivalence ratio of 1.01. Injector fouling was observed through the inspection of the nozzle and its internal parts, indicating carbon build-up similar to that seen in injector coking mechanisms. A comparison of the developed engine to other engine technologies is given, showing that the diesel micro-pilot natural gas engine performance is in good standing among other diesel and gas engines in the market.

Keywords: Micro-Pilot, Stoichiometric, Three-Way Catalyst, Performance, Diesel, Natural Gas

4.2 Introduction

Traditionally, such conventional ‘‘dual-fuel’’ engines have combined a lean premixed natural gas charge with a significant diesel injection [1]. While such engines can achieve reasonable efficiency and low NOx emissions, they suffer from poor combustion efficiency, high unburned methane emissions, and limited reductions in diesel consumption over realistic, on-road duty cycles [2]. As a result, they have not achieved significant market

penetration in on-road vehicle applications. Combining an overall stoichiometric fuel-air mixture with a small diesel pilot injection is an alternative approach. High substitution rates are possible, as only a small amount of diesel is needed to ignite the premixed charge, while

a three-way catalyst (TWC) can be used to achieve extremely low emissions of NOx, CO, and unburned hydrocarbons (UHC), which are predominantly CH4. By maintaining diesel-like compression ratios and efficiency, combined with a low-carbon fuel, significant net fuel cost and greenhouse gas (GHG) emission reductions are possible.

The application of natural gas as an alternative fuel for internal combustion engines (ICEs) has become an attractive field of research as its properties show a great potential to reduce the emissions regarding CO2, and NOx [3]. For applications in ICEs, the high resistance to auto-ignition of methane is particularly suitable for enabling engines with higher compression ratios, resulting in higher efficiency [4,5].

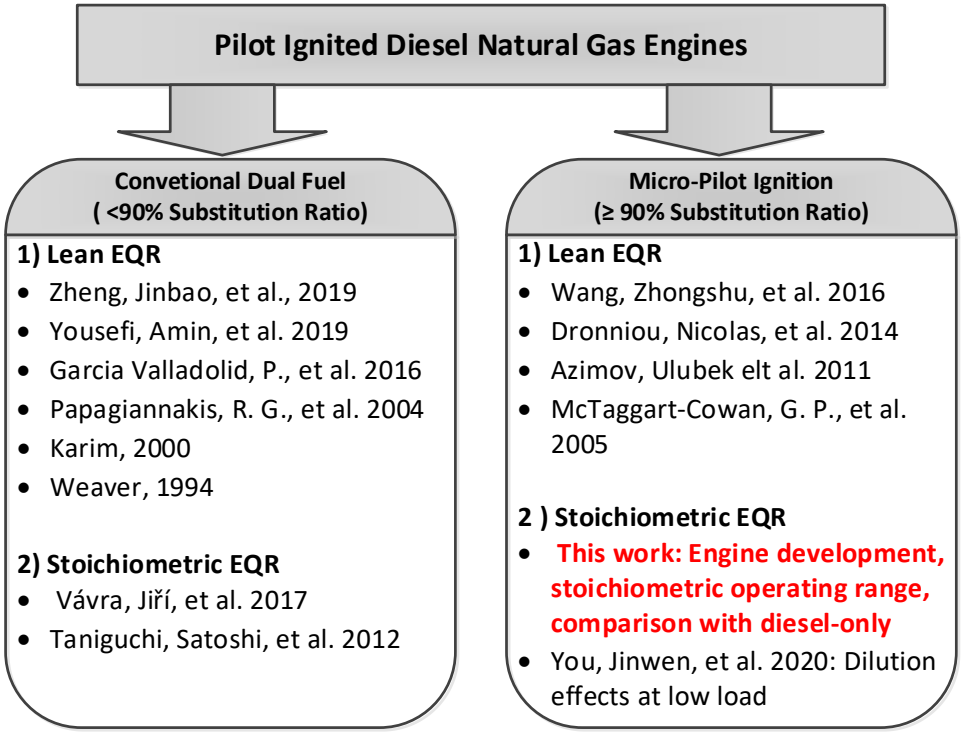

Figure 4-1. Pilot Ignited Diesel Natural Gas Engines Recent Research. EQR stands for equivalence ratio. [6-18]

Figure 4-1 shows the recent research done on pilot-ignited natural gas engines.

The conventional dual fuel operation performance and emissions, including effects of intake manifold air temperature (IMAT) and intake manifold air pressure (MAP), different substitution ratios, the effect of exhaust gas recirculation (EGR), the effect of equivalence ratio, and the effects of injection timing have been extensively studied by multiple researchers [7, 8, 13]. Zheng, J. et al. [6] studied the effect of equivalence ratio. Their work showed that the premixed lean-burn engines have a slower flame propagation while an increase in equivalence ratio increases the heat release rate and exhaust gas temperature, which improves thermal efficiency and reduces methane emissions. However, due to the higher temperatures, NOx emissions are higher if no dilution is used. Papagiannakis [9] showed that at high loads conditions, the fuel consumption under dual fuel operation is similar to the ones seen in the regular diesel operation but are inferior when running partial loads.

The micro-pilot ignition is shown in Figure 4-1 as a diesel substitution ratio greater than 90%. This distinction is made because conventional diesel injection systems degrade the injection pressure and spray characteristics when the pilot quantities are below 10% of the quantity at full load. There are two strategies to achieve micro-pilot injection quantities with an injector sized for full diesel operation: lower injection pressures or shorter injection durations. Low injection pressures lead to poor spray development and large fuel droplets, e.g. [19]. For pilot injection pressures lower than 300 bar, spray breakup and consequent mixing process were negatively affected. For more conventional injection pressures (>600 bar), very short injection durations are required, especially at part loads. For the same injector as utilized in this study, Yang, X. et al. [20] observed that a fully developed spray could be achieved for diesel injection quantities that provide as little as 2% of the total fuel energy at full load; this agrees with similar findings from Zirngibl, S [21]. Maintaining the low diesel energy ratio at lower loads is a substantial challenge due to very small injection quantities requiring short injection durations. These short durations impact the injectors in that the injector needle never fully opens and is always in either the opening or closing phase. This greatly increases variability in performance, including between injectors and

even for the same injector as a function of operating temperature. It also ensures that the fuel in the injector sac is never at full pressure, limiting spray atomization and resulting in broad variations in spray penetration. While not absolutely required, a dedicated injector sized for micro-pilot fuel quantities would allow a longer injection duration at higher injection pressures, resulting in more stable and repeatable injection events.

Moreover, as discussed later in this paper, injector tip temperature management becomes a challenge due to the reduced fuel flow. Therefore, an optimized micro-pilot injection system, as an ignition source only with enhanced cooling, is usually required to achieve low injection quantities [11]. Additionally, conventional dual-fuel engines can run under pure diesel over a great range of the operating map.

Micro-pilot studies have focused on the effect of injection pressure, engine performance and emissions, and pilot injection timing at lean operations [14, 15]. You, J. et al., discuss inert gases' dilution effect (Ar, N2, and CO2) at low load stoichiometric conditions on a 6-cylinder turbocharged engine [18]. With increasing the dilution ratio, Ar and N2 were observed to increase engine power while CO2 (normally available through exhaust gas recirculation systems) deteriorated the combustion process, such as heat release rate, cylinder peak pressure, and combustion phasing. The CO2 dilution resulted in the lowest NOx emissions of the three gases tested due to its lower in-cylinder temperature, while Ar resulted in the highest NOx emission.

No research has been found for the development of a micro-pilot diesel ignition that includes:

- Natural gas stoichiometric premix charge.
- Performance and emissions characteristics and comparison with the diesel-only operation.
- The application of a Three-Way Catalyst aftertreatment in a diesel micro-pilot natural gas operation and its sensitivity to equivalence ratio.

Stoichiometric Micro-Pilot Engine

A micro-pilot diesel and natural gas combustion approach was developed for an efficient, low-cost natural gas engine targeting medium-duty applications (i.e., 1.0 -1.7 L/cylinder). The concept is to combine a stoichiometric combustion event with EGR and a diesel pilot to provide a robust ignition source. Retaining a globally stoichiometric fuel-air ratio enables the use of a low-cost three-way catalyst to meet emissions standards. This is a significant simplification compared to the multi-element aftertreatment systems needed to meet emissions standards in modern diesel engines.

The combination of stoichiometric combustion with EGR is a feature of current natural gas fueled on-road engine products for the medium-duty market, with ignition provided by a spark plug. The concept being developed here uses a small quantity diesel pilot as the ignition source in place of the spark plug. This approach offers higher ignition energy and a more distributed ignition source for the premixed mixture, providing a more robust ignition, premixed turbulent flame combustion, and shorter distances for the flame to propagate through the combustion chamber. It is anticipated that these effects should reduce the potential for knock compared to premixed S.I. approaches, allowing higher brake thermal efficiency through higher compression ratios and more optimized combustion timing while also benefiting from lower COV and shorter combustion duration.

The goal of this work was to design and demonstrate the combustion system with a low diesel contribution (< 5% of total fuel energy), high brake mean effective pressure (BMEP) of 25 bar target, high brake thermal efficiency (>40% BTE) premixed charge natural gas on a multi-cylinder medium-duty engine. The combustion system and engine combined stoichiometric natural gas custom fueling system with diesel micro-pilot ignition and charge dilution via EGR. Low emissions (<0.2 g/kWh NOx) are to be achieved via stoichiometric combustion and a three-way catalyst.

This combustion approach is of particular interest to medium-duty applications. In these cases, the ability to provide a diesel-like torque profile with good efficiency is desirable.

However, relatively low mileage (compared to long-haul heavy-duty) limits the incremental engine system costs that can be accommodated within a reasonable payback. Furthermore, as these engines are typically used in urban and suburban areas, where air quality challenges are most serious, the ability to achieve very low tailpipe emissions of pollutant species such as oxides of nitrogen (NOx) is critical.

The following sections describe the modification process of a stock medium-duty diesel engine system, including the compression ratio (CR), the fuel system, the charge handling system, and the aftertreatment. The results and discussion section includes the combustion characteristics, performance, and emissions comparison of the micro-pilot mode and diesel-only mode, the aftertreatment sensitivity to equivalence ratio, the observed injector fouling, and the operating limits of this engine system.

4.3 Engine Development

The technical approach incorporates a series of standard engine technologies combined on a medium-duty diesel engine platform. A Cummins ISB 6.7Lwas selected as the medium-duty base engine and modified for diesel micro-pilot natural gas stoichiometric combustion operation.

The base engine technical specifications are shown in Table 4-1. The Cummins ISB 6.7L is an in-line 6-cylinder engine with a stock C.R. of 17.3:1. It has a common rail fuel system with a variable geometry turbocharger (VGT), and high pressure cooled EGR.

Table 4-1. Cummins ISB 6.7L Base Engine Specifications

No. of Cylinders	6
Bore & Stroke	107 x 124mm
Connecting rod length	192 mm
Displacement	6.7 L
Compression Ratio	17.3:1

Aspiration	VGT + Charge Air Cooler + HP EGR
Rated Power	224 kW (300 HP) @ 2600 RPM
Rated Torque	895 Nm @ 1600 RPM
Peak BMEP	16.8 bar

The engine was baselined in its original configuration over an extensive set of 26 speeds and loads conditions for later comparison with the micro-pilot mode.

6.7L Medium Duty Engine Modification

Figure 4-2 shows a schematic of the unit under test with the key modifications made to the compression ratio, fuel system, and the charge handling system described in the following sections, including the detailed instrumentation, aftertreatment system, and the controls system.

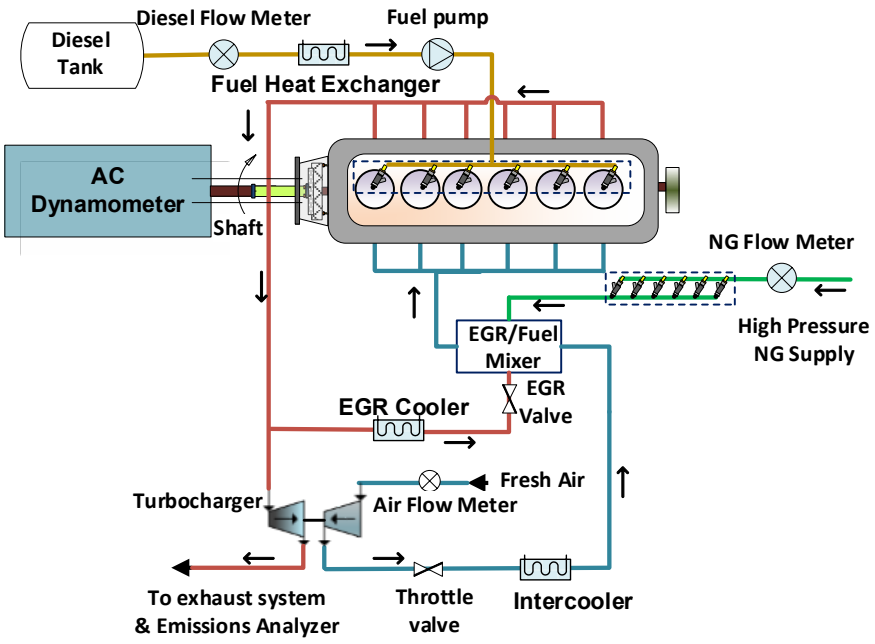

Figure 4-2. Test engine schematics.

Compression Ratio Selection

Despite NG's well-known knock resistance, a stoichiometric mixture of NG can auto-ignite under the conditions found in the end-gas of a high compression ratio engine. To reduce the chance of such engine knock occurring, the geometric compression ratio was reduced from 17.3:1. A preliminary modeling study conducted by the project partner suggested that a CR of between 14.5 and 15.5:1 would provide an acceptable balance of cold-start capability and knock avoidance at the target load up to 25 bar BMEP.

The target of CR 15.0:1 was achieved by combining a thicker head gasket and modified aluminum pistons. The pistons were selected due to their demonstrated production performance in a 30 bar BMEP version of the engine. The piston was customized by milling the top face of the crown to a depth of 2.8mm and machining a 1.7mm deep chamfer at a 45º angle on the periphery, as shown in Figure 4-3.

Apart from the machining modification, the piston bowl geometry was kept the same. Although this design is likely not optimal for the premixed combustion of the NG, the optimization of the combustion chamber geometry outside of the CR was outside the scope of this work.

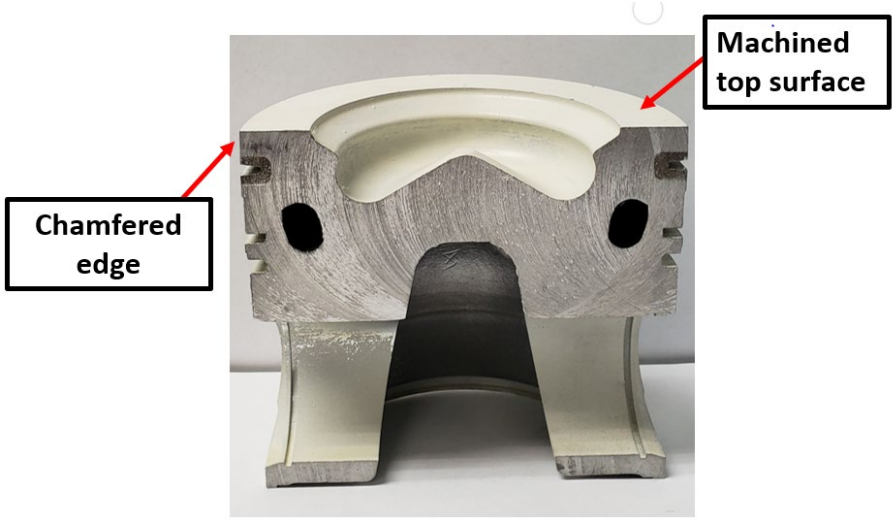

Figure 4-3. Piston machining overview on OEM pistons

Charge Handling System

The shift to stoichiometric operation results in significant changes to the requirements of the air handling system. To control airflow rate and maintain a stoichiometric mixture fraction at part load, a throttle was installed upstream of the intake manifold. This enables advanced control of engine load, specifically for low load control and EGR at stoichiometric combustion. The EGR/Fuel mixer (Figure 4-5) is located downstream of the throttle to ensure that a positive pressure difference between the exhaust and intake manifolds can be maintained.

A better mixing system than seen in typical diesel engines is needed to ensure equal air and EGR distributions between cylinders and charge homogeneity. The fabricated NG-air-EGR mixer system (Figure 4-5 (b)) is therefore designed to deliver the research engine's required homogeneous charge airflow during combustion development.

To achieve the target high load BMEP output, 1-D Engine Simulation performed in GT Suite was used to examine the limitations of the engine's stock turbocharger and the benefits for a smaller compressor. It was determined that the stock turbocharger had a potential for compressor surge, and therefore a pre-production high-boost turbocharger was installed. This unit has a fixed geometry with a smaller compressor and turbine wheels to accommodate the low flow requirements for stoichiometric combustion. This turbocharger is equipped with a wastegate to control boost pressure rather than a VGT as the exhaust temperatures are higher and lower levels of EGR are needed. The 1-D engine simulation model was then utilized to evaluate the potential to achieve 25 bar BMEP at different speeds using the new turbocharger. Through a combination of wastegate and throttle position to drive EGR, the location of the simulated conditions on the compressor map is shown in Figure 4-4.

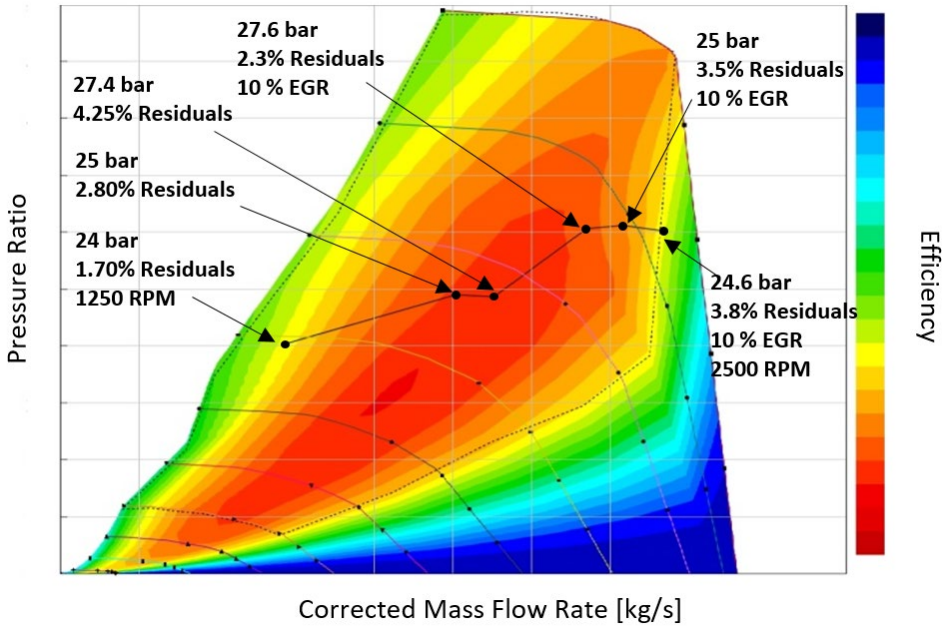

Figure 4-4. Compressor map of the new turbocharger, showing 1-D engine simulation results of the location of peak torque at various speeds. Axis values have been removed per supplier request due to confidentiality.

The simulation results suggest the selected turbocharger is well matched to achieve the target 25 bar BMEP with an anticipated boost pressure of 2.80 bar. The residuals shown are the estimated internal residuals.

For the high-speed cases highlighted in Figure 4-4, the simulation model was run with 10% EGR to avoid combustion knock, and therefore a higher-pressure ratio was required to achieve the target EGR. Overall, while the boost requirements for the application are higher than would be seen in a standard diesel engine, they still fall within the range that is achievable with single-stage compressors.

Fuel System

The diesel micro-pilot injection as low as 2% of total energy contribution is delivered by a direct-injection, high-pressure (common-rail) diesel injection system that includes six

medium-duty 8-hole Bosch diesel injectors with an included angle of 150°. This micro-pilot quantity was successfully achieved by using the engine's stock injector.

The NG is introduced to the engine through a mixing venturi located immediately upstream of the intake manifold. A set of six prototype high flow port injectors (Westport AEC 8 g/s rating) are installed in a custom-designed manifold (Figure 4-5 (a)). The outlet fuel passage connects to an inlet port on an air-fuel mixing block.

The mixing block (Figure 4-5 (b)) is composed of an airfoil installed across the throat of a mixing venturi, with a series of small diameter holes sized to provide an appropriate pressure drop across the mixer. The mixing block includes a cross-flow EGR mixer with a larger flow area than the fuel side to minimize pressure loss and the required pressure differential pressure across the engine. The mixing block is installed in the air system downstream of the throttle but upstream of the intake manifold to allow sufficient mixing time before the fuel-air mixture is inducted into the engine.

Westport Fuel Systems Inc. developed the fuel-air-EGR mixing system seen in Figure 4-5.

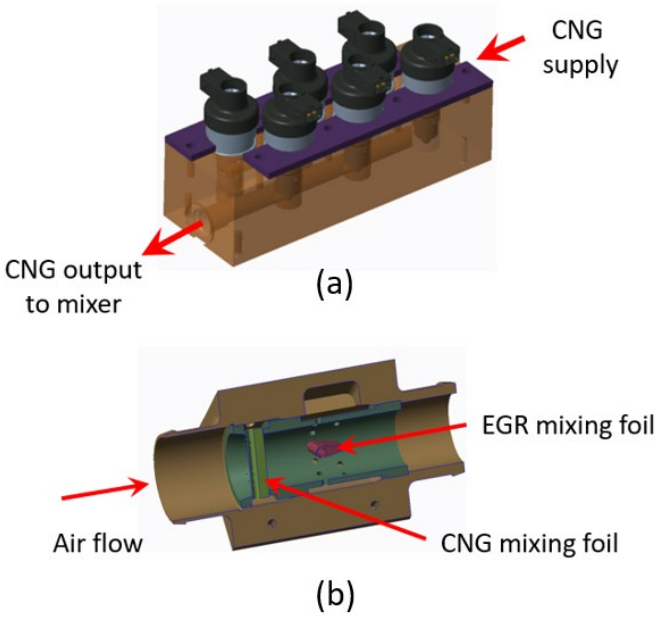

Figure 4-5. (a) Fuel Injector manifold; (b) Fuel-air-EGR mixing block

Aftertreatment System

Twin TWC procured from ACAT/Umicore featuring a novel herringbone metallic substrate were installed. Each unit has a 0.144 m diameter by 0.156 m flow length and a wash-coat technology with 5.65 g/m3 of precious metal loading. All exhaust ducting from the turbine outlet to the catalyst outlet was insulated to maximize exhaust temperature and improve catalyst efficiency. The aftertreatment system is shown in Figure 4-6.

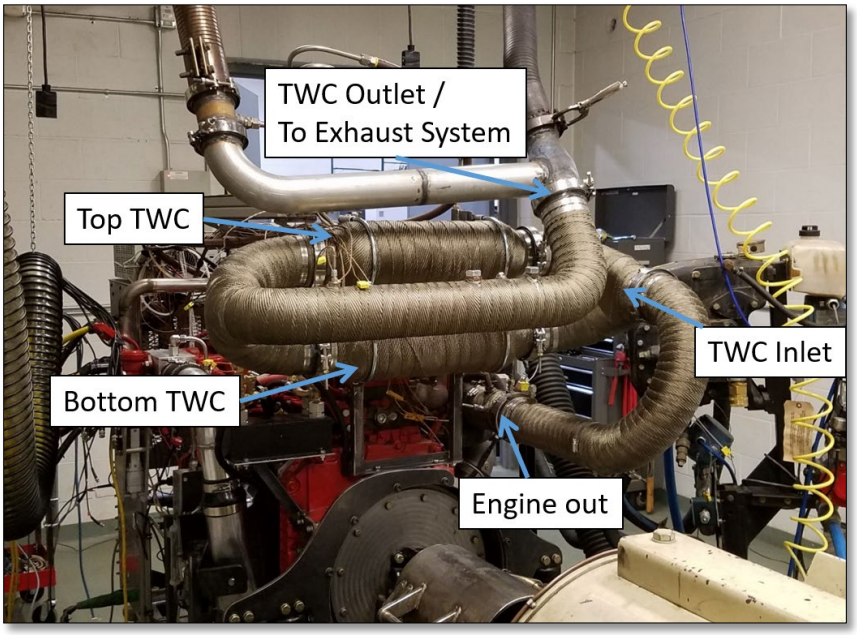

Figure 4-6. Exhaust system with twin TWC

Control System

A standalone MotoHawk ECU565-128 prototype engine control unit (P-ECU) was selected to allow complete control of engine actuators through the Mathworks/Simulink® + Motohawk programming language.

A diesel-only control strategy developed for the standalone ECU allowed 100% diesel operation of the engine, simulating operation with the base engine ECU. This strategy was

used to check and compare baseline operating points. While the full calibration maps were not accessible in the factory ECU, the custom strategy could replicate steady states points.

The micro-pilot diesel functionality was implemented as a modified strategy of the diesel-only operation. The diesel split injection is disabled in this mode, and the pilot injection quantity is reduced to the desired micro-pilot operation condition.

The control system allows the operator to have full authority of all systems, including diesel injection timing, diesel injection pressure, diesel injection quantity, global equivalence ratio, intake manifold conditions (wastegate, charge air cooling, dilution).

Instrumentation and Uncertainty

The test unit is instrumented with six in-cylinder pressure transducers type AVL GH series piezoelectric feeding a real-time combustion analyzer system. The crank angle position is measured by a BEI encoder series H25D with 360 pulses per revolution, and the load and speed are controlled by an AVL A/C Dynoroad 308/4 SX.

The in-cylinder pressure data is recorded by a high-speed data acquisition of 300 cycles in an A&D CAS system featuring a high-speed sampling multiplier that enabled a crank angle resolution of 0.167 (6 samples per degree). The low-speed data acquisition system is done through a NI PCIe chassis with corresponding modules for thermocouples and 0-10V analog inputs.

Two Micro Motion Coriolis Meter ELITE CMFS010P are used to measure the fuel flow rates, one for the liquid diesel and one for the compressed natural gas.

Temperature measurements such as intake, exhaust manifold, and engine coolant are made with type K thermocouples. Intake and exhaust pressures are measured by Omega Absolute Pressure Transducer MMA050V5P4D1T3A5CE. Other pressure measurements (i.e., oil pressure, fuel inlet) are done with Omega Gage Pressure Transducer GP50.

The EGR percentage is calculated as the ratio of intake and exhaust CO2. The measurements are made with CO2 Meter K33 series sensors. Sample ports in the exhaust and intake manifolds were installed to continuously measure CO2 concentration. The sensor output is sent to the prototype ECU, enabling real-time determination of EGR.

Gaseous emissions measurements are made by a Horiba MEXA 1600 emissions bench. One analyzer was used to measure engine out or tailpipe emissions. While operating at a steady-state, the sampling line was selected from either engine out or tailpipe by a 3-way valve.

Measurement errors include sensor accuracy and systematic error due to electrical noise, signal conditioning, signal transmission, hysteresis. To mitigate these factors, several control points are taken during engine testing, along with test repetitions.

The major engine sensors' accuracy and uncertainties for the independent variables are shown in Table 4-2.

Table 4-2. Independent variables accuracy and uncertainty

Measurement	**Accuracy**	**Full scale**	**Uncertainty (absolute)**	**Unit**
In-Cylinder Pressure transducer	±0.30%FS	0-250	± 0.75	bar
Engine crank angle degree (Encoder)	±1.00	360:1	± 1.00	Deg
Fuel flow rate (Diesel & NG)	±0.05 FS	0-30	± 0.015	g/s
Temperature measurement	±2.20	0-800	± 2.20	°C
Intake/Exhaust Manifold Pressure Transducer	±0.08%FS	0-6.89	± 0.0055	bar
Other pressure measurements	±0.50%FS	0-7 / 0-2	±0.035 / 0.010	bar
Torque measurement	±0.05%FS	0 – 5000	±2.50	Nm
CO2 Analyzer	±1.00%FS	0 – 16	±0.16	%

NOx Analyzer	±1.00%FS	0 – 5000	±50.0	ppm
UHC Analyzer	±1.00%FS	0–10000	±100.0	ppm

The uncertainty of the dependent variables shown in Table 4-3 is calculated using the uncertainty propagation analysis according to NIST Technical Report 1297 by Taylor B.N and Kuyatt (Eq. 3). Where Y is the value of the calculated quantity, U represents the variable's uncertainty, and X is the measured variable.

$$U_Y = \sqrt{\sum \left(\frac{\partial Y}{\partial X_i}\right)^2 U_x^2} \qquad \text{(Eq. 1)}$$

Table 4-3. Dependent variables accuracy and uncertainty

Measurement	Range	Uncertainty (absolute)	Unit
NMEP	4.70 – 8.00	± 0.15	Bar
BSFC	215 – 305	± 3.80	g/kWh
DSR	93 - 97	± 0.50	%
Ignition Delay	1.70 – 4.60	± 0.08	ms
EGR	0.00 - 12.0	± 0.20	%
EQR	0.80 – 1.10	± 0.01	-
CA50	12.0 – 32.0	± 0.60	°aTDC
BSNOx	0.20 - 133	± 34.1	g/kWh
BSUHC	2.10 - 37.0	± 5.00	g/kWh
BSCO2	374 - 680	± 11.8	g/kWh

Fuels

The properties of the fuels used in the engine validation are shown in Table 4-4. The CNG supplier provides the fuel property averages in daily reports. The ULSD #2 fuel characteristics were evaluated by a third-party laboratory.

Table 4-4. Properties of liquid and gaseous fuels

Diesel (ULSD)	Density (kg/m^3) @ 15.6°C, 1 atm	Heating value (MJ/kg)	AFR	H/C	Cetane Number
	851.6	42.8	14.60	1.85	51.7
CNG	Density (kg/m^3) @ 20°C, 1 atm	Heating value (MJ/kg)	AFR	H/C	*Methane Number
	0.727	47.5	16.30	3.80	83.0

*Wärtsilä Methane Number

In this project, the Diesel Substitution Ratio (SR) is given on an energy basis as described in Eq.1.

$$SR = \frac{\dot{m}_{CNG} \cdot Q_{LHV,CNG}}{\dot{m}_{CNG} \cdot Q_{LHV,CNG} + \dot{m}_{Diesel} \cdot Q_{LHV,Diesel}} \qquad \text{(Eq. 2)}$$

Where, $\dot{m}$ is the mass flow rate in kilograms per second (kg/s), and QLHV is the lower heating value in MJ/kg, as seen in Table 4-4.

The Equivalence Ratio (φ) is determined as shown in Eq. 2.

$$\varphi = \frac{\dot{m}_{CNG} \cdot AFR_{stoich,CNG} + \dot{m}_{Diesel} \cdot AFR_{stoich,Diesel}}{\dot{m}_{air}} \qquad \text{(Eq. 3)}$$

Where AFR is the stoichiometric mass air to fuel ratio described in Table 4-4.

4.4 Results and Discussion

Overview of the Micro-Pilot Diesel Natural Gas Engine

The diesel micro-pilot ignited natural gas engine's final build specifications are given in Table 4-5.

Table 4-5. Engine's Final Specifications

Compression Ratio	15.0: 1
Aspiration	Turbocharged (Wastegate) + Charge Air Cooler + HP EGR + Throttle Valve
Diesel Micro-Pilot Injection System	HPCR injector 8 holes (168 microns diameter)
Diesel Injection Pressure	600 to 2000 bar
Diesel Micro- Pilot Minimum Fuel Quantity	3.3 mg/injection
Natural Gas Fueling System	6 CNG injectors (Westport AEC 8 g/s)
Aftertreatment	ACAT/Umicore TWC Herringbone metallic substrate

The diesel micro-pilot engine's final configuration with the TWC aftertreatment in the Michigan Tech heavy-duty dynamometer test cell is shown in Figure 4-7.

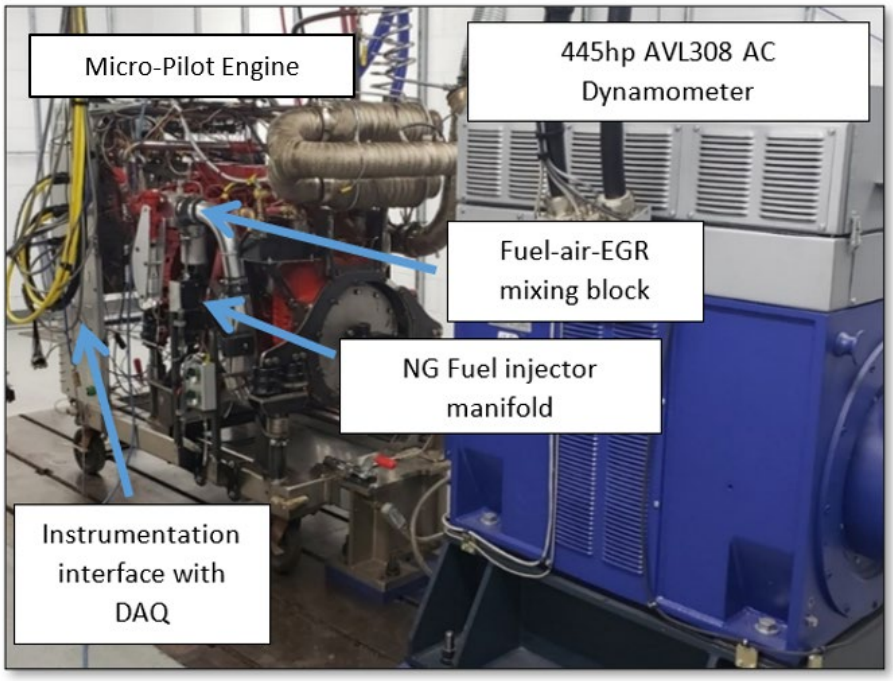

Figure 4-7. Micro-Pilot Diesel Natural Gas Engine.

Diesel Micro-Pilot Natural Gas Stoichiometric Combustion Comparison to Diesel-Only Mode at Medium Load

The diesel-only and micro-pilot part-load operating condition (13 bar BMEP @ 1620 RPM) with engine-out emissions are summarized in Table 4-6.

Table 4-6. Medium load operating conditions for the engine operating at 13 bar BMEP @ 1620 RPM

	Diesel-Only	**Micro-Pilot**
BMEP [bar]	13.0	13.0
Diesel Contribution	100%	4%
Diesel Flowrate [g/s]	6.50	0.29
Natural Gas Flowrate [g/s]	0.0	5.74

MAP [kPa]	184	135
EQR [-]	0.62	1.01
EGR [%]	7.00	5.30
BTE [%]	41.0	40.0
PCP [bar]	106	88
LPP [°aTDC]	14.0	14.0
CA10 [°aTDC]	5.80	5.70
CA50 [°aTDC]	13.0	11.0
CA90 [°aTDC]	29.0	24.0
EGT [°C]	586	720
NOx [g/kWh]	3.50	9.20
UHC [g/kWh]	<0.50	2.60
CO_2 [g/kWh]	603	479

The micro-pilot mode engine out NOx was observed to be higher than the diesel operation. Although the micro-pilot engine operates at lower boost and stoichiometric conditions, therefore, low oxygen available, the main driver for NOx formation is temperature. The exhaust temperatures are observed to be higher, indicating a higher in-cylinder temperature, which leads to an increased NO formation through the dominant thermal (Zeldovich) NOx mechanism. Additional dilution has the potential to reduce this further, and the high EGT is a benefit for the aftertreatment operation to reduce the tailpipe NOx. The unburned hydrocarbons increase is expected; however, the stoichiometric operation enables the use of a TWC aftertreatment. The brake specific CO2 emission was observed to be reduced by 20%.

The in-cylinder pressure and heat release comparison of the two combustion modes are shown in Figure 4-8. The in-cylinder pressure trace difference seen in (a) is due to the

impact of CR change and lower boost in the micro-pilot mode required to achieve the same load as the stock diesel-only configuration. The vertical lines seen in (b) represent the hydraulic start of injection timing of the diesel injection for both Diesel-Only mode (dashed-lines) and Micro-Pilot mode (solid-line). For the Micro-Pilot mode, the start of injection had to be controlled to be in between the main and pilot injection of the Diesel-Only mode in order to match the same combustion phasing (i.e., CA10, CA50).

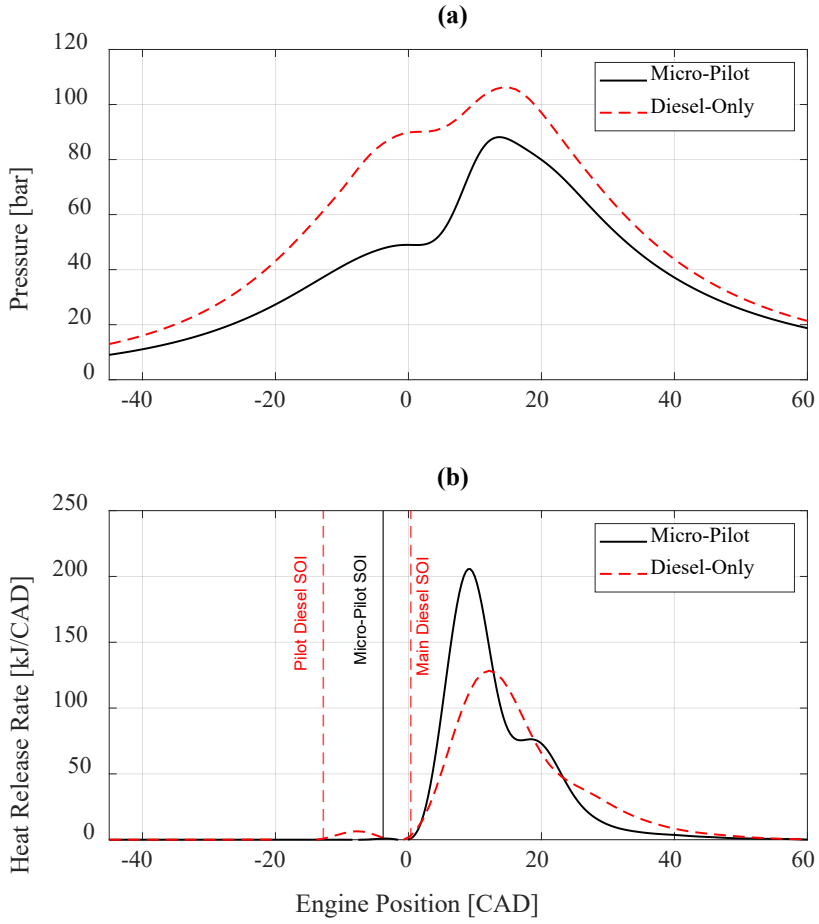

Figure 4-8. Micro-Pilot vs. Diesel Only Comparison. Engine operated at 13 bar BMEP and 1620 RPM. Complete operating conditions are shown in Table 6.

In the micro-pilot mode, the heat release curve seen in Figure 4-8 shows a rapid initial heat release peak followed by a secondary slower peak later in the cycle similar to what has

been seen by Liu, J., and Dumitrescu, C.E. in a Natural Gas SI combustion inside a diesel combustion chamber geometry [22, 23]. According to their work, the rapid first stage occurs in the high turbulence piston bowl, followed by a much slower burn in the squish region.

The CA50 vs. IMEP of the 300 cycles of a single cylinder is shown in Figure 4-9 for each of the operating modes.

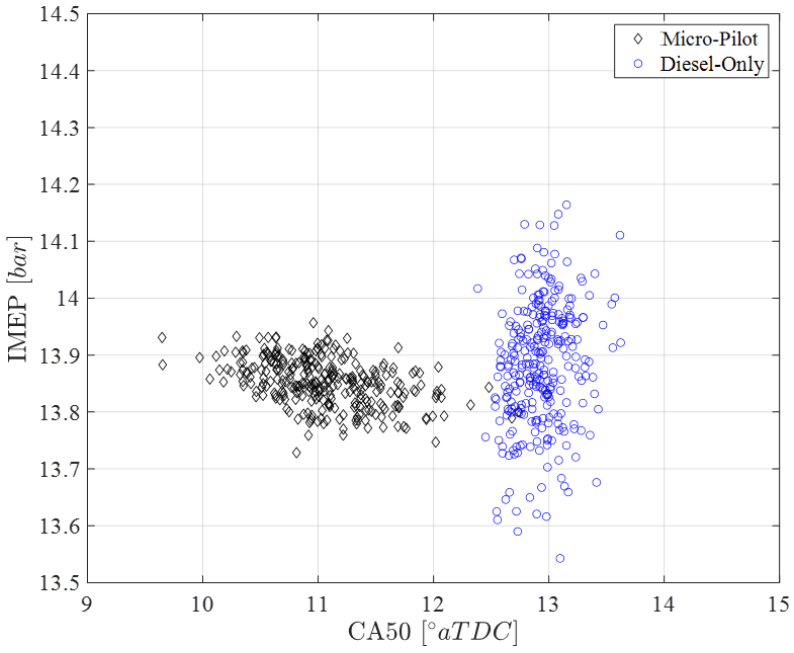

Figure 4-9. CA50 vs. IMEP Distribution in micro-pilot vs. diesel mode for the same conditions as those shown in Figure 8. The Micro-Pilot COVIMEP=0.33% vs. Diesel Only COVIMEP=0.85%. The CA50 Standard Deviation for Micro-pilot=0.48CAD vs. Diesel Only=0.18CAD.

It is observed that combustion is very stable in the micro-pilot mode with COV<0.5%. Compared to diesel, the micro-pilot natural gas stoichiometric combustion shows a smaller variance in IMEP. The CA50 variance of the micro-pilot mode is larger than that of diesel-only, indicating that the micro combustion is similar to that seen in spark-ignited engines as seen in the cycle-to-cycle variation study by Sztenderowicz, M.L., and Heywood, J.B. [24].

A design of experiments study performed in the same micro-pilot engine operating at medium load to quantify the performance sensitivity of combustion control factors is reported in [25]. The results have shown that, among the factors investigated (including MAP, EGR, pilot injection timing, pilot injection pressure, pilot injection duration, intake temperature, and equivalence ratio), EGR and pilot injection timing are the most influential performance control parameters. In contrast, intake temperature and pilot injection pressure were observed to have the least impact on this operating regime.

Emissions Sensitivity to Equivalence Ratio

Figure 4-10 shows results obtained from an equivalence ratio study to determine the catalyst efficiency at partial load. As shown at EQR = 1.01, high conversion >99% of NOx, UHCs, and CO was obtained.

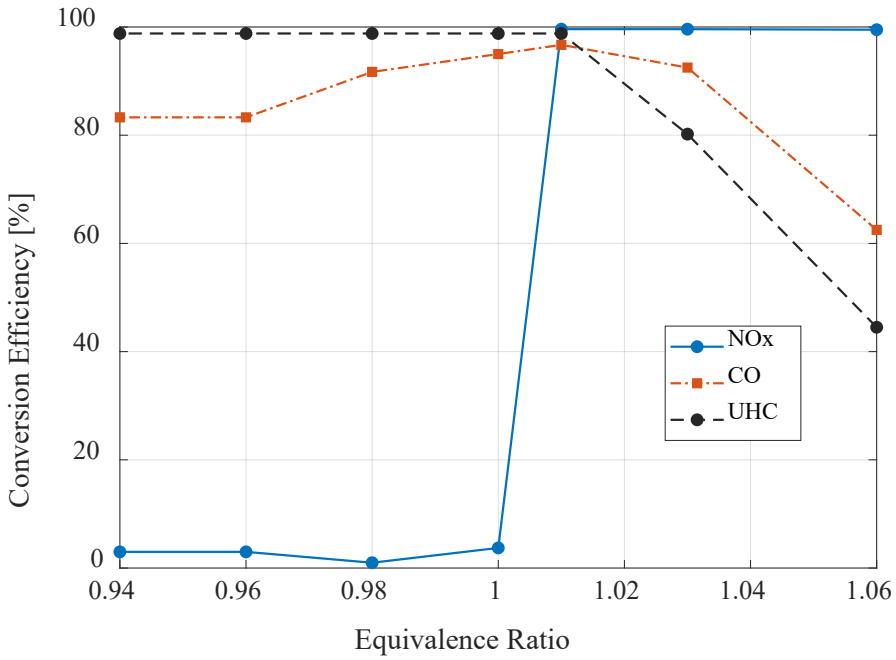

Figure 4-10. TWC conversion efficiency. Engine operating at 1200 RPM/8 bar BMEP/ No EGR/ >90% SR. Catalyst fully warmed up w/ inlet temperature >460 °C

It was observed that the system is sensitive to EQR consistent with TWC operation. In a production scenario, oxygen storage would need to be added along with a control system used in current stoichiometric on-road engines to control the lambda biasing using upstream and downstream oxygen sensors. With this control, it is expected that very low emissions can be achieved as the exhaust temperature is within the operating range for high conversion without excessive catalyst aging.[26]

Diesel Injector Fouling

Inspection on the diesel injectors was carried out post medium/high load operation to investigate potential tip temperature wear as seen by Vávra, J., 2017.[12]. The key finding from the work was that there was a sign of internal carbon build-up inside the injector, likely due to diesel pyrolyzing under relatively high temperatures. Figure 4-11 shows the injector nozzle as inspected under a microscope. As seen in the photos, some holes had internally obstructed flow passages.

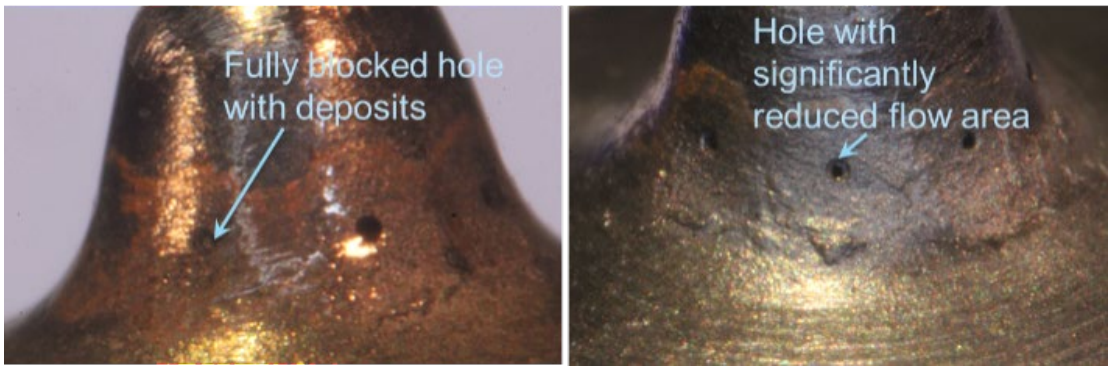

Figure 4-11. Microscope photo of the injector nozzle.

Additionally, the needle showed a significant amount of black residue on its surface, as shown in Figure 4-12. The observed residue is likely caused by the evaporation of lighter compounds, leaving the heavier compounds behind. The residue was not hard and could be removed easily, which indicates the temperature may not have been high enough to create hard coking residue. Although not verified by testing, it is reasonable to assume that the observed residue was caused by high temperatures inside the nozzle due to reduced

diesel flow, leading to less cooling and higher in-cylinder temperatures due to stoichiometric combustion.

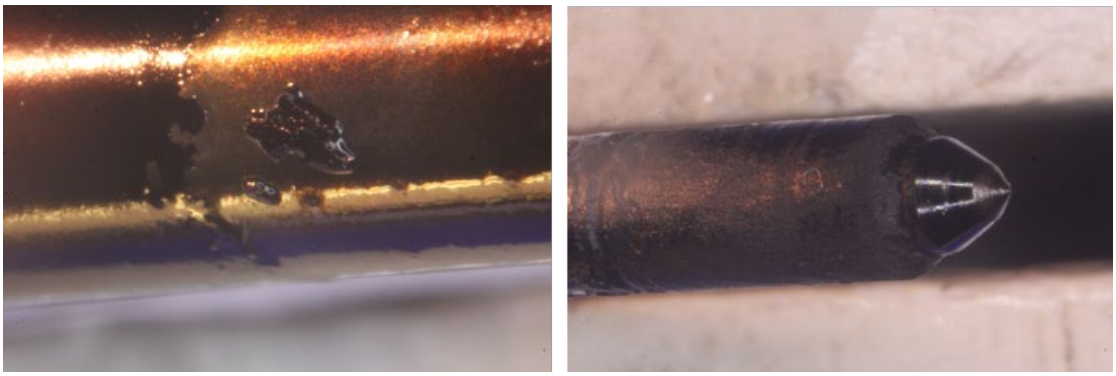

Figure 4-12. Microscope image of pyrolyzed diesel deposit and carbon build-up on injector internal needle.

As a corrective measure, research has shown that specific anti-coking fuel additives can effectively reduce carbon build-up in diesel pilot injection application [27, 28]. In this project, the remaining investigations were carried out after mixing the fuel additive Powerzol 9040 series. No impact was observed at the start of combustion and combustion duration with the addition of the fuel additive, indicating that the additive did not significantly affect the cetane or ignition.

High Load Strategies and Limits

A study was conducted to identify the micro pilot system's maximum and minimum load output. While it was possible to achieve 25 bar BMEP, the high load operation was limited by abnormal combustion (i.e.,combustion knock and pre-ignition) and exhaust (turbocharger inlet) temperature. Adding EGR and controlling pilot SOI enabled 23 bar BMEP with controlled combustion and no knock. Table 4-7 shows the high load operating condition achieved at stoichiometric natural gas diesel micro-pilot combustion at 3% diesel contribution.

Table 4-7. Overview of High Load Operating Condition

Operating Regime	Operating Condition	Constraints
High Load (18 – 25 bar BMEP)	1230 Nm @ 1620 RPM 23 bar BMEP Peak Cylinder Pressure: 130 bar 3% Diesel contribution 41% BTE 2.5% EGR Knock Pk-Pk: 4.5 bar 793 °C EGT CA50: 17 CAD (retarded)	Peak Cylinder Pressure max: 150 bar EQR 1.0 Max EGR: 10% Max Knock Pk-Pk: 10 bar Max EGT: 870°C

Combustion knock was determined via the cylinder pressure signal after band-passing (4 – 12 kHz) and rectifying, then determining the peak-to-peak pressure (Kpp (kPa)) on an individual cylinder basis [29]. The distribution of the KPP was found to be positively skewed, with skewness increasing with knock level. The combustion knock limit was set to 10 bar for the 95th percentile. Combustion knock was primarily controlled by pilot SOI and cooled EGR, as shown in Figure 4-13, enabling the engine load output of 23 bar BMEP with low Kpp.

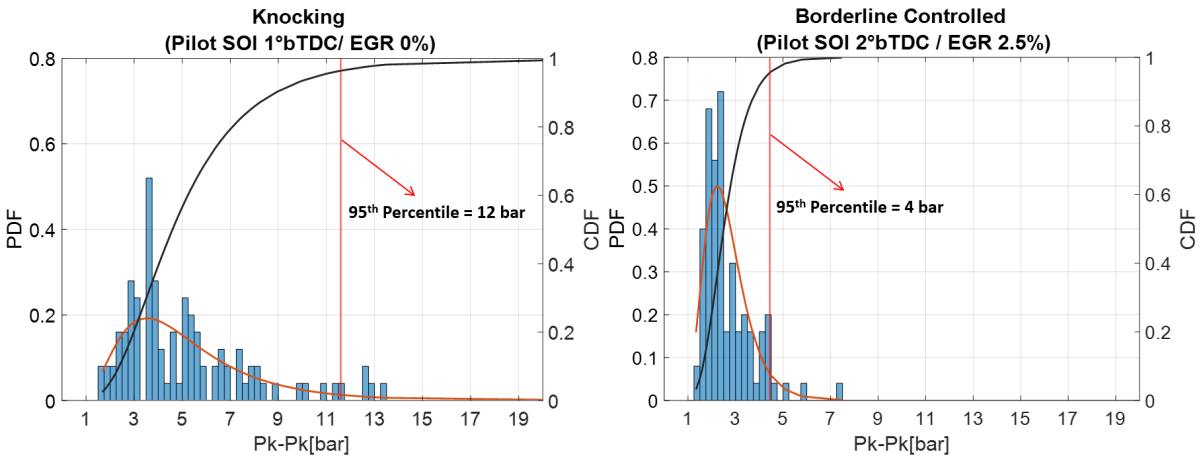

Figure 4-13. Knock Peak-Peak PDF comparison (95th percentiles being 12 and 4.0 bar respectively for the 0% EGR and 2.5% EGR. (Engine Speed=1620 rpm and 23 bar BMEP)

Low Load Strategies and Limits

The low load operation was limited by ignition delay, combustion stability, and throttling to a minimum intake pressure of 80kPa at the stock CR of 17.3 and 85 kPa at the modified CR of 15.0. Reducing load while maintaining stoichiometric combustion requires intake throttling or dilution via EGR. Maintaining stable ignition of the diesel pilot becomes a greater challenge at lower loads, as the diesel quantity is reduced; the chamber pressure at diesel injection is lower, and the presence of a near-stoichiometric mixture of NG will act to inhibit the diesel ignition. As such, a minimum load is encountered below which reliable ignition cannot be achieved.

The low load operation imposes a limit on the stoichiometric micro-pilot concept. The ability to reduce the charge mass through intake throttling is limited by engine design and instability in the diesel ignition leading to high variability in the IMEP. Bonfochi Vinhaes, V. et al. [30] investigated strategies to reduce load, including:

- Increasing charge dilution (EGR) to displace fresh air.
- Reducing diesel pilot injection pressure to provide a more concentrated ignition source in the vicinity of the injector.

- Retarding pilot injection timing to change combustion phasing and how the work potential of the fuel energy is utilized.
- Increasing the pilot injection quantity to increase the strength of the ignition source.
- Leaning the fuel-air mixture to reduce the amount of fuel energy.

Interestingly, a decrease in diesel pilot injection pressure has improved the combustion stability at lower loads. The lower pilot injection pressure keeps the pilot fuel-rich zones in the center of the combustion chamber, making it easier for the flame to ignite and propagate throughout the combustion chamber. This is shown in Figure 4-14, which gives the heat release traces for different diesel injection pressures. The lower pilot injection pressure was observed to reduce the ignition delay time between the hydraulic start of injection and the start of the heat release, resulting in a combustion stability improvement and greater flexibility in fueling and combustion phasing control.

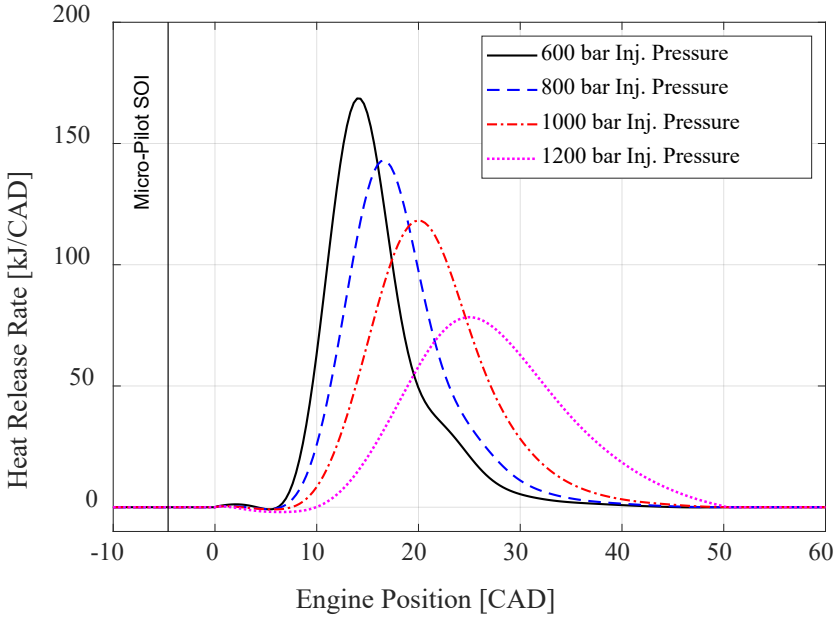

Figure 4-14. Heat release rate at different diesel pilot injection pressures. Engine operating conditions: 85 kPa MAP; 0% EGR; 35 °C IMAT; Constant diesel pilot SOI; Pilot fuel quantity of 3.3 mg/inj.; 1200 RPM; EQR 1.

The lowest load achieved while operating stoichiometric was 5 bar BMEP when operating the engine at 1200 rpm. Table 4-8 shows the low load operating conditions achieved with stoichiometric operation via diesel micro-pilot NG premix combustion with a 7% diesel contribution.

Table 4-8. Overview of Low Load Operating Condition

Operating Regime	Operating Condition	Constraints
Low Load (4 – 10 bar BMEP)	270 Nm @ 1200 RPM 5 bar BMEP 7% Diesel contribution 29% BTE 678 °C EGT 12% EGR CA50: 26 CAD COVIMEP: 3.5%	EQR 1.0 Minimum Catalyst Temperature: >420°C 5% Diesel contribution COVIMEP < 3%

Below this limit, other strategies, such as increased diesel contribution, variable valve timing, cylinder deactivation, lower intake manifold pressure, and hot EGR are potential solutions to further reduce the low-load limit with corresponding implications for the aftertreatment system that will require further investigation. Ultimately, it is possible that low load and idle conditions will be run in diesel-only operation with NOx controlled through charge dilution and combustion phasing optimization. Then the dual-fuel engine can switch to the diesel micro-pilot natural gas mode at the optimum engine load when the combustion is stable and the engine thermal efficiency is comparable to the diesel-only operation.

Performance Comparison to Commercial Diesel and Gas Engines

The minimum brake specific fuel consumption (BSFC), maximum BTE, and CO2 emissions of the micro-pilot engine are compared to those of diesel and SI gas engines manufactured by Cummins, as shown in Table 4-9.

The BSFC data, converted to diesel fuel equivalent for SI natural gas and micro-pilot engines, was obtained either experimentally or from technical paper [31, 32]. The consumption of the micro-pilot engine lies between diesel and spark-ignited natural gas engines. The CO2 emission of the micro-pilot engine is significantly lower than that of diesel engines, showing a significant 25% reduction in CO2 emission at peak torque. The demonstrated BTE of 41% on the micro-pilot engine effectively reduces the efficiency penalty of NG SI engines in comparison to diesel engines (42% diesel compared to 37% for NG SI) while retaining a high compression (15:1).

Table 4-9. Engine Performance Comparison

		SI Natural Gas [31]	**Diesel [32]**	**Micro-Pilot**
	Model	Cummins-Westport ISX12-G	ISB 6.7L Diesel Baseline	**MTU-WPT Micro-Pilot Engine**
Parameter	**Unit**	-	-	**-**
Rated Power	**kW**	238@1800 RPM	224 @ 2600 RPM	232 @ 1800 RPM
Displacement	**L**	11.9	6.7	6.7
Compression Ratio	**-**	11.5:1	17.3:1	15.0:1
BMEP @ Peak Torque	**bar**	16.5	16.5	24.0
Min. BSFC*	**g/kW-hr**	227	200	205
Max. BTE	**%**	37%	42%	41%

CO_2**	**g/kW-hr**	500	630	470
BTE @ Low-Load (5 bar BMEP)	**%**	29%	35%	29%

*BSFC: Diesel fuel equivalent / **CO2: Determine from BSFC and fuel composition.

At the low-load conditions studied, the stoichiometric micro-pilot diesel natural gas engine is observed to have similar brake thermal efficiency to that of the SI engine (29% for Micro-Pilot; 29% for NG SI; 35% for Diesel). This is attributed to SI-like performance, including stoichiometric operation leading to higher heat loss and intake air throttling.

At all operating conditions investigated, the stoichiometric operation was maintained. This enables the use of a TWC to achieve tailpipe NOx and unburned HC emissions at very low levels. Even at the lowest load achieved, exhaust gas temperatures on the order of 650°C were maintained, well above the temperature required for TWC operation. These findings are similar to SI engines, which can achieve NOx levels compliant with CARB's ultra-low NOx requirements (0.02 g/bhph), and do not require the complex system integration and controls required for multi-component aftertreatment systems used in modern diesel engines.

Although a transient operation investigation was not the scope of this work, the authors expect the micro-pilot engine response to transient operation to be similar to that seen in SI engines, owning its transient characteristics to the turbocharging/throttling capabilities of the system. While further investigation of the transient response is required, the extra degrees of freedom offered by the diesel pilot injection system offers extra scope for optimizing the engine transient operation.

The micro-pilot ignition technology provides a robust ignition energy source by the diesel pilot that can be leveraged to initiate the combustion of low-carbon and no-carbon fuels with high resistance to autoignition (i.e., Hydrogen and Ammonia) as well as to ensure stable early frame growth under lean conditions. These fuels have been reported to perform better at lean operation, so the stoichiometric strategy employed here may not be as promising. However, the high NOx emissions are still a critical challenge and make the use

of an aftertreatment a requirement [33, 34]. Moreover, these fuels have been observed to be limited by combustion knock at high-load conditions, which can limit the total diesel substitution ratio to be lower than the micro-pilot strategy. Further research of alternative no-carbon and low-carbon fuels with the micro-pilot ignition strategy is required.

4.5 Summary/Conclusions

The work focused on understanding the limitations for ignition and combustion of the micro-pilot concept. The key conclusions from this work were:

1) At mid-load conditions representative of loaded cruising, the micro-pilot engine had a brake thermal efficiency of 40%, nearly equivalent to the efficiency of the base diesel engine. This high-efficiency results in CO2 emissions 20% below those of the base diesel.
2) A Peak BMEP of 23 bar was achieved. This peak BMEP was limited by abnormal combustion (i.e., combustion knock and pre-ignition) and turbine inlet temperatures.
3) Stable ignition and stoichiometric operation were achieved at BMEPs as low as 5 bar. Below this load, ignition stability was degraded by low in-cylinder pressures and temperatures resulting from throttling and increasing EGR levels. Lower injection pressures were found to help extend the low-load ignition stability limit.
4) High in-cylinder temperatures and reduced cooling from diesel flow through the diesel injectors resulted in internal and external carbon build-up. Anti-fouling fuel additives were successful in preventing long-term degradation of injector performance.
5) At all operating conditions, the exhaust temperature was sufficiently high that tailpipe CO, NOx, and CH4 emissions could be maintained at near-zero conditions through stoichiometric combustion and a three-way catalyst. The maximum conversion was found at a slightly rich global equivalence ratio of 1.01.

In summary, these results demonstrated that the stoichiometric micro-pilot concept can achieve efficiencies that approach those of an equivalent diesel engine with diesel-like

BMEPs, very low NOx levels while reducing CO2 emissions by 20% or more. Further development of this concept will focus on optimizing the combustion and air handling systems to provide higher efficiencies and more robust knock control. Optimized low-flow micro-pilot injectors with enhanced cooling are required to provide stable ignition, better fuel distribution, and reduced risk of injector carboning. Strategies to achieve idling load operation and maintain stoichiometric conditions over transient cycles also need to be developed.

4.6 References

1. Karim GA. A Review of Combustion Processes in the Dual Fuel Engine—the Gas Diesel Engine. Progress in Energy and Combustion Science 1980; 6: 277-285. DOI: https://doi.org/10.1016/0360-1285(80)90019-2.

2. Karim GA. Dual-Fuel Diesel Engines. CRC Press: Boca Raton, FL, USA, 2015, p.Chapters: 3, 5, and 6.

3. Manns HJ, Brauer M, Dyja H, et al. Diesel CNG-The Potential of a Dual Fuel Combustion Concept for Lower CO2 and Emissions. SAE2015-26-0048 2015. DOI: https://doi.org/10.4271/2015-26-0048.

4. Naber J, Siebers D, Di Julio S, et al. Effects of Natural Gas Composition on Ignition Delay Under Diesel Conditions. Combustion and Flame 1994; 99: 192-200. DOI: https://doi.org/10.1016/0010-2180(94)90122-8.

5. Karim GA. Combustion in Gas Fueled Compression Ignition Engines of the Dual Fuel Type. Journal of engineering for gas turbines and power 2003; 125: 827-836. DOI: https://doi.org/10.1002/9783527628148.hoc047.

6. Zheng J, Wang J, Zhao Z, et al. Effect of Equivalence Ratio on Combustion and Emissions of a Dual-Fuel Natural Gas Engine Ignited with Diesel. Applied Thermal Engineering 2019; 146: 738-751. DOI: https://doi.org/10.1016/j.applthermaleng.2018.10.045.

7. Yousefi A, Birouk M and Guo H. An Experimental and Numerical Study of the Effect of Diesel Injection Timing on Natural Gas/Diesel Dual-Fuel Combustion at Low Load. Fuel 2017; 203: 642-657. DOI: https://doi.org/10.1016/j.fuel.2017.05.009.

8. Valladolid PG and Tunestal P. Effects of Intake Manifold Conditions on Dual-Fuel CNG-Diesel Combustion in a Light Duty Diesel Engine Operated at Low Loads. SAE2016-01-0805 2016. DOI: https://doi.org/10.4271/2016-01-0805.

9. Papagiannakis R and Hountalas D. Combustion and Exhaust Emission Characteristics of a Dual Fuel Compression Ignition Engine Operated with Pilot Diesel Fuel And Natural Gas. Energy conversion and management 2004; 45: 2971-2987. DOI: https://doi.org/10.1016/j.enconman.2004.01.013.

10. Karim G. Combustion in Gas-Fuelled Compression Ignition Engines. InASME ICE Fall Technical Conference 2000 Sep 23 (Vol 351) 2000: 35-31.

11. Weaver CS and Turner SH. Dual Fuel Natural Gas/Diesel Engines: Technology, Performance, and Emissions. SAE 940548 1994. DOI: https://doi.org/10.4271/940548.

12. Vávra J, Bortel I, Takáts M, et al. Emissions and Performance of Diesel–Natural Gas Dual-Fuel Engine Operated With Stoichiometric Mixture. Fuel 2017; 208: 722-733. DOI: https://doi.org/10.1016/j.fuel.2017.07.057.

13. Taniguchi S, Masubuchi M, Kitano K, et al. Feasibility Study of Exhaust Emissions in a Natural Gas Diesel Dual Fuel (DDF) Engine. SAE2012-01-1649 2012. DOI: https://doi.org/10.4271/2012-01-1649.

14. Wang Z, Zhao Z, Wang D, et al. Impact of Pilot Diesel Ignition Mode on Combustion and Emissions Characteristics of a Diesel/Natural Gas Dual Fuel Heavy-Duty Engine. Fuel 2016; 167: 248-256. DOI: https://doi.org/10.1016/j.fuel.2015.11.077.

15. Dronniou N, Kashdan J, Lecointe B, et al. Optical Investigation of Dual-fuel CNG/Diesel Combustion Strategies to Reduce CO_2 Emissions. SAE2014-01-1313 2014; 7: 873-887. DOI: https://doi.org/10.4271/2014-01-1313.

16. Azimov U, Tomita E and Kawahara N. Ignition, Combustion and Exhaust Emission Characteristics of Micro-pilot Ignited Dual-fuel Engine Operated under PREMIER Combustion Mode. SAE2011-01-1764 2011. DOI: https://doi.org/10.4271/2011-01-1764.

17. McTaggart-Cowan G, Jones H, Rogak S, et al. The Effects of High-Pressure Injection on a Compression-Ignition, Direct Injection of Natural Gas Engine. Internal Combustion Engine Division Fall Technical Conference 2005; 47365: 161-173. DOI: https://doi.org/10.1115/ICEF2005-1213.

18. You J, Liu Z, Wang Z, et al. Experimental Analysis of Inert Gases in EGR On Engine Power and Combustion Characteristics in a Stoichiometric Dual Fuel Heavy-Duty Natural Gas Engine Ignited with Diesel. Applied Thermal Engineering 2020; 180: 115860. DOI: https://doi.org/10.1016/j.applthermaleng.2020.115860.

19. Wang Z, Ding H, Ma X, et al. Ultra-High Speed Imaging Study of the Diesel Spray Close to the Injector Tip at the Initial Opening Stage with Single Injection. Applied energy 2016; 165: 335-344. DOI: https://doi.org/10.1016/j.apenergy.2015.12.046.

20. Yang X, Bonfochi Vinhaes V, Turcios M, et al. Process for Study of Micro-pilot Diesel-NG Dual Fuel Combustion in a Constant Volume Combustion Vessel Utilizing the Premixed Pre-burn Procedure. SAE2019-01-1160 2019; 1. DOI: https://doi.org/10.4271/2019-01-1160.

21. Zirngibl S and Wachtmeister G. Extensive Investigation of a Common Rail Diesel Injector Regarding Injection Characteristics and the Resulting Influences on the Dual Fuel Pilot Injection Combustion Process. SAE2016-01-0780 2016. DOI: https://doi.org/10.4271/2016-01-0780.

22. Liu J and Dumitrescu CE. Analysis of Two-Stage Natural-Gas Lean Combustion Inside a Diesel Geometry. Applied Thermal Engineering 2019; 160: 114116. DOI: https://doi.org/10.1016/j.applthermaleng.2019.114116.

23. Liu J and Dumitrescu CE. Flame Development Analysis in a Diesel Optical Engine Converted to Spark Ignition Natural Gas Operation. Applied Energy 2018; 230: 1205-1217. DOI: https://doi.org/10.1016/j.apenergy.2018.09.059.

24. Sztenderowicz ML and Heywood JB. Cycle-to-cycle IMEP Fluctuations in a Stoichiometrically-Fueled SI Engine at Low Speed and Load. SAE International 1990: 2291-2309. DOI: https://doi.org/10.4271/902143.

25. Bonfochi Vinhaes V, Yang X, McTaggart-Cowan G, et al. Multi-Variable Sensitivity Analysis and Ranking of Control Factors Impact in a Stoichiometric Micro-Pilot Natural Gas Engine at Medium Loads. 2022. DOI: ISSN: 0148-7191.

26. Smith I, Chiu J, Bartley G, et al. Achieving Fast Catalyst Light-Off from a Heavy-Duty Stoichiometric Natural Gas Engine Capable of 0.02 g/bhp-hr NO X Emissions. SAE2018-01-1136 2018. DOI: https://doi.org/10.4271/2018-01-1136.

27. Williams R, Smith A and Buttery I. Formation and Removal of Injector Nozzle Deposits in Modern Diesel Cars. SAE International Journal of Fuels and Lubricants 2013; 6: 230-240. DOI: https://doi.org/10.4271/2013-01-1684.

28. Caprotti R, Bhatti N and Balfour G. Deposit Control in Modern Diesel Fuel Injection Systems. SAE International Journal of Fuels and Lubricants 2010; 3: 901-915. DOI: https://doi.org/10.4271/2010-01-2250.

29. Naber J, Blough JR, Frankowski D, et al. Analysis of Combustion Knock Metrics in Spark-Ignition Engines. SAE2006-01-0400 2006. DOI: https://doi.org/10.4271/2006-01-0400.

30. Bonfochi Vinhaes V, McTaggart-Cowan G, Munshi S, et al. Experimental Studies of Low-Load Limit in a Stoichiometric Micro-Pilot Diesel Natural Gas Engine. Energies 2022; 15: 728. DOI: https://doi.org/10.3390/en15030728.

31. Mitchell R and Kocsis M. Performance Evaluation of Dedicated EGR on a 12 L Natural Gas Engine. SAE20190-01-1143 2019. DOI: https://doi.org/10.4271/2019-01-1143.

32. Joshi S, Dahodwala M, Koehler EW, et al. Trade-Off Analysis and Systematic Optimization of a Heavy-Duty Diesel Hybrid Powertrain. SAE2020-01-0847 2020. DOI: https://doi.org/10.4271/2020-01-0847.

33. Dimitriou P and Javaid R. A Review of Ammonia as a Compression Ignition Engine Fuel. International Journal of Hydrogen Energy 2020; 45: 7098-7118. DOI: https://doi.org/10.1016/j.ijhydene.2019.12.209.

34. Dimitriou P and Tsujimura T. A Review of Hydrogen as a Compression Ignition Engine Fuel. International Journal of Hydrogen Energy 2017; 42: 24470-24486. DOI: https://doi.org/10.1016/j.ijhydene.2017.07.232.

5 MULTI-VARIABLE SENSITIVITY ANALYSIS AND RANKING OF CONTROL FACTORS IMPACT IN A STOICHIOMETRIC MICRO-PILOT NATURAL GAS ENGINE AT MEDIUM LOADS

This paper was published in the proceedings of the SAE Technical Conference WCX, 2022.

Bonfochi Vinhaes, V., Yang, X., Eggart, B., Naber, J.D.

Michigan Technological University

Gordon McTaggart-Cowan

Simon Fraser University

Mahdi Shahbakhti

University of Alberta

Sandeep Munshi

Westport Fuel Systems Inc.

Michigan Technological University

Department of Mechanical Engineering – Engineering Mechanics

1400 Townsend Drive, Houghton, Michigan, USA 49931

Email: vbvinhae@mtu.edu, jnaber@mtu.edu

5.1 Abstract

A diesel piloted natural gas engine's performance varies depending on operating conditions and has performed best under medium to high loads. It can often equal or better the fuel conversion efficiency of a diesel-only engine in this operating range. This paper presents a study performed on a multi-cylinder Cummins ISB 6.7L diesel engine converted to run stoichiometric natural gas/diesel micro-pilot combustion with a maximum diesel contribution of 10%. This study systematically quantifies and ranks the sensitivity of control factors on combustion and performance while operating at medium loads. The effects of combustion control parameters, including the pilot start of injection, pilot injection pressure, pilot injection quantity, exhaust gas recirculation, and global equivalence ratio, were tested using a design of experiments orthogonal matrix approach. Specific outcomes from this research lead to fundamental and essential new knowledge in identifying the dominant factors for optimizing engine performance (i.e., thermal efficiency, combustion stability, combustion duration). The results provide a path forward for developing a high-efficiency engine and an optimized fuel and air handling system by ranking different controlling parameters for each performance metric studied. It was observed that exhaust gas recirculation and diesel pilot start of injection are the most influential parameters controlling medium load performance. In contrast, intake air temperature and pilot injection pressure have the least impact on the condition studied.

5.2 Introduction

Over 25% of the world's power utilization still relies on oil-based fossil fuel to power internal combustion engines (ICEs) [1]. Engine researchers have, for several years, focused on greenhouse gas emissions reduction, and therefore, ICE engine research has seen a shift towards low carbon fuel options [2]. An attractive field of research in ICE is the application of natural gas (NG) as an alternative fuel due to its great potential to reduce CO2 and NOx emissions [3]. NG's high resistance to auto-ignition is suitable for application in high compression ratio ICEs, resulting in a higher fuel conversion efficiency potential [4].

Conventional dual-fuel engines have traditionally combined the lean-burn of a premixed NG charge with a large amount of diesel injection [5]. Such engines have shown diesel-like fuel conversion efficiencies and low NOx emissions. However, poor combustion efficiency and high unburned methane emissions have posed a challenge for system development and on-road vehicle application [6, 7].

The combination of a stoichiometric fuel-air mixture with a small diesel pilot ("micro-pilot") is an alternative approach. Current diesel fueling technologies have made high substitution rates possible [8]. At the same time, stoichiometric operation enables the use of a three-way catalyst (TWC) to achieve extremely low emissions of NOx, CO, and hydrocarbons. The diesel-like efficiencies, paired with the low carbon fuel, can significantly reduce fuel costs and CO2 greenhouse gas emissions.

Recent researchers have focused on the effects of engine control parameters on the performance and emissions of diesel/NG engines. Belgiorno et al.[9] investigated the effect of engine calibration parameters, seen in Table 1, on the combustion characteristics, emissions, and performance of a lean dual-fuel engine operated with >10% diesel contribution while operating the engine at low-medium load conditions. They reported that unburned hydrocarbons (UHC) and methane hydrocarbons (MHC) are a function of the substitution ratio. Reducing compression ratio (CR) led to about a 30% reduction in MHC values. However, this had a negative impact on indicated thermal efficiency. Exhaust gas recirculation (EGR) and intake throttling showed a beneficial effect on the MHC emissions with a slight decrease in the indicated fuel consumption but an increase in smoke emission. Hydrocarbons and CO emissions were shown to be insensitive to rail pressure variation, and the combustion phasing advancement improves indicated thermal efficiency due to a reduction in heat rejection.

Rochussen et al.[10] studied the effect of fueling in a lean, naturally aspirated diesel/natural gas engine. Their work focused on parameters such as substitution ratio, diesel pilot start of injection (SOI), pilot injection pressure, and the equivalence ratio of both liquid and gaseous fuel. They observed a two-stage apparent heat release curve, in which stage 1

exhibited the behavior consistent with the auto-ignition of diesel, gas, and air premix mixture. In stage 1, the combustion seemed to be strongly influenced by the diesel injection parameters (quantity and pressure). Stage 2 of the heat release curve was observed to begin immediately after the end of stage 1, for which the gaseous fuel equivalence ratios greater than 0.4 showed a strong correlation with turbulent flame propagation. Below this limit, the fuel seemed to be converted by another mechanism that is not yet understood and needs further investigation.

Azimov et al.[11] focused on the sensitivity study of a supercharged dual-fuel engine running with various Syngas fuel compositions. Their work expanded on what was introduced as Premixed Mixture Ignition in the End-gas Region (PREMIER) combustion mode. In this mode, a two-stage heat release is observed. The first stage is the gaseous fuel flame propagation, and the second stage is the end-gas mixture auto-ignition. It was found that the second stage is mainly controlled by the pilot fuel SOI, gas equivalence ratio, and EGR. An increase in mass fraction burn in the second stage was observed as the hydrogen content in the syngas is increased, indicating an increase in combustion temperature, indicated mean effective pressure and efficiency with a significant increase in NOx emissions. The results also showed that with an increase in the Syngas CO2 content, the pressure rise rate, combustion temperature, thermal efficiency, and NOx decreases, despite increasing the mass fraction burned in the second stage of the combustion heat release.

Papagiannakis et al.[12] studied a single cylinder, naturally aspirated, direct injection diesel engine modified to run dual fuel. Their work focused on the effect of the natural gas substitution ratio (up to 90% NG) on the emissions and combustion performance at different speeds and loads. For dual fuel operating mode, it was reported that there is a reduction in engine efficiency for all operating points compared to diesel-only operation. A positive reduction in NOx and soot was observed while CO and UHC increased.

Table 5-1 summarizes the reviewed references and the parameters investigated in prior sensitivity analysis studies on dual fuel natural gas-diesel engines.

Table 5-1. Prior sensitivity analysis diesel pilot ignited natural gas engine studies [9-12]. IMAT stands for Intake Manifold Air Temperature; MAP stands for Manifold Air Pressure.

Reference	Parameters studied	Ranking of control factors
Belgiorno, G., et al.	1. Compression ratio 2. Substitution ratio 3. Injection pressure 4. Pilot quantity 6. Combustion phasing 7. EGR 8. Air-Fuel Ratio	No
Rochussen, J., et al.	1. Substitution ratio 2. Pilot SOI 3. Pilot injection pressure 4. NG EQR 5. Pilot EQR	No
Azimov, U., et al.	1. Pilot fuel pressure 2. Pilot quantity 3. Gaseous fuel composition 4. Pilot SOI 5. EGR	No
Papagiannakis, R., et al.	1. Engine Load 2. Engine Speed 3. Diesel substitution ratio	No
This work	1. Pilot SOI 2. Pilot injection pressure 3. Pilot pulse width 4. IMAT 5. EGR 6. EQR 7. MAP	Yes; Using Taguchi orthogonal matrix methodology

All the previously reviewed literature does a factor sensitivity study by investigating the effect of an isolated change in the parameter of interest. As of the time of this work, the authors of this paper have not found any recent research done on a modern turbocharged micro-pilot (high diesel substitution ratio of >90% total energy contribution) stoichiometric NG engine platform that quantifies and ranks the sensitivity of the control factors using a multi-variable orthogonal matrix approach. This paper addresses this limitation in the literature and provides a rank of the most influential parameters controlling combustion and performance of a micro-pilot NG engine.

In this study, a Cummins ISB 6.7L diesel engine was modified to run micro-pilot diesel and natural gas combustion engine targeting medium-duty applications with a maximum of 10% diesel contribution of the total fuel energy. The concept combines an overall stoichiometric combustion, composed predominantly of premixed NG with EGR for charge temperature control and a micro-pilot injection of diesel to provide a robust ignition source.

Stoichiometric combustion with EGR is a feature of current state-of-the-art spark-ignited NG fueled engines where the spark plug serves as the ignition source. The diesel micro-pilot approach offers higher ignition energy and a more distributed ignition source for the premix mixture, resulting in a more robust ignition, premixed turbulent flame combustion, and shorter distances for the flame to propagate through the combustion chamber. This makes such an approach of particular interest to medium duty applications, in which the ability to provide a torque profile and fuel conversion efficiency similar to that of a diesel engine is desirable.

Operating at a globally stoichiometric fuel-air ratio also enables the use of a low-cost three-way catalyst to meet both current and future emissions standards. Spark-ignited stoichiometric natural gas engines with EGR in the medium-heavy duty range (9-12 L) have been developed that meet California's ultra-low NOx (0.02 g/bhph); similar aftertreatment effectiveness should be achievable with a micro-pilot ignition source. Compared to the multi-element aftertreatment systems present in modern diesel engines, this approach allows a significant simplification and potential cost reduction. For the purposes of this study, a highly effective aftertreatment system was assumed, including effectiveness at oxidizing unburned methane (CH4) and reducing oxides of nitrogen (NOx). As a result, the engine-out emissions are not considered in this assessment, which is focused on engine performance and efficiency. CO2 emissions are not explicitly considered, but given the small contribution of the diesel, higher thermal efficiencies will equate almost linearly with lower CO2.

This paper focuses on the medium load operation, systematically studying, quantifying, and ranking controlling factors for the combustion and performance of diesel micro-pilot natural gas engines. The medium load is chosen as it has been seen as the optimum operating condition of turbocharged piloted ignited natural gas engines, often performing equal to or better the fuel conversion efficiency of a diesel-only application [6, 13]. At this condition, maximization of fuel conversion efficiency is needed while keeping combustion knock levels under control. The results in this work provide an understanding of the main controlling factors for the development and optimization of a high-efficiency engine.

It is important to note that the ranking of the controlling factors will likely differ at different operating regimes. At low-loads, where the stability of the ignition process is a critical limitation, Bonfochi Vinhaes et al.[14] have shown that, for the same engine studied in this paper, the reduction in micro-pilot diesel injection pressure is an important factor as it improves combustion stability by shortening the ignition delay. The reduced injection pressure keeps the pilot fuel-rich zone close to the injector tip, enabling the flame to start and propagate more easily. This observation agrees with the work reported by Khosravi et al.[15].

The following sections will cover the experimental apparatus, including an overview of the modified diesel engine to run micro-pilot diesel natural gas mode, the instrumentation and fuels used, and a description of Taguchi's orthogonal matrix approach, followed by results and conclusions.

5.3 Experimental Apparatus

Micro Pilot Diesel Natural Gas Engine

Figure 5-1 (a) shows the engine setup in the dyno test cell, and Figure 5-1 (b) shows a schematic of the engine system developed for this work. An overview of the key modifications made to the engine is described in this section, including the compression ratio reduction, fuel, the air handling system, and instrumentation. A detailed description of the modifications is provided in [16]; a few key points are discussed briefly here.

(a)

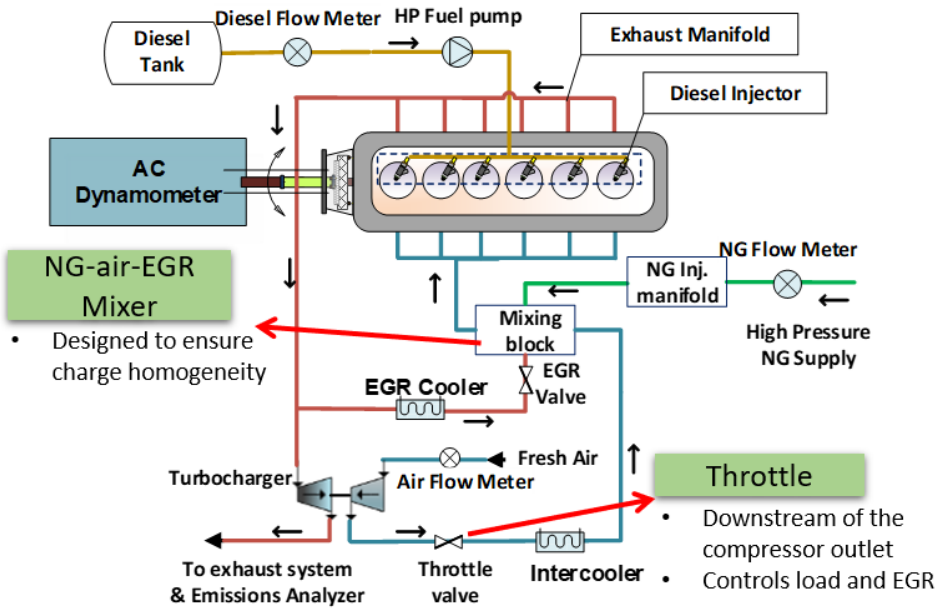

(b)

Figure 5-1.Engine Setup. (a) Engine cart in the dyno test cell. (b) Detailed schematics

The geometric compression ratio was reduced from 17.3:1 to 15.0:1 by installing a thicker head gasket and reducing the piston's top face crown height by 2.8mm to reduce the chance of abnormal combustion occurrence. Apart from the machining modification, the piston

bowl geometry was kept the same. Although this design is likely not optimal for the premixed combustion of the NG, the optimization of the combustion chamber geometry was outside the scope of this work.

The shift to stoichiometric operation results in significant changes to the air handling system requirements. For airflow rate and stoichiometric mixture control, a throttle valve was installed upstream of the intake manifold and the mixing block, enabling advanced engine load control.

A mixing system that ensures consistent air and EGR distribution and mixture homogeneity is critical for the NG premix operation. A custom fabricated NG-air-EGR mixer system was designed to deliver these flow requirements. The mixer system comprises a natural gas injector manifold with six prototype high-flow port injectors rated for 8 g/s each that supply the gaseous fuel into the NG-air-EGR mixer. The mixer is composed of an airfoil installed across the throat of a mixing venturi, with a series of small diameter holes sized to provide an appropriate pressure drop across the mixer. The mixer is installed downstream of the throttle but upstream of the intake manifold to allow sufficient mixing time before the premix mixture is inducted into the engine.

Table 5-2 shows the final build specifications of the diesel micro-pilot natural gas engine.

Table 5-2. Engine's Specifications.

No. of Cylinders	6
Bore & Stroke	107 x 124mm
Connecting rod length	192 mm
Displacement	6.7 L
Compression Ratio	15.0:1
Aspiration	Turbocharged + Charge Air Cooler + HP EGR + Throttle Valve

Diesel Micro Pilot Injection System	HPCR injector 8 holes (168 microns diameter)
Diesel Injection Pressure	600 to 2000 bar
Diesel Micro- Pilot Minimum Fuel Quantity	3.3 mg/injection
Rated Power	231 kW (310 hp) @ 1800 RPM
Rated Torque	1230 Nm @ 1620 RPM
Peak BMEP	24 bar

As for the control system, a standalone MotoHawk ECU565-128 engine control unit is used with a custom-built strategy developed to allow complete control of engine actuators, including pilot injection timing, diesel injection pressure, pilot injection quantity, equivalence ratio, intake air pressure, charge air cooling, and dilution.

Instrumentation and Measurement Uncertainty

The engine's six cylinders are instrumented with pressure transducers type AVL GH series piezoelectric that feeds a real-time combustion analyzer system. A BEI encoder series H25D with 360 pulses per revolution measures the crank angle position, and the engine's speed and load are controlled by a 445 hp AVL A/C Dynoroad 308/4 SX.

The A&D CAS system makes the combustion analysis for high-speed, crank angle resolution of 6 samples per degree for 300 cycles. Although the H25D encoder only outputs one pulse per degree, a feature enabled in the combustion analysis system increased the encoder resolution.

A NI PCIe chassis logs thermocouple and 0-10V analog input signals. Type K thermocouples are used for temperature measurements, including the intake air manifold, engine coolant, engine oil, exhaust gas temperature, turbocharger inlet, and outlet. Omega Absolute Pressure Transducer MMA050V5P4D1T3A5CE measures the intake and exhaust

pressures. Other pressure measurements (i.e., oil pressure, fuel inlet) are done with Omega Gage Pressure Transducer GP50.

Two Micro Motion Coriolis Meter ELITE CMFS010P are used to measure the fuel flow rates, one for the diesel and the other for the natural gas. A Bosch LSU 4.9 lambda sensor measures the equivalence ratio.

The EGR percentage is calculated as the ratio of intake and exhaust CO2. The measurements were made with CO2 Meter K33 series sensors. Sample ports in the exhaust and intake manifolds were installed to measure CO2 concentration, enabling real-time determination of EGR.

Transducer accuracies and uncertainties for the independent variables are shown in Table 5-3.

Table 5-3. Sensor's accuracy and measurement uncertainty

Measurement	**Accuracy**	**Full scale**	**Uncertainty (absolute)**	**Unit**
In-Cylinder Pressure transducer	±0.30%FS	0-250	± 0.75	bar
Engine crank angle degree (Encoder)	±1.00	360:1	± 1.00	Deg
Fuel flow rate (Diesel & NG)	±0.05 FS	0-30	± 0.015	g/s
Thermocouples	±2.20	0-800	± 2.20	°C
Intake/Exhaust Manifold Pressure Transducer	±0.08%FS	0-6.89	± 0.0055	bar
Oil and Fuel Inlet Pressure	±0.50%FS	0-7 / 0-2	±0.035 / 0.010	bar
Torque	±0.05%FS	0 – 5000	±2.50	Nm
CO2 (Intake & Exhaust)	±200	0-300000	±200	ppm
Lambda Sensor	±0.01	0.8-1.2	±0.01	-

The uncertainty for each parameter, including the engine control factors and response, is shown in Table 5-4. For the independent factors and responses, the uncertainty is calculated based on the uncertainty value provided by the sensor manufacturer. For the dependent variables, the uncertainties are determined using equation (1) from the uncertainty propagation approach described in [17].

$$U_Y = \sqrt{\sum \left(\frac{\partial Y}{\partial X_i}\right)^2 U_x^2} \qquad (1)$$

Where Y represents the calculated quantity's value, U represents the variable's uncertainty, and X represents the measured variables.

Table 5-4. Uncertainty of the engine controlling factors and observed engine responses. °aTDC stands for Degrees after Top Dead Center; °bTDC stands for Degrees before Top Dead Center; CA50 is the Crank Angle position at which 50% of the heat from combustion has been released.

Measurement	**Range**	**Uncertainty (absolute)**	**Unit**
Brake Mean Effective Pressure	8.0-12	±0.05	bar
Brake Thermal Efficiency	32-43	±0.40	%
CA50	10-30	±0.60	°aTDC
Combustion Duration	10-18	±0.60	Deg
Combustion Stability (COV_{IMEP})	0.2-2.5	±0.05	%
Equivalence Ratio	0.9-1.1	±0.01	-
Exhaust Gas Recirculation	0.0-15	±0.20	%
Ignition Delay	0.65-2.1	±0.08	ms
Intake Manifold Air Temp.	25-40	±2.20	°C
Knock Peak-Peak 95th Percentile	0.3-8.1	±0.75	Bar

Manifold Air pressure	110-125	±0.01	kPa
Peak Cyl. Pressure	48-110	±0.75	bar
Pilot Inj. Pressure	800-1200	±5.00	bar
Pilot Pulse Width	250-350	>0.1	µs
Pilot SOI	1.0-3.5	±0.25	°bTDC

Fuels

Table 5-5 shows the fuel properties and characteristics for both diesel and line natural gas. The composition of the natural gas was measured by the gas supply company (SEMCO) and represented an average composition of the gas during the testing program. The primary constituents were 89% CH4, 8% C2H6, 0.4% C3H8, and 2.6% inert (all % by volume).

Table 5-5. Diesel and Natural Gas fuel properties

Diesel (ULSD)	**Density (kg/m³) @ 15.6°C, 1 atm**	**Heating value (MJ/kg)**	**AFR**	**H/C**	**Cetane Number**
	851.6	42.8	14.60	1.85	51.7
CNG	Density (kg/m³) @ 20°C, 1 atm	Heating value (MJ/kg)	AFR	H/C	*Methane Number
	0.727	47.5	16.30	3.80	83.0

*Wärtsilä Methane Number[18]

In this project, the Diesel Substitution Ratio (DSR) is given on an energy basis as described in equation (2).

$$DSR = \frac{\dot{m}_{CNG} \cdot Q_{LHV,CNG}}{\dot{m}_{CNG} \cdot Q_{LHV,CNG} + \dot{m}_{Diesel} \cdot Q_{LHV,Diesel}} \qquad (2)$$

Where, $\dot{m}$ is the fuel mass flow rate, and QLHV is the lower heating value of each fuel, as described in Table 5-5.

The Equivalence Ratio (φ) is determined as shown in equation (3).

$$\varphi = \frac{\dot{m}_{CNG} \cdot AFR_{stoich,CNG} + \dot{m}_{Diesel} \cdot AFR_{stoich,Diesel}}{\dot{m}_{air}} \quad (3)$$

Where AFR is the stoichiometric mass air to fuel ratio of each fuel, as described in Table 5-5.

5.4 Experimental Procedure

Taguchi's Orthogonal Matrix design

Taguchi's Orthogonal Matrix design was selected to rank the control factors as it provides an efficient method to systematically determine parameters for performance and cost [19]. The Taguchi design estimates the effects of factors on the response mean and variation using orthogonal arrays. The orthogonal array balances the design so that each factor level is equally weighted. This allows each factor to be assessed independently, so the effect of one factor does not affect the estimation of a different factor. This approach significantly reduces the time and cost associated with the design of experiments in which factorial designs are used [20-22]. Although a small number of experiments are used, their conclusions are applicable over the entire experimental region.

Figure 5-2 shows the flowchart used to design Taguchi's experimental approach based on [23].

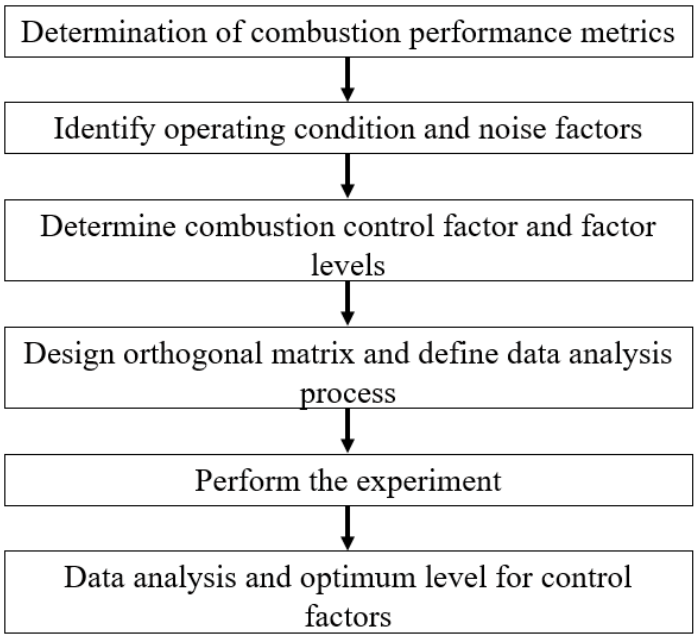

Figure 5-2. Taguchi's method flowchart

The first step from the flowchart was to determine the performance metrics to be studied. This paper's sensitivity study prioritized identifying the controlling factors that have a stronger effect (more sensitive) in maximizing efficiency and minimizing combustion knock. Additionally, other commonly used combustion metrics that characterize combustion and performance were also evaluated. These included:

- Brake Mean Effective Pressure (BMEP)
- Combustion Stability (COV of IMEP)
- Peak Cylinder Pressure
- Combustion Phasing (CA10, CA50)
- Combustion Duration (CA0-10, CA10-90)

The second step was to identify the noise factors and test conditions. The engine was initially operated at a single speed and load condition of 10 bar BMEP at 1620 RPM to minimize the chances of exceeding engine operating constraints (peak cylinder pressure, exhaust temperature, and knock index) and maintaining a stable operation. This mid-load

operating point is representative of loaded cruising conditions for a typical medium-duty commercial vehicle.

The noise factors are uncontrolled parameters that can cause an impact on the system, such as NG gas supply composition, diesel injection variability, cylinder charge distribution, and ambient air humidity. Three repetitions of the test matrix were performed to minimize the noise effects.

In the third step, the control parameters and their levels were defined. Based on the previously reviewed research articles from Table 5-1, the controlling parameters identified to be the most studied are:

- Diesel pilot start of injection (Pilot SOI)
- Diesel pilot injection pressure
- Substitution ratio of diesel to the total fueling on an energy basis, controlled by NG and diesel pilot quantity (Pilot pulse width)
- Dilution including exhaust residuals (EGR%)
- Global Equivalence Ratio (EQR)
- Intake Manifold Air Temperature (IMAT)
- Manifold air pressure (MAP)

The levels of each beforementioned factor were determined during a preliminary screening study that was conducted to define a stable operating condition and to avoid a combination of levels that would render operation unviable (i.e., high knock, high peak pressure rise rate, and combustion stability). Three levels were selected for each factor, except for Pilot SOI, where six levels were selected. Then the 7-factor orthogonal array was created, resulting in a total of 18 experiments (L18). As a comparison, a full factorial test program would involve 4374 individual tests, not including any replications. Applying the Taguchi approach reduced this to a tractable number of experiments at the expense of losing the ability to resolve interactions between factors. The L18 test plan is shown in Table 5-6.

Table 5-6. L18 Test Matrix

Test No.	Pilot SOI	Pilot Inj. Press.	Pilot Pulse Width	IMAT	EGR %	EQR	MAP
-	° bTDC	bar	µs	° C	%	-	kPa
1	2	1000	300	35	0	1.0	116
2	2	800	250	25	7.5	1.1	125
3	2	1200	350	40	15	0.9	110
4	3	1000	300	25	7.5	0.9	110
5	3	800	250	40	15	1.0	116
6	3	1200	350	35	0	1.1	125
7	1	1000	250	35	15	1.1	110
8	1	800	350	25	0	0.9	116
9	1	1200	300	40	7.5	1.0	125
10	2.5	1000	350	40	7.5	1.1	116
11	2.5	800	300	35	15	0.9	125
12	2.5	1200	250	25	0	1.0	110
13	1.5	1000	250	40	0	0.9	125
14	1.5	800	350	35	7.5	1.0	110
15	1.5	1200	300	25	15	1.1	116
16	3.5	1000	350	25	15	1.0	125
17	3.5	800	300	40	0	1.1	110
18	3.5	1200	250	35	7.5	0.9	116

5.5 Results and Discussion

Brake Thermal Efficiency Analysis and Factor Ranking

One of the main outputs of the Taguchi Design is the mean factor effect estimation. Figure 5-3 shows the main effect plot for means in the brake thermal efficiency (BTE) analysis.

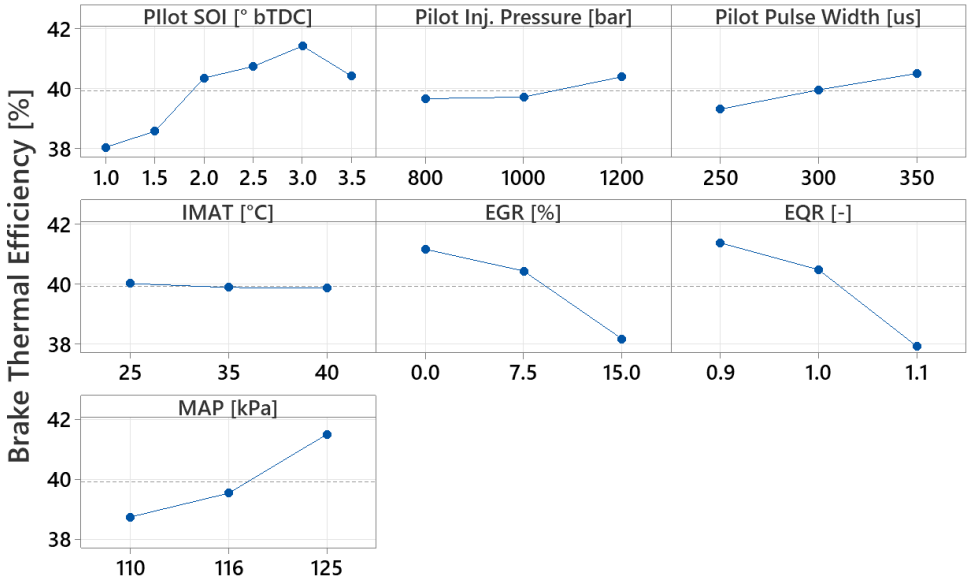

Figure 5-3. Brake thermal efficiency main effect plots for means. The engine operated at an average BMEP of 10 bar and 1620 RPM.

From each plot shown in Figure 5-3, it is possible to calculate the delta between the maximum and minimum BTE. For instance, for the EQR plot, the delta between levels 0.9 (maximum BTE) and 1.1 (minimum BTE) is 3.45 percentage points of BTE. It is the largest delta in the BTE analysis and ranks EQR as its most influential parameter for the operating condition studied. It should be noted that while EQR did have the strongest effect on BTE, in actual use, this would be maintained very close to stoichiometric level (~1.0) to ensure the effectiveness of the TWC aftertreatment. The delta of each factor was calculated and is used to determine the sensitivity rank of that factor shown in Table 7 from the largest to the lowest delta.

It is also possible to quantify the sensitivity of BTE as each control factor level is increased. Figure 5-3 shows that, as Pilot SOI levels are increased from 1.0°bTDC to 3.5°bTDC, the BTE value increases. The effects of each factor were analyzed and are shown in Table 5-7 by the use of directional arrows: the arrow pointing upwards means that the increase of the given factor level increases BTE, the arrow pointing downwards means that there is a

decrease in BTE as that factor level is increased, and the star symbol means that the factor did not show a directional trend.

Table 5-7. Brake thermal efficiency factor ranks. The effect of each factor is described using direction arrows: ↑ mean the increase of the given factor increases the response, ↓ mean the increase of the given factor decreases the response, * mean the increase of the given factor has not impacted the response.

Rank	Factor	Level for Maximization	Effect on BTE
1	EQR [-]	0.9	↓
2	Pilot SOI [°bTDC]	3.0	↑
3	EGR [%]	0.0	↓
4	MAP [kPa]	125	↑
5	Pilot Pulse Width [μs]	350	↑
6	Pilot Inj. Pressure [bar]	1200	↑
7	IMAT [°C]	25	*

From Table 5-7, EQR, Pilot SOI, and EGR are the top three most influential factors in the BTE analysis and ranks. EQR directly impacts BTE and combustion development in the combustion chamber, ranking first in thermal efficiency control. The increase in EQR decreased BTE (as indicated by the downwards pointing arrow in Table 5-7). This trend represents one of the spark-ignited engine performance characteristics discussed by Heywood in [24]; the BTE decreases primarily due to a decrease in combustion efficiency associated with the enrichment of the mixture. A study that shows the effect of change in EQR near stoichiometric conditions (0.9 to 1.1) in a diesel pilot natural gas engine was not found in the literature. While standard operation would retain a stoichiometric condition (~1.0), excursions could be encountered during transients or cold-start conditions when the aftertreatment system is not functioning effectively. EQRs greater than 1.0 would generally be avoided for an NG-fueled engine due to the probability of emitting high levels of unburned methane.

Pilot SOI, ranked second, impacts the start of combustion and combustion phasing. It has been seen by Rochussen et al. [10], and Abd Alla et al. [25] that advancing combustion phasing improves the indicated thermal efficiency due to lower exhaust heat rejection and higher peak cylinder pressures, confirming the trend observed in this work. Overly advanced timing results in lower efficiencies due to increasing in-cylinder pressures prior to the piston reaching top-dead-center. Much like a spark-ignition engine, the pilot SOI timing is representative of an optimum advance for best torque/efficiency.

EGR ranked third, and the increase in EGR led to a decrease in BTE. This trend was also observed by Tomita et al. [26]. In their work, the loss of fuel conversion efficiency was due to a longer combustion duration and ignition delay caused by the increase in EGR, confirming the trends seen in this paper's analysis for ignition delay and combustion duration shown in Appendix A2 and A3, respectively. The analysis for CA50 is also shown in Appendix A6, and the trends also agree with this observation.

The inflection seen on the Pilot SOI plot from levels 3.0°bTDC to 3.5°bTDC was mainly due to the combination of other factor levels in Test 17 in Table 5-6, resulting in a more dominant-negative effect than the benefit from advancing pilot SOI.

Table 5-7 also shows the expected levels at which efficiency will be maximum. The levels for maximization are the factor levels from Figure 5-3, at which BTE is the highest. Interestingly, from the orthogonal test matrix shown in Table 5-6, Test Number 6 is almost a perfect combination of the levels for maximization. As a result, the brake thermal efficiency was the highest among the tests conducted (43%; the minimum. and median BTEs for all tested combinations were 32% and 40%, respectively), indicating that the analysis is pointing towards the right direction.

Combustion Knock Analysis and Factor Ranking

Combustion knock was another metric of interest for this study. Combustion knock was determined via the cylinder pressure signal after band-passing (4 – 12 kHz) and rectifying, then determining the peak-to-peak pressure (Kpp) on an individual cylinder basis, as it has

been done by Naber et al. [27]. The combustion knock limit was 10 bar peak-to-peak for the 95th percentile. Figure 4 shows the main response plot for means for the knock peak-to-peak 95th percentile.

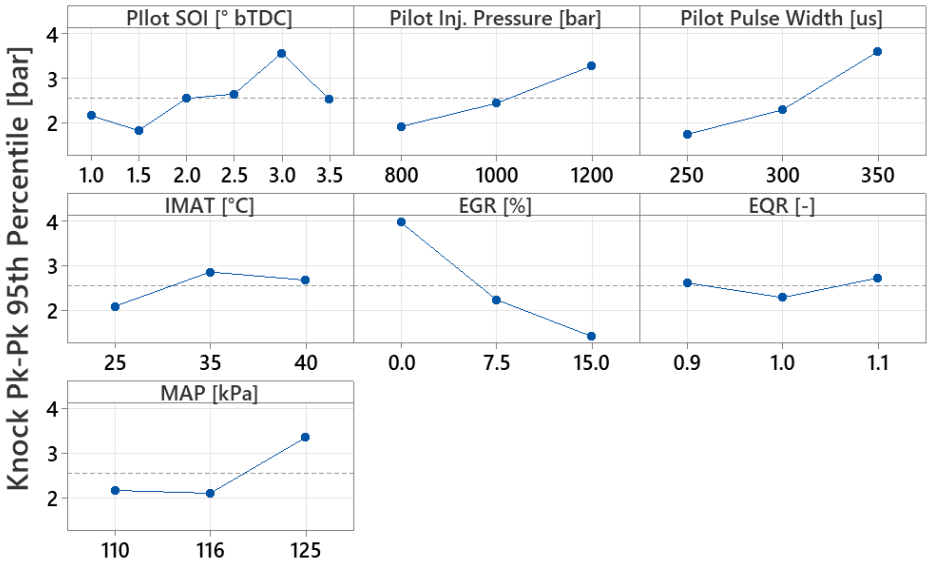

Figure 5-4. Combustion knock response plot. The engine operated at an average BMEP of 10 bar and 1620 RPM.

This data set allows the determination of the control factor ranking, the effect on knock peak-peak by each factor, and the expected levels to minimize it using the same approach previously discussed in the BTE analysis section. The results are shown in Table 5-8.

Table 5-8. Combustion knock factor ranks. The effect of each factor is described using direction arrows: ↑ mean the increase of the given factor increases the response, ↓ mean the increase of the given factor decreases the response, * mean the increase of the given factor has not impacted the response.

Rank	Factor	Level for Minimization	Effect on Knock Peak-Peak
1	EGR [%]	15	↓
2	Pilot Pulse Width [µs]	250	↑
3	Pilot SOI [°bTDC]	1.5	↑

4	Pilot Inj. Pressure [bar]	800	↑
5	MAP [kPa]	116	↑
6	IMAT [°C]	25	↑
7	EQR [-]	1.0	*

In this case, it was observed that EGR, Pilot Pulse Width, and Pilot SOI are the top three factors in the combustion knock analysis. As EGR increases, the charge heat capacity also increases, thus reducing the overall end gas temperature and knock propensity. This trend is confirmed by Tomita et al. [26], and by this work's analysis represented by the downwards pointing arrow shown in Table 5-8.

Pilot pulse width determines the amount of diesel pilot injected in the cylinder, which impacts the reactivity of the mixture, influencing ignition delay and combustion duration. This is confirmed by the trend observed in Appendix A2 and A3: the increase in fuel quantity injected reduces the ignition delay and the combustion duration. Abd Alla et al. [28] also observed that the increase in pilot fuel quantity increases the knock tendency. For a given global EQR, an increase in pilot quantity results in a reduction in premixed EQR; however, the differences were relatively small, as the pilot was smaller than 10% of the total fuel (on an energy basis), with only one test condition at 11%.

Pilot SOI, as previously discussed, affects the start of combustion and combustion phasing. As pilot SOI is advanced (increased), the earlier combustion phasing leads to higher in-cylinder temperature, which, similar to spark-ignited engines, leads to a higher knock peak-peak[29]. Therefore, the knock behavior seen in dual-fuel engines can be compared to combustion knock in spark-ignited engines [30].

Multi-Variable Analysis and Factor Ranking

Taguchi's design analysis was also applied to other combustion metrics commonly used in engine development to describe performance, including BMEP, combustion stability, ignition delay, peak cylinder pressure, CA50, and combustion duration. The same analysis discussed in this section was applied for each metric. The reader can find each factor

analysis result, including plots, ranking tables with levels for optimization, and the sensitivity effect trend in the Appendix of this paper. Table 5-9 shows the overall summary of all the results.

MAP, EGR, and Pilot SOI are the top three most influential factors with the highest deltas in the BMEP study. As MAP was increased, an increase in BMEP was observed due to more NG fuel that had to be added to maintain EQR at the required level for the test. The increase in total fuel quantity increases the amount of energy available to produce work, resulting in a higher BMEP.

EGR has the exact opposite effect. The fresh air displacement by EGR led to a reduction in total fueling to maintain EQR, reducing the energy available to produce work. Therefore, the trend observed was the reduction in BMEP as EGR is increased. As the Pilot SOI level increases, the earlier combustion phasing leads to higher in-cylinder pressures and lower heat loss to the exhaust and heat transfer, increasing the total work produced and increasing BMEP.

The combustion stability, denoted as the coefficient of variance (COV), was calculated as the ratio of the standard deviation of the indicated mean effective pressure (IMEP) and the mean value of the 300 cycles logged. For the COVIMEP, the top three factors are Pilot SOI, EGR, and EQR. In this case, the reduction of COVIMEP is desirable, and advancing the pilot SOI reduced the combustion variability. On the other hand, increasing EGR and EQR increased the COVIMEP, resulting in less stable combustion. 90% of the tests had a COVIMEP value below 1% during this study.

In this work, the ignition delay has been defined as the time between the diesel injection (hydraulic start of injection) and the 10% mass fraction burn (CA10). EGR, Pilot SOI, and MAP have shown a stronger effect for this metric, ranking at the top three. The effect of EGR and MAP can be associated with the change in in-cylinder charge temperature during compression due to the presence of unburned gases, in the case of EGR, and higher charge density, in the case of MAP. For the Pilot SOI levels studied, the more advanced the

injection timing, the shorter the ignition delay was. These effects are confirmed by Liu and Karim in [31].

In the case of peak cylinder pressure, EGR, Pilot SOI, and MAP are the top three most influential control factors. Interestingly, the trend of the top factors in the peak cylinder pressure is opposite of the ignition delay.

Table 5-9. Controlling factors ranking for different combustion metrics. The effect of each factor is described using direction arrows: ↑ mean the increase of the given factor increases the response, ↓ mean the increase of the given factor decreases the response, * mean the increase of the given factor has not impacted the response.

Rank	BMEP	BTE	Knock Pk-Pk 95th Pct	Combustion Stability (COV_{IMEP})	Ignition Delay	Peak Cyl. Pressure	CA50	Combustion Duration
1	MAP (↑)	EQR (↓)	EGR (↓)	Pilot SOI (↓)	EGR (↑)	EGR (↓)	EGR (↑)	EGR (↑)
2	EGR (↓)	Pilot SOI (↑)	Pilot Pulse Width (↑)	EGR (↑)	Pilot SOI (↓)	Pilot SOI (↑)	Pilot SOI (↓)	Pilot Pulse Width (↓)
3	Pilot SOI (↑)	EGR (↓)	Pilot SOI (↑)	EQR (↑)	MAP (↓)	MAP (↑)	Pilot Pulse Width (↓)	Pilot SOI (↓)
4	EQR (*)	MAP (↑)	Pilot Inj. Pressure (↑)	MAP (↓)	EQR (↑)	Pilot Pulse Width (↑)	MAP (↓)	EQR (*)
5	Pilot Pulse Width (*)	Pilot Pulse Width (↑)	MAP (↑)	Pilot Inj. Pressure (↑)	Pilot Pulse Width (↓)	Pilot Inj. Pressure (↑)	EQR (↑)	Pilot Inj. Pressure (↓)

6	IMAT (↓)	Pilot Inj. Pressure (↑)	IMAT (↑)	Pilot Pulse Width (↓)	IMAT (↓)	EQR (*)	Pilot Inj. Pressure (*)	MAP (*)
7	Pilot Inj. Pressure (*)	IMAT (*)	EQR (*)	IMAT (↓)	Pilot Inj. Pressure (*)	IMAT (*)	IMAT (*)	IMAT (*)

CA50 is one of the combustion phasing metrics described as the Crank Angle position at which 50% of the heat from combustion has been released. EGR, Pilot SOI, and pilot pulse width are at the top three for this investigation. As discussed, all three of these factors directly impact the ignition delay, which strongly influences CA50.

Lastly, the combustion duration is primarily influenced by EGR, pilot pulse width, and the Pilot SOI. This work defined the combustion duration as the time between CA10 and CA90. Interestingly, the same parameters that impact combustion phasing the most are seen impacting combustion duration.

Overall, it was observed that EGR and Pilot SOI appear in the top three ranks for all the different responses, indicating that these are the most influential control factors in a diesel pilot natural gas engine operating at medium loads. Conversely, IMAT and Pilot injection pressure were determined to have the least impact on the responses analyzed. These factors will likely differ at low loads, where the stability of the ignition process is a critical limitation, and at high loads, where knock avoidance becomes more critical. Further work is needed to elucidate these effects at higher- and lower-load operating conditions.

5.6 Summary/Conclusions

This work focused on systematically studying, quantifying, and ranking the controlling factors for the combustion and performance of a diesel micro-pilot natural gas engine operating at a mid-load condition.

The orthogonal array approach is an appropriate method for independent multi-variable assessment of control factors as it uses a balanced design of experiments so that each factor level is equally weighted.

It was identified in the literature that the combustion control parameters mainly studied for a diesel pilot ignition natural gas engine included the diesel pilot start of injection and injection pressure, charge dilution, substitution ratio of diesel to total fuel, boost pressure, and intake manifold air temperature. These were used for the design of experiments in this study. Sensitivity analysis and ranking of each control factor were provided for multiple performance metrics, showing which factors are the most influential and the impact on the metric studied. The key findings from this work were:

1. For the brake thermal efficiency, global EQR, diesel pilot start of injection, and EGR were observed to be the most influential factors. Of these, global EQR is fixed in a stoichiometric engine, therefore pilot injection timing should be advanced, and EGR minimized to achieve the highest possible efficiency.

2. EGR, pilot pulse width, and the pilot start of injection are the dominant factors for minimizing combustion knock at the condition studied.

3. EGR and diesel pilot start of injection were the most prominent control parameters across the different performance metrics assessed in this work. This indicates that, at this operating regime, these are the most influential parameters for controlling combustion and performance.

4. Intake temperature and diesel injection pressure were observed to have the least sensitivity for the mid-load, near-stoichiometric, micro-pilot operating condition studied.

In summary, these results provided an understanding and an overall guideline of what are the main controlling factors and their responses for combustion development and robust

control in the diesel micro-pilot ignition of natural gas stoichiometric engine operation at medium loads. The Taguchi design of experiments provides a method to reduce the number of required experiments to analyze the engine performance; thus, this method reduces testing time and cost. However, cross-validation of this paper's findings over a wider range of the engine operational space would be necessary to confirm the findings and understand the micro-pilot engine operation and optimization and is part of the future work.

5.7 References

1. Reitz, R., H. Ogawa, R. Payri, T. Fansler, et al., "IJER Editorial: The Future of the Internal Combustion Engine." Int. J. Engine Res., 21, 3-10, 2020, doi: https://doi.org/10.1177/1468087419877990.

2. Reitz, R.D., "Directions in Internal Combustion Engine Research." Combustion and Flame. 160(1): p. 1-8., 2013, doi: https://doi.org/10.1016/j.combustflame.2012.11.002.

3. Manns, H.J., M. Brauer, H. Dyja, H. Beier, et al.," Diesel CNG-The Potential of a Dual Fuel Combustion Concept for Lower CO2 and Emissions." SAE Technical Paper 2015-26-0048, 2015, doi: https://doi.org/10.4271/2015-26-0048.

4. Karim, G.A., "Combustion in Gas Fueled Compression Ignition Engines of the Dual Fuel Type." Journal of engineering for gas turbines and power. 125(3): p. 827-836, 2003, doi: https://doi.org/10.1002/9783527628148.hoc047.

5. Karim, G.A.," Dual-Fuel Diesel Engines, 1st Edition," (CRC Press, 2015), Chapters: 3, 5, and 6, doi: https://doi.org/10.1201/b18163

6. Weaver, C.S. and S.H. Turner, "Dual Fuel Natural Gas/Diesel Engines: Technology, Performance, and Emissions." SAE Technical Paper 940548, 1994, doi: https://doi.org/10.4271/940548.

7. Daisho, Y., T. Yaeo, T. Koseki, T. Saito, et al.," Combustion and Exhaust Emissions in a Direct-injection Diesel Engine Dual-Fueled with Natural Gas," SAE Technical Paper 950465, 1995, doi: https://doi.org/10.4271/950465.

8. Vávra, J., I. Bortel, M. Takáts, and M. Diviš, "Emissions and Performance of Diesel–Natural Gas Dual-Fuel Engine Operated With Stoichiometric Mixture," Fuel. 208: p. 722-733, 2017, doi: https://doi.org/10.1016/j.fuel.2017.07.057.

9. Belgiorno, G., G. Di Blasio, and C. Beatrice, "Parametric Study and Optimization of the Main Engine Calibration Parameters and Compression Ratio of a Methane-Diesel Dual Fuel Engine," Fuel. 222: p. 821-840, 2018, doi: https://doi.org/10.1016/j.fuel.2018.02.038.

10. Rochussen, J., J. Yeo, and P. Kirchen," Effect of Fueling Control Parameters on Combustion and Emissions Characteristics of Diesel-Ignited Methane Dual-Fuel Combustion." SAE Technical Paper 2016-01-0792, 2016, doi: https://doi.org/10.4271/2016-01-0792.

11. Azimov, U., E. Tomita, and N. Kawahara," Ignition, Combustion and Exhaust Emission Characteristics of Micro-pilot Ignited Dual-fuel Engine Operated under PREMIER Combustion Mode." SAE Technical Paper 2011-01-1764, 2011, doi: https://doi.org/10.4271/2011-01-1764.

12. Papagiannakis, R.G., D.T. Hountalas, C.D. Rakopoulos, and D.C. Rakopoulos," Combustion and Performance Characteristics of a DI Diesel Engine Operating from Low to High Natural Gas Supplement Ratios at Various Operating Conditions." SAE Technical Paper 2008-01-1392, 2008, doi: https://doi.org/10.4271/2008-01-1392.

13. Yao, M., J. Shen, and J. Qin," Turbocharged Diesel/CNG Dual-fuel Engines with Intercooler: Combustion, Emissions and Performance." SAE Technical Paper 2003-01-3082, 2003, doi: https://doi.org/10.4271/2003-01-3082.

14. Bonfochi Vinhaes, V., G. McTaggart-Cowan, S. Munshi, M. Shahbakhti, et al., (2022) "Experimental Studies of Low-Load Limit in a Stoichiometric Micro-Pilot Diesel Natural Gas Engine." Energies. 15(3): p. 728, 2022, doi: https://doi.org/10.3390/en15030728.

15. Khosravi, M., J. Rochussen, J. Yeo, P. Kirchen, et al." Effect of Fuelling Control Parameters on Combustion Characteristics of Diesel-Ignited Natural Gas Dual-Fuel Combustion in an Optical Engine." Presented at the ASME 2016 Internal Combustion Engine Division Fall Technical Conference., USA, October 2016, doi: https://doi.org/10.1115/icef2016-9399.

16. Naber, J.D., Henes, R.; Henes, E., "High Brake Mean Effective Pressure and High Efficiency Micro Pilot Ignition Natural Gas Engine (Final Project Report)," Office of Scientific and Technical Information (OSTI): Oak Ridge, TN, USA, 2020 doi: https://doi.org/10.2172/1605097.

15. Taylor, B.N. and C.E. Kuyatt, "Guidelines for Evaluating and Expressing the Encertainty of NIST Measurement Results." National Institute of Standards and Technology: Gaithersburg, MD, USA, 1994, doi: https://doi.org/10.6028/nist.tn.1297 .

16. "Wärtsilä Methane Number Calculator". https://www.wartsila.com/marine/build/gas-solutions/methane-number-calculator, Accessed on June 2021.

17. Unal, Resit, and Edwin B. Dean. "Taguchi Approach to Design Optimization for Quality and Cost: An Overview." In 1991 Annual Conference of the International Society of Parametric Analysts, 1990.

18. Kacker, R.N., E.S. Lagergren, and J.J. Filliben, "Taguchi's Orthogonal Arrays are Classical Designs of Experiments." Journal of research of the National Institute of Standards and Technology. 96(5): p. 577, 1991 doi: https://doi.org/10.6028/jres.096.034.

19. Byrne, Diane M. "The Taguchi Approach to Parameter Design." ASQ's Annu Qual Congr Proc, 1986 40: 168, 1986.

20. Inc., A.S.I." Taguchi Methods: Implementation Manual." 1989. ASI Dearborn, MI. (1989).

21. Phadke, M.S.," Quality Engineering Using Robust Design." Prentice Hall PTR., 1995

22. Heywood, J.B.," Internal Combustion Engine Fundamentals." (McGraw-Hill Education: New York, NY, USA, 2018). Chapter: 15. ISBN: 1260116107.

23. Abd Alla, G., H. Soliman, O. Badr, and M. Abd Rabbo, (2002) "Effect of Injection Timing on the Performance of a Dual Fuel Engine." Energy conversion and Management. 43(2): p. 269-277., 2002, doi: https://doi.org/10.1016/S0196-8904(00)00168-0.

24. Tomita, E., Y. Harada, N. Kawahara, and A. Sakane," Effect of EGR on Combustion and Exhaust Emissions in Supercharged Dual-Fuel Natural Gas Engine Ignited with Diesel Fuel." SAE Technical Paper 2009-01-1832, 2009, doi: http://doi.org/10.4271/2009-01-1832.

25. Naber, J., J.R. Blough, D. Frankowski, M. Goble, et al.," Analysis of Combustion Knock Metrics in Spark-Ignition Engines." SAE Technical Paper 2006-01-0400, 2006, doi: https://doi.org/10.4271/2006-01-0400.

26. Abd Alla, G.H., H.A. Soliman, O.A. Badr, and M.F. Abd Rabbo,"Effect of Pilot Fuel Quantity on the Performance of a Dual Fuel Engine." SAE Technical Paper 1999-01-3597, 1999, doi: https://doi.org/10.4271/1999-01-3597.

27. Wang, Z., H. Liu, and R.D. Reitz, "Knocking Combustion in Spark-Ignition Engines." Progress in Energy and Combustion Science. 61: p. 78-112., 2017, doi: https://doi.org/10.1016/j.pecs.2017.03.004.

28. Lounici, M., M. Benbellil, K. Loubar, D. Niculescu, et al., "Knock Characterization and Development of a New Knock Indicator for Dual-Fuel Engines." Energy. 141: p. 2351-2361, 2017, doi: https://doi.org/10.1016/j.energy.2017.11.138.

29. Liu, Z. and G.A. Karim," The Ignition Delay Period in Dual Fuel Engines." SAE Technical Paper 950466, 1995, doi: https://doi.org/10.4271/950466.

5.8 Appendix

This section contains the plots and tables of the analysis for combustion stability, ignition delay, combustion duration, BMEP, peak cylinder pressure and CA50. The summary of the data presented here is shown in Table 9.

A1: Combustion stability (COV IMEP) data analysis plots

Figure 5-5 shows the combustions stability sensitivity analysis for each combustion control factor.

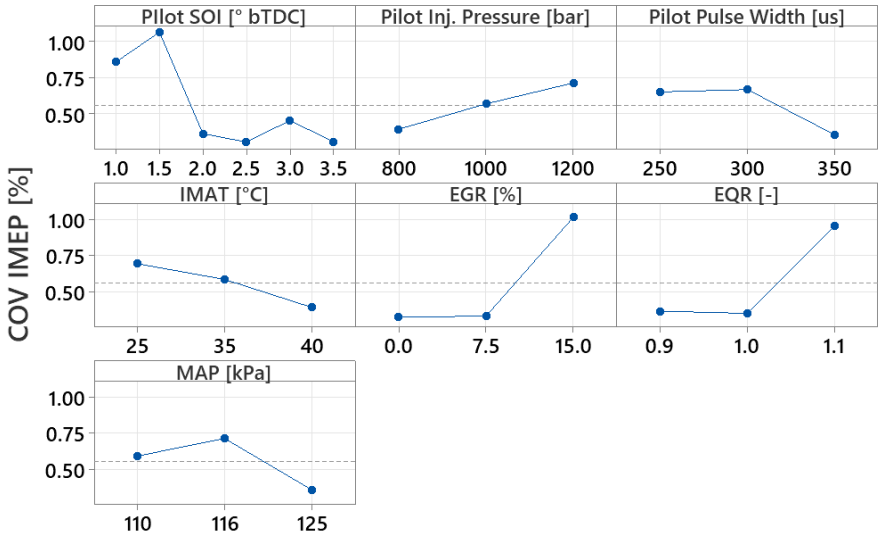

Figure 5-5. Combustion stability main effect plots for means

Table 5-10 shows the factor ranking, level for minimizing, level for maximizing combustion stability for each factor. The effect on combustion stability is based on the increase of each factor level.

Table 5-10. Combustion stability factor ranks

Rank	Factor	Level for Minimization	Level for Maximization	Effect on combustion stability
1	Pilot SOI [°bTDC]	2.5	1.5	↓
2	EGR [%]	0.0	15	↑
3	EQR [-]	1.0	1.1	↑
4	MAP [kPa]	125	116	↓
5	Pilot Inj. Pressure	800	1200	↑
6	Pilot Pulse Width [µs]	350	300	↓
7	IMAT [°C]	40	25	↓

A2: Ignition delay data analysis plots

Figure 5-6 shows the ignition delay sensitivity analysis for each combustion control factor. In this work, ignition delay was determined as the time between the hydraulic start of injection to 10% mass fraction burn (CA10).

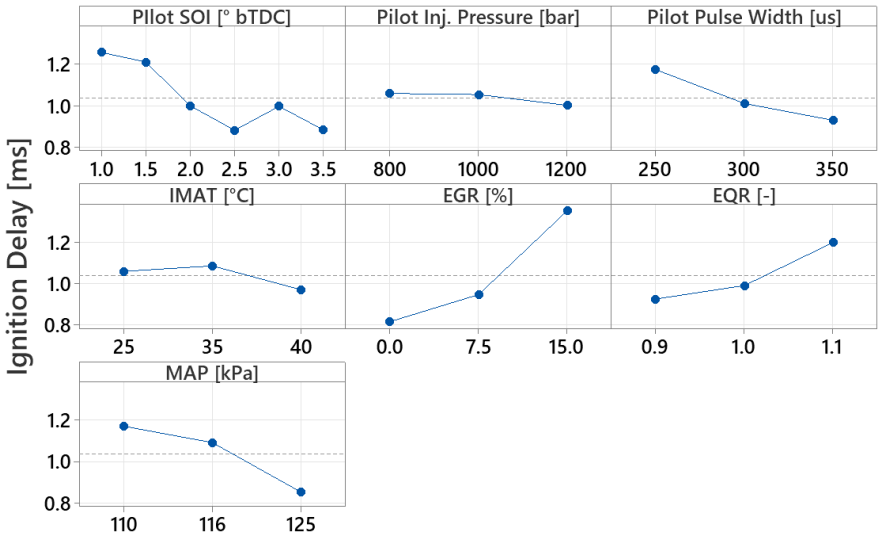

Figure 5-6. Ignition delay main effect plots for means

Table 5-11 shows the factor ranking, level for minimizing, level for maximizing ignition delay for each factor. The effect on ignition delay is based on the increase of each factor level.

Table 5-11. Ignition delay factor ranks

Rank	Factor	Level for Minimization	Level for Maximization	Effect on ignition delay
1	EGR [%]	0.0	15	↑
2	Pilot SOI [°bTDC]	2.5	1.0	↓
3	MAP [kPa]	125	110	↓
4	EQR [-]	0.9	1.1	↑
5	Pilot Pulse Width [µs]	350	250	↓
6	IMAT [°C]	40	35	↓
7	Pilot Inj. Pressure [bar]	1200	800	*

A3: Combustion duration (CA10-90) data analysis plots

Figure 5-7 shows the combustion duration sensitivity analysis for each combustion control factor. In this work, combustion duration was determined as the time between CA10 to CA90.

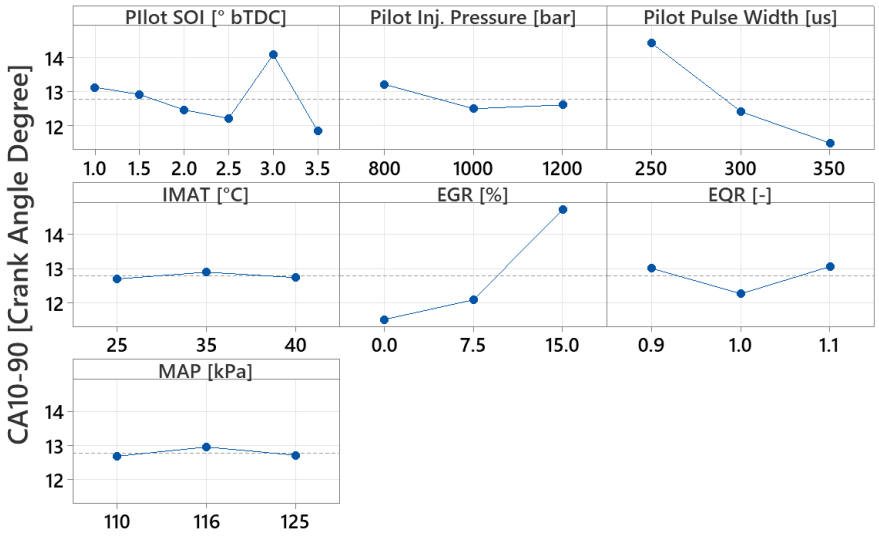

Figure 5-7. Combustion duration main effect plots for means

Table 5-12 shows the factor ranking, level for minimizing, level for maximizing combustion duration for each factor. The effect on combustion duration is based on the increase of each factor level.

Table 5-12. Combustion duration factor ranks

Rank	Factor	Level for Minimization	Level for Maximization	Effect on combustion duration
1	EGR [%]	15	0.0	↑
2	Pilot Pulse Width [µs]	350	250	↓
3	Pilot SOI [°bTDC]	3.5	3.0	↓
4	EQR [-]	1.0	1.1	*
5	Pilot Inj. Pressure [bar]	1000	800	↓
6	MAP [kPa]	110	116	*
7	IMAT [°C]	25	35	*

A4: BMEP data analysis plots

Figure 5-8 shows the BMEP sensitivity analysis for each combustion control factor.

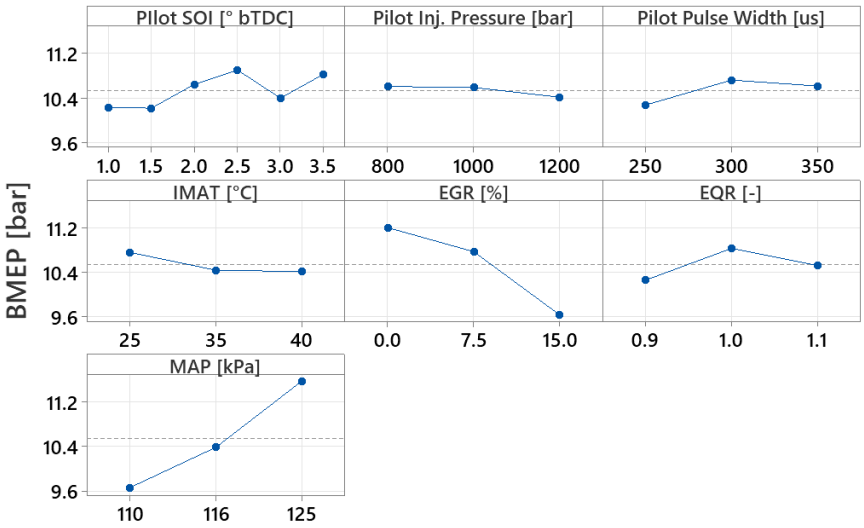

Figure 5-8. BMEP main effect plots for means

Table 5-13 shows the factor ranking, level for minimizing, level for maximizing BMEP for each factor. The effect on BMEP is based on the increase of each factor level.

Table 5-13. BMEP duration factor ranks

Rank	Factor	Level for Minimization	Level for Maximization	Effect on BMEP
1	MAP [kPa]	110	125	↑
2	EGR [%]	15	0.0	↓
3	Pilot SOI [°bTDC]	1.5	2.5	↑
4	EQR [-]	0.9	1.0	*
5	Pilot Pulse Width [µs]	250	300	*
6	IMAT [°C]	40	25	↓
7	Pilot Inj. Pressure [bar]	1200	800	*

A5: Peak cylinder pressure data analysis plots

Figure 5-9 shows the peak cylinder pressure sensitivity analysis for each combustion control factor.

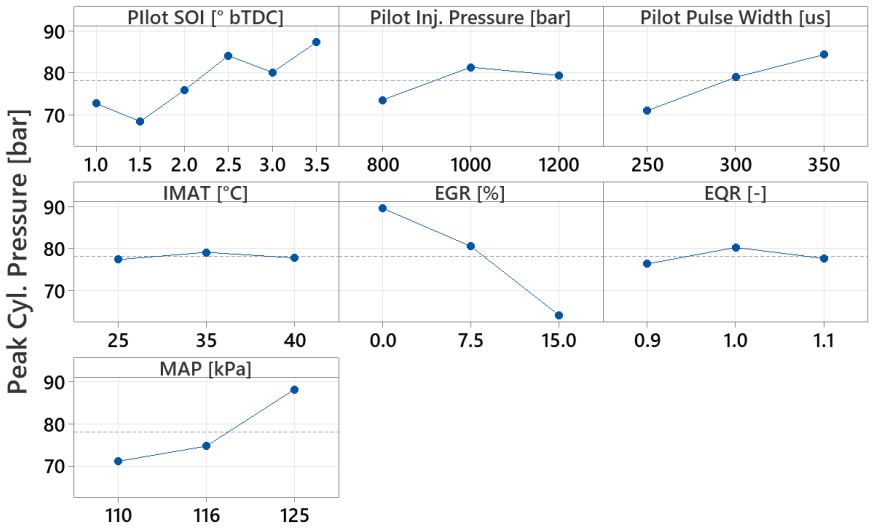

Figure 5-9. Peak Cylinder Pressure main effect plots for means

Table 5-14 shows the factor ranking, level for minimizing, level for maximizing peak cylinder pressure for each factor. The effect on PCP is based on the increase of each factor level.

Table 5-14. Peak Cylinder Pressure factor ranks

Rank	Factor	Level for Minimization	Level for Maximization	Effect on peak cylinder pressure
1	EGR [%]	15	0.0	↓
2	Pilot SOI [°bTDC]	1.5	3.5	↑
3	MAP [kPa]	110	125	↑
4	Pilot Pulse Width [µs]	250	350	↑
5	Pilot Inj. Pressure [bar]	800	100	↑
6	EQR [-]	0.9	1.0	*
7	IMAT [°C]	25	35	*

A6: CA50 data analysis plots

Figure 5-10 shows the CA50 sensitivity analysis for each combustion control factor.

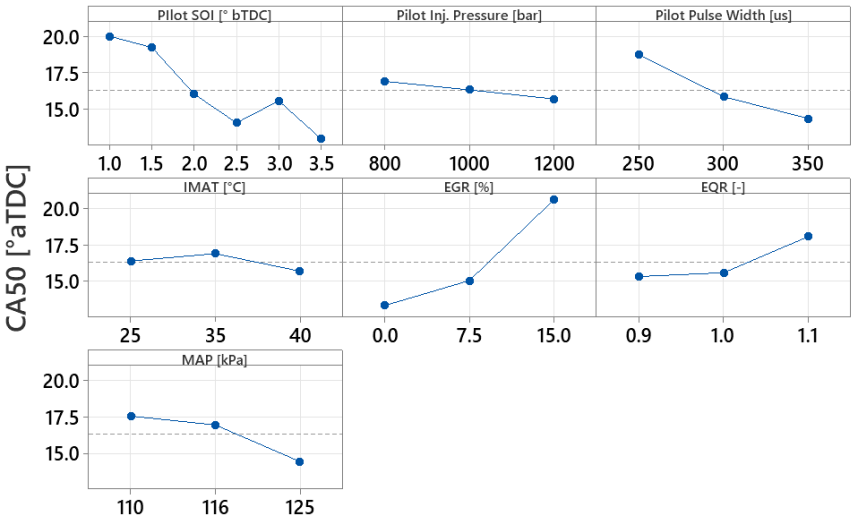

Figure 5-10. CA50 main effect plots for means

Table 5-15 shows the factor ranking, level for minimizing, level for maximizing CA50 for each factor. The effect on CA50 is based on the increase of each factor level.

Table 5-15. CA50 factor ranks

Rank	Factor	Level for Minimization	Level for Maximization	Effect on CA50
1	EGR [%]	0.0	15	↑
2	Pilot SOI [°bTDC]	3.5	1.0	↓
3	Pilot Pulse Width [μs]	350	250	↓
4	MAP [kPa]	125	110	↓
5	EQR [-]	0.9	1.1	↑
6	Pilot Inj. Pressure [bar]	1200	800	↓
7	IMAT [°C]	40	35	*

6 EXPERIMENTAL STUDIES OF LOW-LOAD LIMIT IN A STOICHIOMETRIC MICRO-PILOT DIESEL NATURAL GAS ENGINE

This article was published in the MPDI Energies Journal, 2022.

Bonfochi Vinhaes, V., Naber, J.D.

Michigan Technological University

Gordon McTaggart-Cowan

Simon Fraser University

Mahdi Shahbakhti

University of Alberta

Sandeep Munshi

Westport Fuel Systems Inc.

Michigan Technological University

Department of Mechanical Engineering – Engineering Mechanics

1400 Townsend Drive, Houghton, Michigan, USA 49931

Email: vbvinhae@mtu.edu, jnaber@mtu.edu

6.1 Abstract

While operating at light loads, diesel pilot-ignited natural gas engines with lean premixed natural gas suffer from poor combustion efficiency and high methane emissions. This work investigates the limits of low-load operation for a micro-pilot diesel natural gas engine that uses a stoichiometric mixture to enable methane and nitrogen oxide emission control. By optimizing engine hardware, operating conditions, and injection strategies, this study focused on defining the lowest achievable load while maintaining a stoichiometric equivalence ratio and with acceptable combustion stability. A multi-cylinder diesel 6.7 L engine was converted to run natural gas premix with a maximum diesel micro-pilot contribution of 10%. With the base diesel compression ratio of 17.3:1, the intake manifold pressure limit was 80 kPa(absolute). At a reduced compression ratio of 15:1, this limit increased to 85 kPa, raising the minimum stable load. Retarding the combustion phasing, typically used in spark-ignition engines to achieve lower loads, was also tested but found to be limited by degraded diesel ignition at later timings. Reducing the pilot injection pressure improved combustion stability, as did increasing pilot quantity at the cost of lower substitution ratios. The lean operation further reduced load but increased NOx and hydrocarbon emissions. At loads below the practical dual-fuel limit, a transition to lean diesel operation will likely be required with corresponding implications for the aftertreatment system.

Keywords: High-efficiency engine, Micro-Pilot Diesel, Natural Gas, Stoichiometric Operation, Low Load

6.2 Introduction

Modern society relies on the transportation of products and people, and due to the abundant supply, convenience, and affordability of liquid fuels, transportation is virtually entirely powered by conventional internal combustion engines (ICE). Furthermore, stationary combustion engines (i.e., generators) are essential in medical facilities, industries, and many other services [1]. Demand for high-efficiency engines with high specific power output, low greenhouse gas emissions, and ever lower pollutant emissions is expected to

continue to grow[2]. Natural gas (NG) as an alternative fuel is an exciting subject of research in ICE because of its significant potential to reduce CO2 and oxides of nitrogen (NOx) emissions [3].

Compression ignition engine types that burn two distinct fuels in different mixture quantities simultaneously are often described as dual-fuel engines. The combination of lean-burn of a premixed NG-air mixture with a considerable quantity of diesel injection as the combustion pilot is a characteristic of the conventional dual fuel engines [4]. Diesel-like fuel conversion efficiencies and relatively low NOx emissions have been demonstrated in such engines. However, system development and on-road vehicle use have been limited by low combustion efficiency, limited diesel replacement, and high unburned methane emissions [5, 6]. As a result, lean-burn engines have not been able to gain a large share of the on-road vehicle market. Combining an overall stoichiometric fuel-air combination with a small diesel pilot injection ("micro-pilot") is another option. Because only a small quantity of diesel is required to ignite the premixed charge, high substitution rates are attainable. The overall stoichiometric mixture enables use of a three-way catalyst (TWC to obtain extremely low NOx, Carbon Monoxide (CO), and hydrocarbon emissions (which are predominantly CH4) [7]. At moderate- and high-load conditions, significant net fuel cost and greenhouse gas (GHG) emission reductions are feasible by keeping diesel-like compression ratios (CR) and efficiency when paired with a low-carbon fuel. At low loads, the inducted air mass needs to be reduced to maintain stoichiometric operation. This leads to low end-of-compression pressure which, when combined with a near-stoichiometric premixed fuel concentrations, can impede ignition of the diesel pilot. This imposes a fundamental limit on the feasible operating range of such a stoichiometric micro-pilot engine.

Multiple researchers have studied the performance and emissions of conventional dual fuel operation, including the effects of intake manifold air temperature (IMAT) and manifold air pressure (MAP), substitution ratios, exhaust gas recirculation (EGR), equivalence ratio, and the effects of injection timing. Figure 6-1 summarizes the recent work in pilot ignited

natural gas engines that included the low load operation regime that is the focus of the current study.

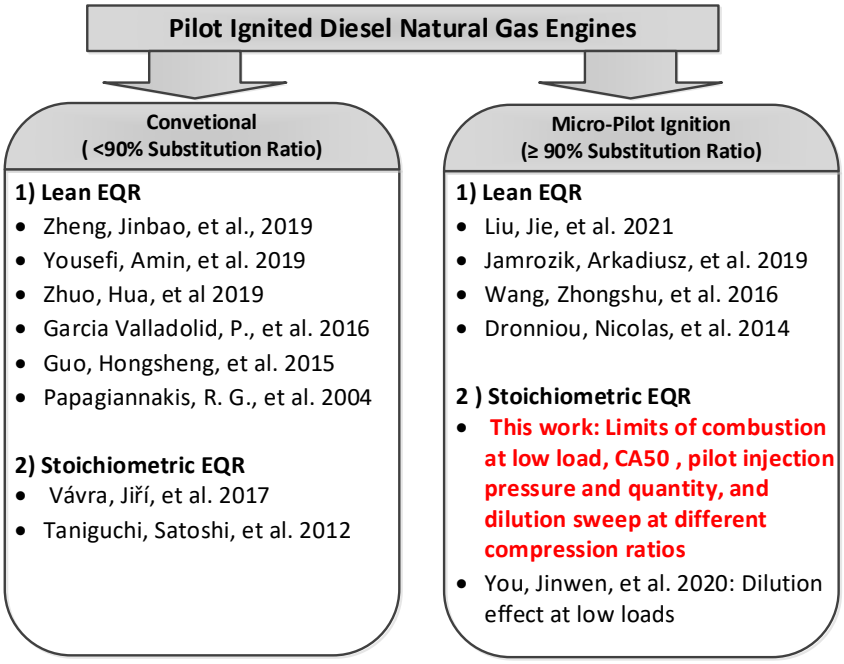

Figure 6-1. Recent pilot ignited diesel natural gas engines in the low to medium load operation range research and contributions of this work compared to the state-of-the-art. EQR: Equivalence Ratio. CA50: Crank Angle position at which 50% of the heat from combustion has been released.

The influence of the equivalence ratio was investigated by Zheng, et al. [8]. Their research revealed that premixed lean-burn engines have a slower flame propagation, whereas increasing the equivalence ratio increases the heat release rate and exhaust gas temperature, resulting in improved thermal efficiency and reduced methane emissions. However, NOx emissions are higher if no dilution is used because of the higher temperatures. The effect of diesel pilot start of injection (SOI) was investigated by Yousefi, et al. [9] and Zhou, et al. [10] in a range of operating conditions varying from low to high load and speeds. Both researchers agree that for all the engine load-speed conditions studied, the results demonstrated that the pilot diesel SOI advance increases peak cylinder pressure, thermal efficiency, and undesirable NOx emissions increase due to higher in-cylinder temperatures

driven by the higher pressure. Under the low load-low speed and medium load-high speed conditions, advancing the SOI significantly reduced unburned methane and CO2 emissions. Their findings also show that under low load-low speed and medium load-high speed conditions, the central part of the combustion chamber is the primary source of unburned methane emissions, and advancing diesel pilot SOI significantly improves premixed mixture combustion in this region of the combustion chamber.

The study by Valladolid and Tunestal [11] shows the effect of intake manifold conditions while operating a light-duty diesel pilot natural gas engine at low loads. The results show that the IMAT plays an essential role in flame propagation under high dilution conditions and that the higher air temperature allows for reducing the total unburnt hydrocarbon emissions. Under high dilution conditions, throttling effectively reduces emissions and increases fuel conversion efficiency through higher combustion efficiency due to a richer premixed NG-air mixture. When the engine was operated above 5 bar indicated mean effective pressure (IMEP), it is possible to achieve unburned hydrocarbon levels below the legislated limit and with exhaust gas temperatures high enough to enable methane oxidation in the aftertreatment. Their work also suggested that the stoichiometric operation would allow a three-way catalyst usage. However, this approach introduces a penalty on CO emissions and thermal efficiency.

Guo, et al. [12] investigated the combustion and emissions performance of the diesel pilot natural gas engines in a range of load and speed varying from low to medium loads. In their work, as the natural gas substitution ratio was increased, a pilot injection timing sweep was conducted. They reported that a maximum of 50% natural gas fraction was reached at the low load condition while 70% natural gas fraction was achieved in the medium load. The minimum diesel pilot pulse width was the substitution ratio limiting factor in their study. The increase in natural gas ratio led to a retarded combustion phasing at a constant pilot injection timing, and brake thermal efficiency decreased significantly at low loads. The natural gas substitution increased methane emissions while reducing CO2 emissions. At low loads, the CO emissions increased due to decreased combustion efficiency. This observation is also consistent with other researches [13-15].

Poorghasemi, et al. [16] employed a detailed chemical kinetics mechanism in a commercial Computational Fluid Dynamics software to investigate the effects of the direct injection strategy on the combustion and emissions characteristics of a light duty engine fueled with natural gas and diesel. While considering a split injection strategy for the diesel fuel, a reduction in NOx emissions and controllable HC and CO emissions was achieved by increasing the NG fraction and advancing the diesel pilot injection timing, increasing the diesel fuel injection quantity, and lowering the pressure of the first diesel injection.

A typical definition for micro-pilot ignition is where more than 90% of the net chemical energy is from the premixed NG (i.e., diesel substitution ratio ≥ 90%, Figure 6-1) at all engine operating conditions. This distinction is made because traditional diesel injection systems tend to have degraded spray quality (e.g., penetration, atomization, and mixing) when the pilot quantities are between 10% to 1% of the full load quantity. To reliably deliver the low injection quantities that are solely needed to ignite a near-stoichiometric premixed fuel-air mixture, the diesel injection system needs to be reoptimized. Such a fuel system modification would mean that, unlike a traditional dual fuel engine, a micro-pilot engine is typically restricted from operating in a diesel-only configuration. .

While many studies have recently focused on pilot-ignited natural gas engines operated at low loads, only a few focused on micro-pilot ignition[15, 17, 18]. Jamrozik, et al. [19] work focused on the effect of NG substitution ratio from 0% to 95%. They reported that the increase in NG substitution ratio increases the ignition delay of the diesel pilot and shortens the overall combustion duration. Only one study was found that paired the micro-pilot ignition in a globally stoichiometric mixture [20]. In this work, You et al. discusses the dilution effect of inert gases (Ar, N2, and CO2) under low load stoichiometric conditions on a 6-cylinder turbocharged engine. Ar and N2 were shown to boost engine power as the dilution ratio was increased. However, CO2 (generally supplied through exhaust gas recirculation systems) degraded the combustion process, including heat release rate, cylinder peak pressure, and combustion phasing. Because of the lower cylinder temperature, CO2 dilution resulted in the lowest NOx emissions of the three gases tested, while Ar resulted in the greatest NOx emission.

To the best of the authors' knowledge, there is no published research that has investigated the limits of combustion and the minimum stable load that can be maintained at stoichiometric conditions through optimization of engine hardware (compression ratio), operating condition (EGR, Injection timing), and micro-pilot injection strategy (pressure, quantity). The diesel micro-pilot strategy is an attractive area of study as it aims at minimizing the diesel combustion contribution to GHG emissions while leveraging its high ignition energy potential. Therefore, the purpose of this research is to determine the limits of a natural gas diesel micro-pilot engine's light load operation and its controlling parameters by optimizing engine hardware, operating conditions, and injection strategies to achieve the lowest possible load while operating in a stoichiometric equivalence ratio and maintaining combustion stability. Furthermore, the TWC requirements for operating the system at low load and the engine out emissions implications of transitioning to lean operation below the minimum NG operating load are also investigated.

This paper is divided into three sections. The experimental apparatus is explained in Chapter 6.3, which includes an overview of the modified diesel engine to run micro-pilot diesel natural gas mode, the instrumentation and fuels used, and a description of the test approach. Section 3 centers on presenting engine results and discussing the reported results. The last section concludes this study.

6.3 Materials and Methods

Micro Pilot Diesel Natural Gas Engine

This section summarizes the engine's major modifications, including compression ratio reduction, fuel, air handling system, and instrumentation. The modifications are described in [21], but the essential features are briefly mentioned here.

A Cummins 6.7L diesel engine was adapted for this project to run under micro-pilot diesel and natural gas combustion with a maximum diesel contribution of 10% of total fuel energy. The approach combines overall stoichiometric combustion consisting primarily of premixed NG with EGR for combustion temperature management and a micro-pilot

injection of diesel to offer a reliable ignition source. Stoichiometric operation enables the use of a three-way catalyst to meet emissions criteria. This is a substantial simplification compared to the multi-element aftertreatment systems required to meet emissions standards in modern diesel engines.

For the medium-duty market, a feature of modern NG-fueled on-road engine products is the coupling of stoichiometric combustion with EGR, and with a spark plug to ignite the fuel-air mixture. The method being investigated here uses a very small quantity diesel pilot as the ignition source instead of a spark plug. This strategy provides a more robust ignition, premixed turbulent flame combustion, and shorter distances for the flame to propagate across the combustion chamber by providing higher ignition energy and a more distributed ignition source for the premixed mixture. Compared to premixed SI methods, these effects are expected to lessen the chance for knock, allowing for higher thermal efficiency through higher compression ratio, better combustion timing, and lower coefficient of variance (COV) of net indicated mean effective pressures (NMEP) and shorter combustion duration.

Converting the engine to stoichiometric premixed operation resulted in significant changes to the air handling system (shown in Figure 6-2). A throttle valve was installed downstream of the compressor discharge to manage airflow rate, primarily to maintain stoichiometric mixtures at all loads. A specially constructed mixer system was created to meet the flow requirements for both NG and EGR, with an aim of maximizing the uniformity of the premixed fuel-air-EGR mixture being supplied to the intake manifold. A natural gas injector manifold with six prototype high-flow port injectors rated at 8 g/s each supplies gaseous fuel to the NG-air-EGR mixer in the mixer system. An airfoil is fitted across the throat of a mixing venturi, with a series of small diameter holes sized to give a suitable pressure drop over the mixer. To allow enough mixing time before the premix mixture is inducted into the engine, the mixer is situated downstream of the throttle but upstream of the intake manifold.

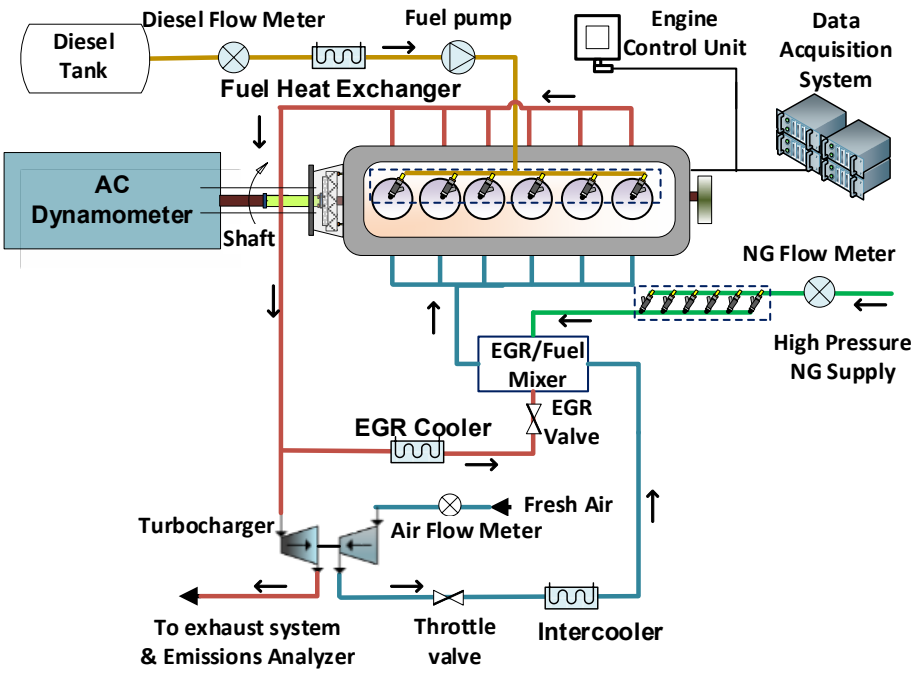

Figure 6-2. Engine experimental setup.

While this work focuses on low-load operation, a key target for the stoichiometric micro-pilot engine is to achieve a high maximum power (24 bar BMEP). To avoid end gas auto-ignition at high loads, it was necessary to decrease the compression ratio from 17.3 to 15:1. This was achieved through a thicker head gasket and lowering the pistons' top face crown heights by 2.8mm. Apart from the machining change, the piston bowl geometry remained unchanged from the stock diesel engine configuration.

Table 6-1 shows the engine's specifications. A MotoHawk ECU565-128 engine controller is utilized in conjunction with a custom-built strategy to manage the engine actuators, including pilot SOI, pilot injection pressure, injection quantity, equivalence ratio, wastegate position, charge air cooling, and dilution.

Table 6-1. Engine's specifications. HP stands for High Pressure, and VGT stands for Variable Geometry Turbocharger

No. of Cylinders	6
Bore & Stroke	107 x 124 mm
Connecting Rod Length	192 mm
Displacement Volume	6.7 L
Compression Ratio	15.0:1
Aspiration	Turbocharged (VGT) + Charge Air Cooler + HP EGR + Throttle Valve
Diesel Micro Pilot Injection System	HPCR injector 8 holes (168 microns diameter)
Diesel Injection Pressure	600 to 2000 bar
Diesel Micro- Pilot Minimum Fuel Quantity	3.3 mg/injection

Instrumentation and Measurement Uncertainty

In-cylinder pressure is measured using AVL GH series piezoelectric pressure transducers installed in each of the engine's six cylinders, feeding a real-time combustion analyzer system. A BEI encoder series H25D with 360 pulses per revolution is used to measure crank angle position in the A&D CAS system for high-speed combustion analysis. The engine's speed and load are regulated by a 445 hp AVL A/C Dynoroad 308/4 SX dynamometer.

Thermocouple and 0-10V analog input signals are logged using an NI PCIe chassis. The intake air manifold, engine coolant, engine oil, exhaust gas temperature, turbocharger inlet, and output are equipped with Type K thermocouples for temperature readings. The MMA050V5P4D1T3A5CE Omega Absolute Pressure Transducer measures the intake and

exhaust pressures. The Omega Gage Pressure Transducer GP50 measures other pressures, including oil pressure and fuel input.

The fuel flow rates are measured using two Micro Motion Coriolis Meters ELITE CMFS010P, one for diesel and the other for natural gas. The intake and exhaust CO2 concentrations, used to calculate the EGR rate, are measured using CO2 Meter K33 series sensors. These are installed in the exhaust and intake manifolds to allow for real-time EGR determination. A Horiba MEXA 1600 emissions bench is used to monitor gaseous emissions. Engine-out emissions were measured using a single analyzer.

Table 6-2 shows the transducer accuracies and uncertainties for the independent variables based on the information provided by the sensor manufacturers.

Table 6-2. Instrumentation accuracy and measurement uncertainty. FS stands for Full Scale.

Measurement	**Accuracy**	**Full scale**	**Uncertainty (absolute)**	**Unit**
In-Cylinder Pressure Transducer	±0.30%FS	0-250	± 0.75	bar
Engine Crank Angle Degree (Encoder)	±1.00	360:1	± 1.00	Deg
Fuel Flow Rate (Diesel & NG)	±0.05 FS	0-30	± 0.015	g/s
Thermocouples	±2.20	0-800	± 2.20	°C
Intake/Exhaust Manifold Pressure Transducer	±0.08%FS	0-6.89	± 0.0055	bar
Oil and Fuel Inlet Pressure	±0.50%FS	0-7 / 0-2	±0.035 / 0.010	bar
Torque	±0.05%FS	0 – 5000	±2.50	Nm
NOx Analyzer	±1.00%FS	0 – 5000	±50.0	ppm
UHC Analyzer	±1.00%FS	0 – 10000	±100.0	ppm

The uncertainty of the dependent variables in Table 6-3 is determined using Equation 1 from the uncertainty propagation approach described in [22].

$$U_Y = \sqrt{\sum \left(\frac{\partial Y}{\partial X_i}\right)^2 U_x^2} \qquad (1)$$

Where Y represents the calculated quantity's value, U represents the variable's uncertainty, and X represents the measured variables.

Table 6-3. Uncertainty propagation to the dependent variables

Measurement	**Range**	**Uncertainty (absolute)**	**Unit**
NMEP	4.70 – 8.00	± 0.15	Bar
Combustion Stability (COV_{NMEP})	0.40 – 9.0	±0.05	%
Ignition Delay	1.70 – 5.0	± 0.08	ms
Diesel Substitution Ratio	86.0 – 93.2	± 0.50	%
CA50	12.0 – 32.0	± 0.60	°aTDC
Exhaust Gas Recirculation	0.00 – 12.0	±0.20	%
Equivalence Ratio	0.80-1.0	±0.01	-
BSNOx	0.20 - 133	± 34.1	g/kWh
BSUHC	2.10 - 37.0	± 5.00	g/kWh

Fuels

The fuel qualities and characteristics for both diesel and natural gas are shown in Table 6-4. The gas supply company (SEMCO) measured the composition of the natural gas, which reflects an average composition of the gas during the testing program. The main constituents were 89% CH4, 8% C2H6, 0.4% C3H8, and 2.6% inert (all percent by volume).

Table 6-4. Fuel Properties. AFR stands for Air Fuel Ratio.

Diesel (ULSD)	Density (kg/m^3) @ 15.6 °C, 1 atm	Lower Heating Value (MJ/kg)	Stoichiometric AFR	H/C	Cetane Number
	851.6	42.8	14.60	1.85	51.7
CNG	Density (kg/m^3) @ 20 °C, 1 atm	Lower Heating Value (MJ/kg)	Stoichiometric AFR	H/C	Methane Number*
	0.727	47.5	16.30	3.80	83.0

*Wärtsilä Methane Number [23]

The Diesel Substitution Ratio (DSR) is calculated on an energy basis in this study, as shown in Equation (2).

$$DSR = \frac{\dot{m}_{CNG} \cdot Q_{LHV,CNG}}{\dot{m}_{CNG} \cdot Q_{LHV,CNG} + \dot{m}_{Diesel} \cdot Q_{LHV,Diesel}} \quad (2)$$

Where, $\dot{m}$ is the fuel mass flow rate in kilograms per second (kg/s), and QLHV is the lower heating value of each fuel in MJ/kg, as described in Table 6-4.

The Equivalence Ratio (φ) is determined as shown in Equation (3).

$$\varphi = \frac{\dot{m}_{CNG} \cdot AFR_{stoich,CNG} + \dot{m}_{Diesel} \cdot AFR_{stoich,Diesel}}{\dot{m}_{air}} \quad (3)$$

Where AFR is the stoichiometric mass air to fuel ratio of each fuel, as described in Table 6-4. Equation (3) is based on fresh airflow. As the mixture was stoichiometric, any recirculated exhaust gases had negligible oxygen content and therefore did not impact the global equivalence ratio.

Experimental Procedure

The experimental procedure consisted of varying selected combustion control parameters while keeping all other control parameters constant. The investigated parameters include CA50 (controlled by the diesel pilot SOI), exhaust gas recirculation, diesel pilot injection

pressure, and diesel pilot injection quantity. The research team has previously shown that pilot start of injection timing and EGR are the dominant control parameters at medium loads in a stoichiometric micro-pilot engine (Bonfochi Vinhaes, et al. [24]). However, for the low load operation, the engine operating controls are constrained differently than those at medium load. For instance, reducing the intake manifold pressure to reduce load while maintaining a stoichiometric mixture is constrained by the minimum in-cylinder conditions required for pilot ignition and stable combustion.. Therefore, the MAP and equivalence ratio are kept at a constant value for all tests in this study. The intake manifold temperature was shown in the prior work to be the least impactful parameter in combustion stability and thus will not be studied in this work.

All tests were performed at 1200 RPM and at a stoichiometric global equivalence ratio, and the intake temperature was kept constant at 35 °C. For the original compression ratio of 17.3:1, the intake manifold pressure of 80kPa was the minimum throttled value determined in preliminary testing below which the combustion was unstable (instability, in this study, is defined as COVNMEP greater than 3%). This instability was a result of weak and unstable diesel pilot ignition, resulting from the low in-cylinder pressure and temperatures under throttled operation. To establish this minimum pressure, an injection timing sweep was conducted to find the minimum combustion variability, and then the intake manifold pressure was gradually reduced by closing the intake throttle. The minimum acceptable pressure was identified as the throttle position before which the combustion became unstable (COVNMEP > 3%). A further restriction on intake pressure results from the unmodified piston rings and valve stem seals for the diesel-based combustion system. These were not designed for sub-atmospheric intake manifold or in-cylinder pressures, limiting the degree of throttling that could be applied without excessive oil carry-over into the intake ports and cylinders. For the reduced compression ratio (i.e., 15.0), the minimum intake manifold pressure was 85kPa (absolute).

To study the effect of different compression ratios, the CA50, pilot injection pressure, and EGR sweeps were done with both the stock compression ratio of 17.3:1 and the reduced compression ratio of 15.0:1. The pilot quantity sweep was only performed at the reduced

compression ratio of 15.0:1 using the maximum EGR quantity identified in the previous sweep. For every parameter swept, the combustion stability limit was set to 3% COV of NMEP. Table 6-5 shows the test conditions summary, including the parameters swept and their range.

Table 6-5. Experimental test summary

	Range of operating conditions tested								
	Speed	**EQR**	**MAP**	**Intake Temp.**	**CR**	**Diesel Pilot SOI**	**Diesel Inj. Pressure**	**EGR**	**Diesel Pilot Quantity**
	RPM	-	kPa	°C	-	°bTDC	bar	%	mg/injection
CA50 Study	1200	1.0	80 (CR17.3); 85 (CR15.0)	35	15.0; 17.3	2.0 to 15	1000	0	3.3
Diesel Inj. Pressure Study					15.0; 17.3	2.5 (CR17.3); 7.0 (CR15.0)	600 to 1200	0	3.3
EGR Study					15.0	7.0 to 15	600	0 to 12	3.3
Pilot quantity Study					15.0	15	600	12	3.3 to 6.6

6.4 Results and Discussion

CA50 Study

In this study, the combustion phasing was swept by changing the diesel pilot start of injection. The investigation was performed at the original and reduced compression ratio. Figure 6-3 shows how the engine load, represented by the NMEP, varies as the CA50 is retarded. The minimum stable loads achieved for each compression ratio are highlighted

in Figure 6-3(a). These conditions correspond to the maximum combustion stability limit represented by the COVNMEP of 3%, as seen in Figure 6-3(b). At the original CR of 17.3:1, the minimum load observed was of 6.5 bar NMEP, while at the reduced CR of 15.0:1 the minimum load observed was 7.2 bar NMEP. These loads correspond to about 30% of the engine's maximum load.

The load difference of 0.7 bar seen between the original CR and reduced CR is expected due to the higher intake manifold pressure required to operate the engine when at the reduced CR configuration. This is a direct result of the lower end-of-compression temperature with the reduced compression ratio, impacting both diesel pilot ignition and subsequent flame propagation. Interestingly, in Figure 6-3(a), both curves show a similar trend as CA50 increases.

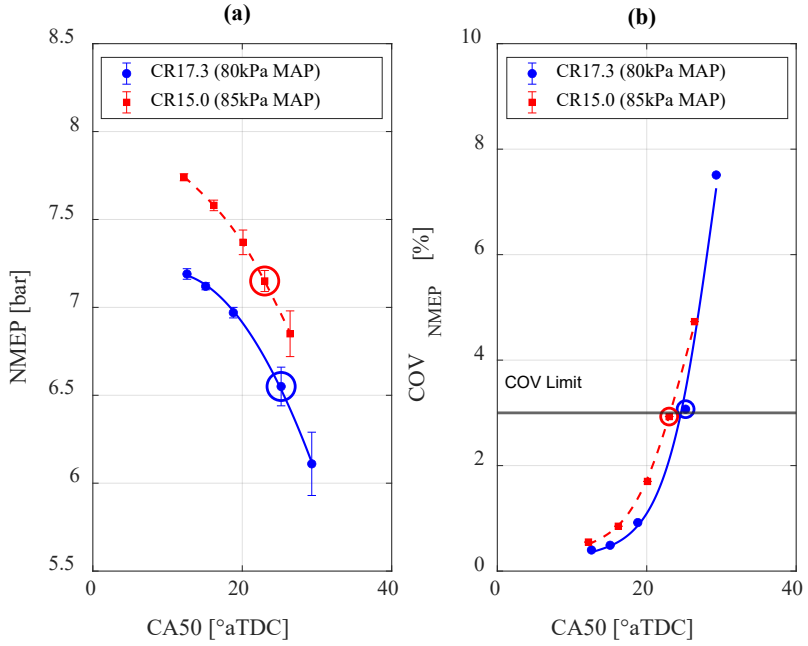

Figure 6-3. Results for the CA50 sweep test. (a) NMEP vs. CA50. (b) COVNMEP vs CA50. Engine operating conditions: 80 kPa MAP (for CR17.3) and 85 kPa MAP (for CR15.0); 0% EGR ; 35 °C IMAT ; pilot quantity of 3.3 mg/inj. at 1000 bar inj. pressure; 1200 RPM ; EQR 1. The circled data points correspond to the lowest load achieved at the combustion stability limit.

Retarding the combustion phasing is a common strategy utilized in spark-ignition (SI) engines to reduce engine load. The effect of the combustion retard on NMEP is discussed by Heywood, et al. [25]. Their work tested the impact of combustion retard over a wide range of spark-ignited operating conditions and collapsed into one universal curve given by Equation (4), where MBT stands for the maximum brake torque. This correlation demonstrates the impact of combustion phasing on the engine load and thermal efficiency. Figure 6-4 shows the correlation for the effect of combustion retard on the normalized load presented by Heywood.

$$\frac{NMEP}{NMEP_{MBT}} = 1 - 0.168[(1 + 4.443 \cdot 10^{-3}(CA50 - CA50_{MBT})^2)^{0.5} - 1] \quad (4)$$

It was observed that the micro-pilot natural gas engine trend is similar to that of SI engines and could be approximated by the same correlation with different parameters, shown in Equation (5), with the modification highlighted by the bold number.

$$\frac{NMEP}{NMEP_{MBT}} = 1 - \mathbf{0.210}[(1 + 4.443 \cdot 10^{-3}(CA50 - CA50_{MBT})^2)^{0.5} - 1] \quad (5)$$

The difference between these correlations could be explained by the higher heat transfer in the micro-pilot engine caused by the micro-pilot engine's larger combustion chamber volume to surface area ratio compared to the SI engine in [25]. Other potential hypotheses include:

1. The higher compression ratio of the micro-pilot engine vs. the SI engine;
2. Different combustion chamber geometries;
3. Natural gas premix flame speed versus gasoline premix flame speed;

These hypotheses could further be investigated in future work.

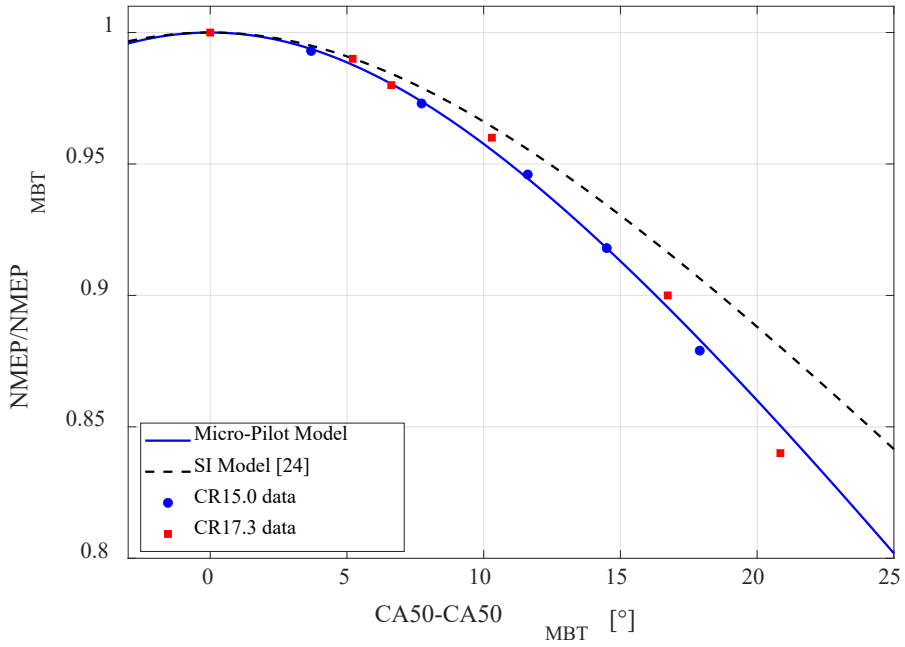

Figure 6-4. Effect of combustion phasing retard on normalized NMEP. Engine operating conditions: 80 kPa MAP (for CR17.3) and 85 kPa MAP (for CR15.0); 0% EGR ; 35 °C IMAT ; pilot quantity of 3.3 mg/inj. at 1000 bar inj. Pressure ; 1200 RPM ; EQR 1

Figure 6-4 also shows that, when compared to the SI engine correlation, the micro-pilot engine combustion phasing retard causes a stronger load loss penalty. This shows the importance of the optimum combustion phasing in diesel micro-pilot NG engines.

Diesel Injection Pressure Study

For this study, the pilot diesel injection pressure was swept from 600 bar to 1200 bar in both original and reduced compression ratios while keeping everything else constant. Figure 6-5 shows how NMEP and the COVNMEP vary with the pilot injection pressures while the injection timing is constant. When injection pressure is decreased from 1000 bar to 600 bar, it results in a load increase from 6.5 bar NMEP to 6.8 bar NMEP for the original compression ratio and from 7.2 bar NMEP to 7.5 bar NMEP for the reduced compression ratio. The operation with an injection pressure of 1200 bar resulted in unstable combustion in both CRs.

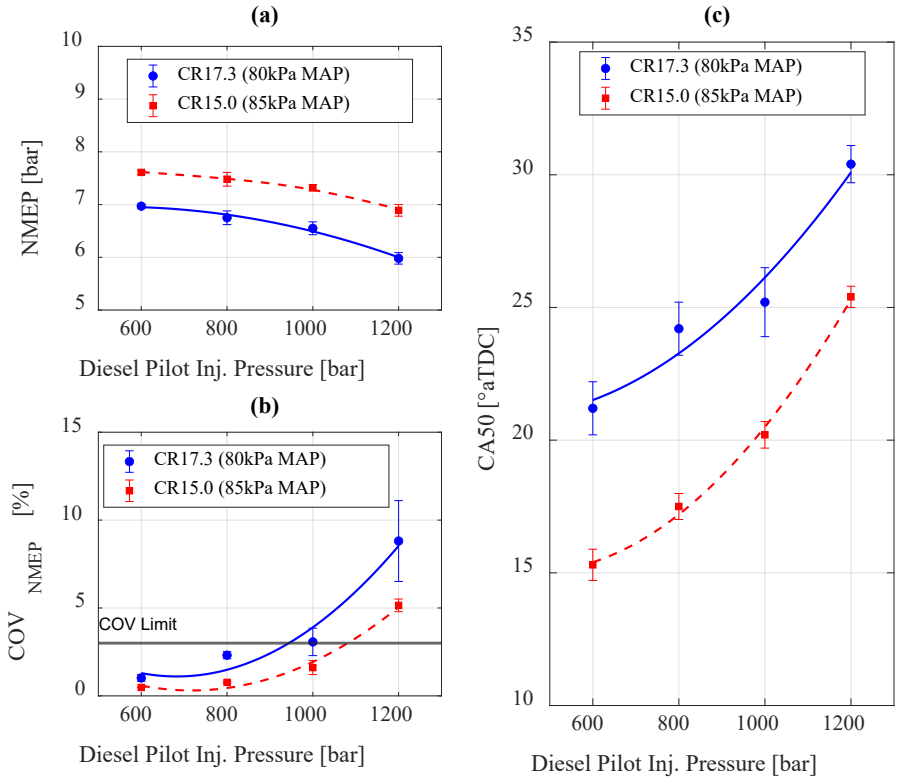

Figure 6-5. Results for the pilot diesel injection pressure sweep. (a) NMEP vs. Inj. Pressure (b) COVNMEP vs. Inj. Pressure (c) CA50 vs. Inj. Pressure. Engine operating conditions: 80 kPa MAP (for CR17.3) and 85 kPa MAP (for CR15.0); 0% EGR ; 35 °C IMAT ; Constant diesel pilot SOI ; Pilot quantity of 3.3 mg/inj. ; 1200 RPM ; EQR 1

The load increase seen by reducing the injection pressure can be attributed to the occurrence of an earlier CA50, as shown in Figure 6-5c. The CA50 location is observed to be up to 5 degrees earlier in the cycle as injection pressure is changed from 1000 bar to 600 bar. This earlier CA50 may be a result of either a shorter combustion duration and/or an earlier start of combustion. Of these, the average combustion duration was 15 degrees with a standard deviation of only a couple of degrees for all operating conditions of this investigation. In this work, combustion duration is calculated using the integrated heat release rate and is defined as the number of degrees between the crank angle at which 10% and 90% of the total energy release has occurred (CA10-90). The ignition delay, however, was reduced by up to 15% when comparing the operation at 600 bar to the 1000 bar

injection pressure for both compression ratios, as shown in Figure 6-6. Interestingly, the compression ratio did not seem to affect the ignition delay. This could be explained by the difference in MAP and NMEP (i.e., higher load observed in the reduced compression ratio) leading to equivalent in-cylinder pressure and temperature conditions at SOI for both CRs.

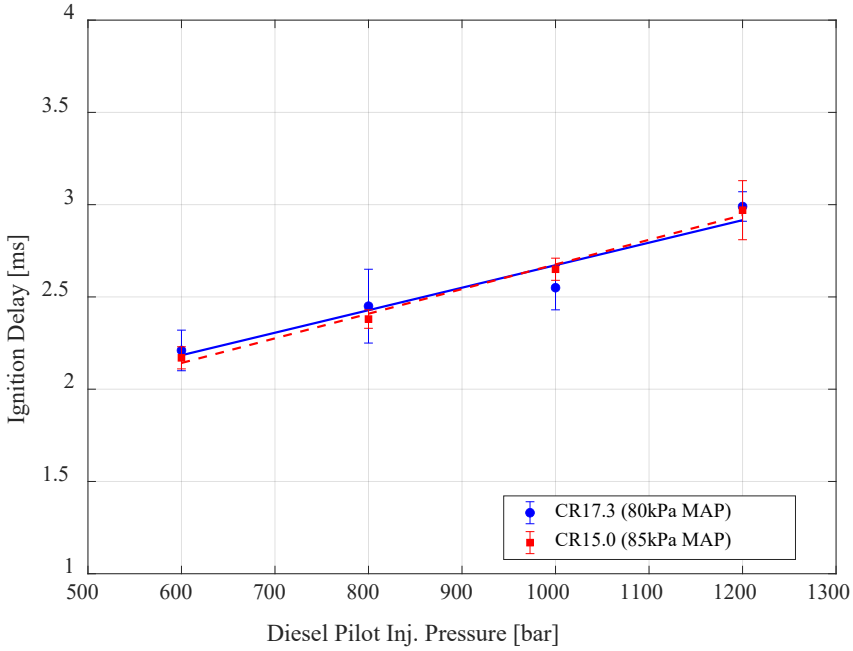

Figure 6-6. Ignition delay vs Inj. Pressure. Engine operating conditions: 80 kPa MAP (for CR17.3) and 85 kPa MAP (for CR15.0) ; 0% EGR ; 35 °C IMAT ; Constant diesel pilot SOI ; Pilot quantity of 3.3 mg/inj ; 1200 RPM ; EQR 1. Ignition delay is calculated by the time between the hydraulic start of injection and CA10.

The shorter ignition delay behavior could be due to the shorter diesel pilot penetration due to the lower pressure. This shorter penetration would concentrate the ignition locations nearer the center of the combustion chamber for lower injection pressures, facilitating the initiation of the propagating flame through the premixed natural gas/air mixture. This also agrees with what has been reported by Khosravi et al. [26].

The shorter ignition delay with lower injection pressure increases the NMEP and advances the combustion phasing (Figure 6-6 (a) and (c)). By applying the approach discussed for

the injection timing study (Figure 6-3), the effect of the combustion phasing retard on NMEP can be assessed relative to the to the Micro-Pilot correlation (i.e., Eq.(5)). This is shown in Figure 6-7; interestingly, the injection pressure study agrees with the model, indicating that the combustion phasing retard, caused by the change in injection pressure, has the same effect on NMEP as the combustion phasing retard caused by the change in pilot SOI.

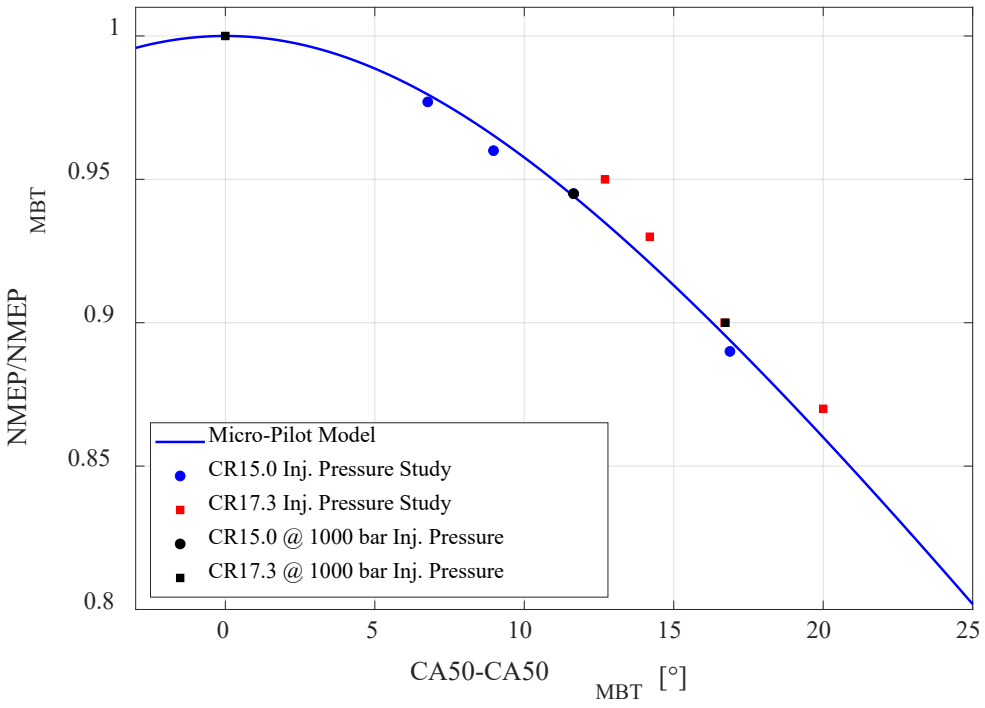

Figure 6-7. Effect of the pilot injection pressure combustion phasing retard caused by on normalized NMEP. Engine operating conditions: 80 kPa MAP (for CR17.3) and 85 kPa MAP (for CR15.0) ; 0% EGR ; 35 °C IMAT ; pilot quantity of 3.3 mg/inj. ; Pilot SOI 2.5°bTDC (CR17.3) and Pilot SOI 7.0°bTDC (CR15.0) ; 1200 RPM ; EQR 1

EGR Study

In this section, the results of the EGR study are shown and discussed. Increasing the EGR concentration will reduce the mass of air inducted for a given intake manifold pressure.

This will result in a lower total fuel quantity needed to maintain a globally stoichiometric mixture. The process used in this study was to increase the EGR level from the minimum achievable load point at a constant intake manifold pressure. As indicated by Figure 6-8, the increase in EGR at a constant pilot injection timing results in unstable combustion. The inclusion of EGR increases the specific heat of the premixed charge, resulting in lower in-cylinder temperature; simultaneously, the oxygen content of the intake charge is reduced. These effects lead to a longer ignition delay for the micro-pilot diesel operation. The ignition processes have more time to occur by advancing the diesel injection timing, and combustion stability can be recovered.

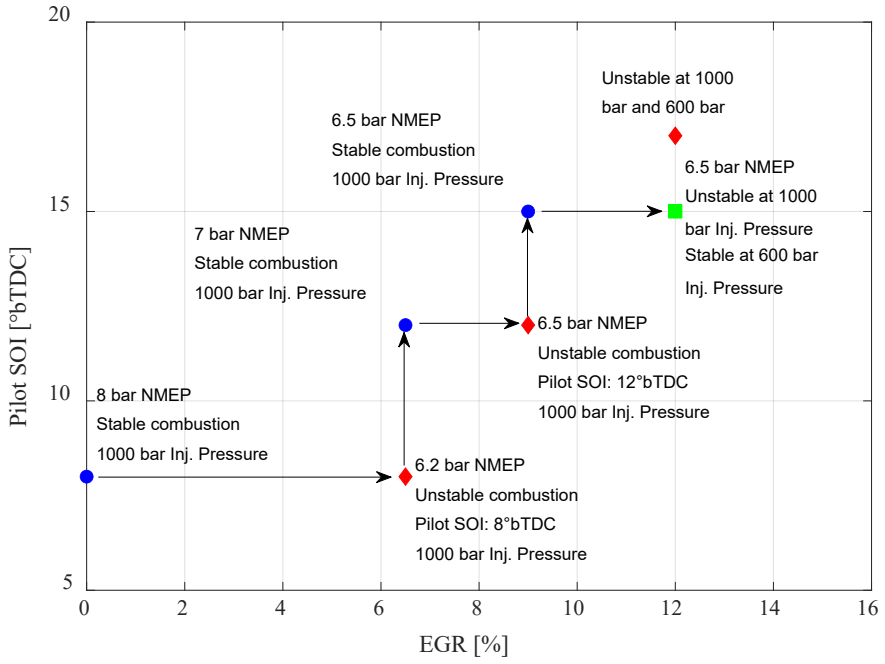

Figure 6-8. Approach to maintain combustions stability during EGR study by adjusting injection pressure and injection timing. CR 15 Engine operating conditions: 85 kPa MAP; 35 °C IMAT; Pilot Quantity of 3.3mg/inj. ; 1200 RPM; EQR 1.

In Figure 6-8, for the 0% EGR data point shown at Pilot SOI of 7°bTDC, 8 bar NMEP with stable combustion at 1000 bar injection pressure (blue circle), EGR was gradually added until COVNMEP was greater than 3%, indicating that combustion was unstable (shown in

red diamond on Figure 6-8 at 6.2% EGR). From there, the EGR quantity was kept at a constant rate while the pilot SOI was advanced until combustion stability was recovered (shown in Figure 6-8 by the blue circle at 6.2% EGR at 12°bTDC). This process was repeated until further advancing the pilot SOI did not reduce the COVNMEP below 3%. A maximum level of 9% EGR was achieved at an SOI limit of 15 ° bTDC and injection pressure of 1000 bar. At this point, further advancing SOI showed no effect at regaining stability. The previously observed ignition delay shortening due to lower injection pressure strategy was applied, enabling the maximum EGR level to be increased to 12%. This EGR maximum quantity agrees with a recent study published by You et al. [20] for micro-pilot diesel natural gas engines operating at low loads.

The results in Figure 6-8 served as a guideline to develop a strategy for achieving lower loads while keeping a globally stoichiometric equivalence ratio. The combination of diluted intake mixture, advanced pilot SOI, and low injection pressure provided the lowest observed load of 6.5 bar NMEP (5.5 bar BMEP)

Diesel Pilot Injection Quantity Study

Lastly, the pilot injection quantity was investigated at the combustion stability limit condition encountered in the EGR study. The increase in diesel pilot quantity aimed to improve combustion stability by increasing the strength of the ignition source. The investigation was performed only in the reduced compression ratio setup and at the EGR limit of 12%. All operating conditions were kept constant while the pilot quantity was increased from 3.3 mg/inj. to 6.6 mg/inj. Natural gas fueling was reduced to maintain a stoichiometric fuel-air ratio. The total diesel substitution ratio reduces by increasing the diesel pilot quantity, as shown in Figure 6-9.

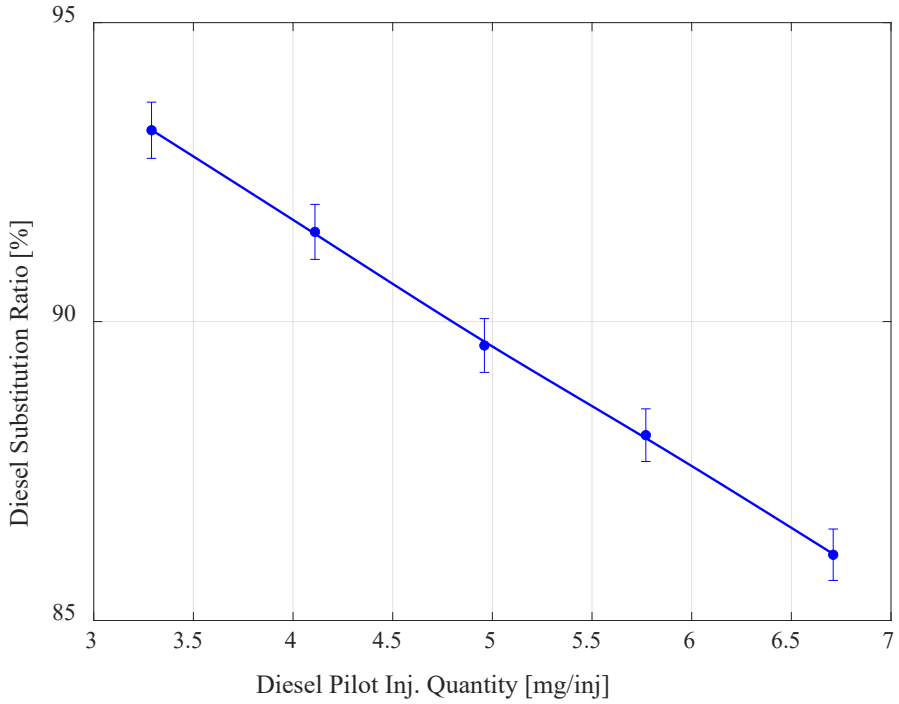

Figure 6-9. Diesel fuel substitution ratio vs. Inj. Quantity for the operating point at the stability limit with 12% EGR from Figure 6-8. CR15 Engine operating conditions: 85 kPa MAP ; 35 °C IMAT ; 600 bar Injection Pressure ; Diesel Pilot SOI 15°bTDC ; 1200 RPM ; EQR 1 ; 12% EGR.

At the minimum injection quantity, the combustion stability is borderline with a COVNMEP slightly above 3% (shown in Figure 6-10(b)) and the lowest achieved load output. Increasing the pilot quantity improves combustion stability and leads to a small increase in NMEP. To maintain the pilot quantity below the targeted 10% of total energy a maximum diesel injection of, 4.11 mg/injection is permitted; this results in improved stability and a small load increase of 0.2 bar NMEP.

The changes in load and COVNMEP are shown in Figure 6-10(a) and Figure 6-10(b), respectively. As expected, when more diesel fuel is added, the COVNMEP reduces as more pilot fuel is available to initiate and maintain the combustion through the premixed charge. With the increase in pilot quantity, the load also increased due to the earlier combustion

phasing resulting from, the shorter ignition delay shown in Figure 6-10(c). These results agree well with the previous studies that have shown a similar sensitivity to the pilot quantity, albeit in globally lean conditions [27-30].

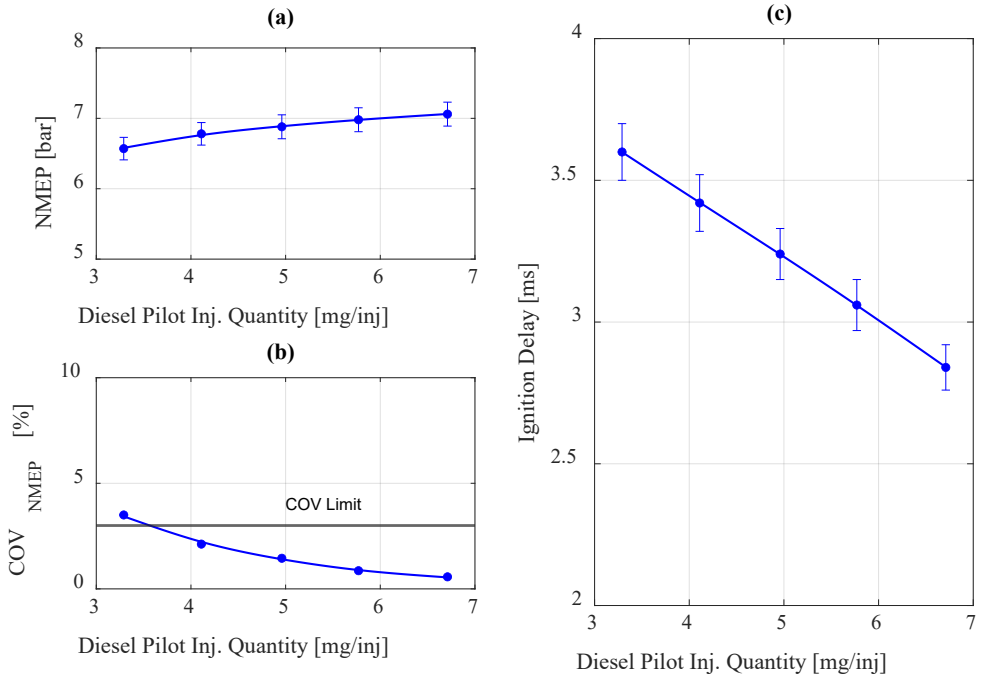

Figure 6-10. Diesel pilot injection quantity sweep results. (a) NMEP vs. Inj. Quantity (b) COVNMEP vs. Injection Quantity (c) Ignition Delay vs. Inj. Quantity. CR15 Engine operating conditions: 85 kPa MAP ; 35 °C IMAT ; 600 bar Injection Pressure ; Diesel Pilot SOI 15°bTDC ; 1200 RPM ; EQR 1 ; 12% EGR.

Optimizing the SOI timing, EGR level, and injection pressure at higher pilot quantity conditions could result in a small further reduction in NMEP. However, the results from the current study indicate that only incremental reductions in NMEP will be achievable through this optimization. The low in-cylinder temperature and lack of available oxygen and reactive species, due to the presence of both premixed NG and EGR, pose a fundamental limit to achieving robust and stable diesel pilot ignition at very low load engine conditions.

Lowest Stable Load Achievable in Stoichiometric Operation

By combining the results from the previous investigations, the lowest load achieved while operating stoichiometric was 6.20 bar NMEP at the reduced compression ratio (CR 15.0) and 5 bar NMEP at the original compression ratio (CR 17.3). Table 6-6 summarizes the minimum low load operating conditions achieved for the micro pilot natural gas engine while maintaining a stoichiometric EQR and stable combustion.

Table 6-6. Minimum load achieved at the stoichiometric operation.

	Reduced Compression Ratio (15.0)	**Original Compression Ratio (17.3)**
Load (NMEP) [bar]	6.20	5.20
Indicated Fuel Conversion Efficiency [%]	35.7	36.3
Diesel Substitution Ratio [%]	93.2	91.0
Equivalence Ratio [-]	1.00	1.00
EGR [%]	12.0	12.0
Pilot Injection Pressure [bar]	600	600
Pilot Injection Quantity [mg/inj]	3.30	3.30
CA50 [°aTDC]	26.0	24.0
COV NMEP [%]	3.50	3.30
MAP [kPa]	85.0	80.0
Intake Manifold Temp. [°C]	35.0	35.0
EGT [°C]	587	515
Brake Specific NOx [g/kWh]	0.50	0.25
Brake Specific CO2 [g/kWh]	590	538
Brake Specific UHC [g/kWh]	4.20	8.90

To reduce the minimum load, it is necessary to reduce the fuel quantity without further reducing the in-cylinder end-of-compression temperature. This can be achieved by transitioning from stoichiometric to lean operation. Reducing the EQR from 1 to 0.83 enabled the minimum load to be reduced by 12% (Figure 6-11 (a)) with the tradeoff of increase in engine-out unburned HC (UHC) by 160% (Figure 6-11 (d)). At this condition, the engine-out NOx emission was also observed to be increased by 40% (Figure 6-11(c)).

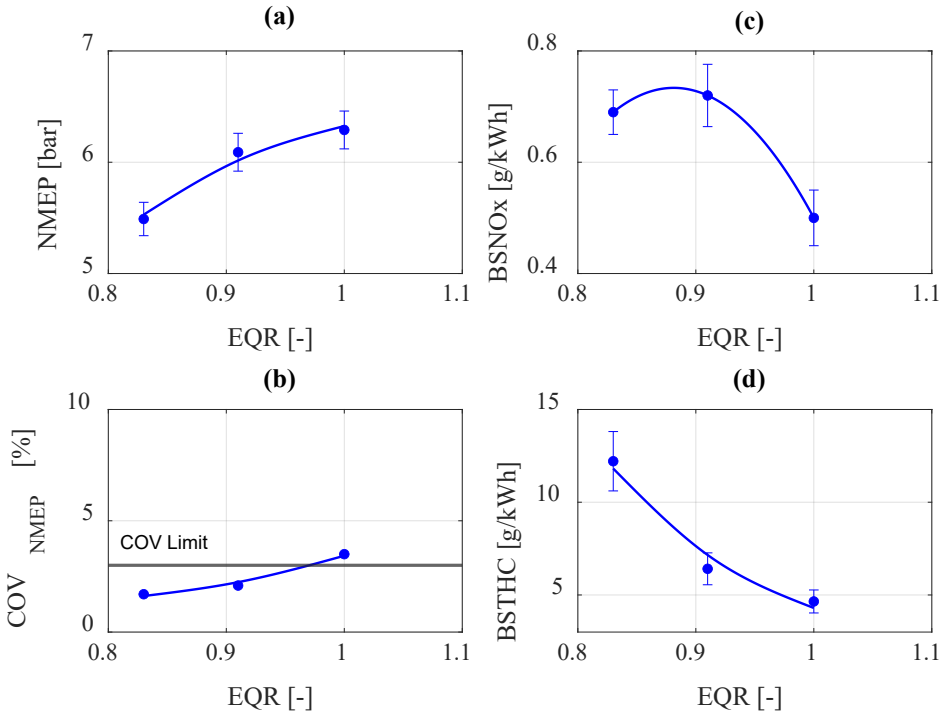

Figure 6-11. Lean operation impacts on load, stability, and engine out emissions. (a) EQR vs NMEP. (b) EQR vs. COVNMEP. (c) EQR vs Brake Specific NOx (BSNOx). (d) EQR vs Brake Specific UHC (BSUHC). CR 15.0 ; 85 kPa MAP ; 35 °C IMAT ; 600 bar Injection Pressure ; Diesel Pilot SOI 15°bTDC ; 1200 RPM ; Pilot Quantity 3.3 mg/inj. ; 12% EGR.

The increase in unburned HC and NOx shown in Figure 6-11 agrees with the literature [31] and makes this strategy undesirable as a traditional TWC aftertreatment system would not be able to reduce NOx emissions in an oxygen-rich exhaust stream. As such, a lean NOx trap or another aftertreatment approach would be needed. Furthermore, the TWC enabled

through stoichiometric operation can effectively control CH4 emissions at operating temperatures as low as 420 °C [32]. However, the effectiveness of these systems for unburned methane control, which is the predominant component of the UHC emissions, under lean conditions is uncertain. In all studies performed in this work, the lowest and the highest post-turbine exhaust gas temperature observed were 523°C and 726°C, respectively, confirming that a TWC could be applied to effectively control CO, NOx and CH4 emissions under stoichiometric conditions. Preliminary testing with a custom TWC system demonstrated >95% reductions in all criteria pollutants and CH¬4 under stoichiometric conditions. Further development of the engine air handling and fueling control systems are needed to ensure robust, low-emission operation over a wider range of steady-state and transient operating conditions.

6.5 Summary and Conclusions

In summary, this work focused on studying the limits of low load operation of a micro-pilot diesel natural gas engine and the effect of controlling parameters including engine hardware by reducing compression ratio and finding the optimum operating condition by sweeping the diesel pilot start of injection and dilution with cooled EGR, as well as adjusting the pilot injection strategy by sweeping injection pressure and injection quantity. These factors were independently investigated with the goal of reaching the minimum load limit while constrained by the need to operate at stoichiometric equivalence ratio, minimum intake manifold pressure, and having stable combustion.

The key conclusions from this work for the tested engine conditions are:

1. The compression ratio impacts the minimum intake manifold pressure that maintains combustion stable. By reducing the compression ratio from 17.3:1 to 15.0:1, the intake manifold pressure had to be increased by 5 kPa, which raised the lowest load achievable by 1 bar NMEP due to the extra premix fuel required to maintain a globally stoichiometric premix.
2. Combustion phasing retard controlled by the diesel micro-pilot start of injection is a way to achieve lower loads. This is a common strategy utilized in spark-ignited

engines. A modified version of the correlation for SI engines is proposed in this work to fit the diesel micro-pilot natural gas combustion system. The micro-pilot engine combustion phasing retard has a slightly stronger impact on the minimum possible load than an SI engine. This shows the importance of the optimum combustion phasing in diesel micro-pilot NG engines.

3. The reduction of pilot injection pressure improves combustion stability by the observed shortening of ignition delay. The lower injection pressure helps keep the pilot fuel-rich zones near the injector tip, facilitating the flame to initiate and spread inside the combustion chamber. The combustion phasing retard caused by the change in injection pressure agrees with the micro-pilot correlation, indicating that the change in injection pressure does not affect the negative impact of combustion phasing retard on NMEP.
4. The effect of diesel injection pressure was observed to be more dominant in low in-cylinder temperatures (i.e., T<900K). This is an important finding to help the development of low-temperature combustion strategies. As the in-cylinder charge temperature is near the diesel auto-ignition limit, the lower injection pressure can improve flame development and combustion stability. This effect becomes negligible as the in-cylinder temperature increases.
5. Adding exhaust gas to the intake can reduce the total fuel ingested while maintaining a stoichiometric mixture, leading to longer diesel pilot ignition delays. The exhaust gas recirculation limit at low load was observed to be 12% as increasing delay in ignition results in unstable combustion beyond this limit, independent of injection pressure and timing.
6. Increasing the diesel pilot quantity can improve the combustion stability at a given operating condition by providing a robust and stable ignition source. This comes at the cost of reducing the total diesel substitution ratio.
7. Lean operations enabled lower loads by reducing the total fuel quantity in the intake premix for a given intake pressure. Lean operation increased NOx and unburned hydrocarbon emissions by 40% and 160%, respectively, while lean operation precludes using a TWC to control NOx emissions.

6.6 References

1. Reitz, R., H. Ogawa, R. Payri, T. Fansler, S. Kokjohn, Y. Moriyoshi, A. Agarwal, D. Arcoumanis, D. Assanis, and C. Bae, (2020) IJER Editorial: The Future of the Internal Combustion Engine. SAGE Publications Sage UK: London, England. DOI: https://doi.org/10.1177/1468087419877990.

2. Karim, G.A., (2015) Dual-Fuel Diesel Engines. CRC Press. Chapters: 3, 5, and 6. DOI: https://doi.org/10.1201/b18163

3. Manns, H.J., M. Brauer, H. Dyja, H. Beier, and A. Lasch, (2015) Diesel CNG-The Potential of a Dual Fuel Combustion Concept for Lower CO2 and Emissions. SAE2015-26-0048. DOI: https://doi.org10.4271/2015-26-0048.

4. Karim, G.A., (2003) Combustion in Gas Fueled Compression Ignition Engines of the Dual Fuel Type. Journal of engineering for gas turbines and power. 125(3): p. 827-836. DOI: https://doi.org/10.1115/1.1581894.

5. Weaver, C.S. and S.H. Turner, (1994) Dual Fuel Natural Gas/Diesel Engines: Technology, Performance, and Emissions. SAE 940548. DOI: https://doi.org/10.4271/940548.

6. Daisho, Y., T. Yaeo, T. Koseki, T. Saito, R. Kihara, and E.N. Quiros, (1995) Combustion and Exhaust Emissions in a Direct-injection Diesel Engine Dual-Fueled with Natural Gas. SAE950465. DOI: https://doi.org/10.4271/950465.

7. Vávra, J., I. Bortel, M. Takáts, and M. Diviš, (2017) Emissions and Performance of Diesel–Natural Gas Dual-Fuel Engine Operated With Stoichiometric Mixture. Fuel. 208: p. 722-733. DOI: https://doi.org/10.1016/j.fuel.2017.07.057.

8. Zheng, J., J. Wang, Z. Zhao, D. Wang, and Z. Huang, (2019) Effect of Equivalence Ratio on Combustion and Emissions of a Dual-Fuel Natural Gas Engine Ignited with

Diesel. Applied Thermal Engineering. 146: p. 738-751. DOI: https://doi.org/10.1016/j.applthermaleng.2018.10.045.

9. Yousefi, A., M. Birouk, and H. Guo, (2017) An Experimental and Numerical Study of the Effect of Diesel Injection Timing on Natural Gas/Diesel Dual-Fuel Combustion at Low Load. Fuel. 203: p. 642-657. DOI: https://doi.org/10.1016/j.fuel.2017.05.009.

10. Zhou, H., H.-W. Zhao, Y.-P. Huang, J.-H. Wei, and Y.-H. Peng, (2019) Effects of Injection Timing on Combustion and Emission Performance of Dual-Fuel Diesel Engine under Low to Medium Load Conditions. Energies. 12(12): p. 2349. DOI: https://doi.org/10.3390/en12122349.

11. Garcia Valladolid, P. and P. Tunestal, (2016) Effects of Intake Manifold Conditions on Dual-Fuel CNG-Diesel Combustion in a Light Duty Diesel Engine Operated at Low Loads. SAE2016-01-0805. DOI: https://doi.org/10.4271/2016-01-0805.

12. Guo, H., W.S. Neill, and B. Liko. An Experimental Investigation on the Combustion and Emissions Performance of a Natural Gas–Diesel Dual Fuel Engine at Low and Medium Loads. in ASME 2015 Internal Combustion Engine Division Fall Technical Conference. 2015. American Society of Mechanical Engineers. DOI: https://doi.org/10.1115/ICEF2015-1041.

13. Papagiannakis, R.G., D.T. Hountalas, C.D. Rakopoulos, and D.C. Rakopoulos, (2008) Combustion and Performance Characteristics of a DI Diesel Engine Operating from Low to High Natural Gas Supplement Ratios at Various Operating Conditions. SAE2008-01-1392. DOI: https://doi.org/10.4271/2008-01-1392.

14. Taniguchi, S., M. Masubuchi, K. Kitano, and K. Mogi, (2012) Feasibility Study of Exhaust Emissions in a Natural Gas Diesel Dual Fuel (DDF) Engine. SAE2012-01-1649. DOI: https://doi.org/10.4271/2012-01-1649.

15. Liu, J., Q. Guo, J. Guo, and F. Wang, (2021) Optimization of a Diesel/Natural Gas Dual Fuel Engine Under Different Diesel Substitution Ratios. Fuel. 305: p. 121522. DOI: https://doi.org/10.1016/j.fuel.2021.121522.

16. Poorghasemi, K., R.K. Saray, E. Ansari, B.K. Irdmousa, M. Shahbakhti, and J.D. Naber, (2017) Effect of Diesel Injection Strategies on Natural Gas/Diesel RCCI Combustion Characteristics in a Light Duty Diesel Engine. Applied Energy. 199: p. 430-446. DOI: https://doi.org/10.1016/j.apenergy.2017.05.011.

17. Wang, Z., Z. Zhao, D. Wang, M. Tan, Y. Han, Z. Liu, and H. Dou, (2016) Impact of Pilot Diesel Ignition Mode on Combustion and Emissions Characteristics of a Diesel/Natural Gas Dual Fuel Heavy-Duty Engine. Fuel. 167: p. 248-256. DOI: https://doi.org/10.1016/j.fuel.2015.11.077.

18. Dronniou, N., J. Kashdan, B. Lecointe, K. Sauve, and D. Soleri, (2014) Optical Investigation of Dual-fuel CNG/Diesel Combustion Strategies to Reduce CO_2 Emissions. SAE2014-01-1313. 7(2): p. 873-887. DOI: https://doi.org/10.4271/2014-01-1313.

19. Jamrozik, A., W. Tutak, and K. Grab-Rogaliński, (2019) An Experimental Study on the Performance and Emission of the diesel/CNG Dual-Fuel Combustion Mode in a Stationary CI Engine. Energies. 12(20): p. 3857. DOI: https://doi.org/10.3390/en12203857.

20. You, J., Z. Liu, Z. Wang, D. Wang, and Y. Xu, (2020) Experimental Analysis of Inert Gases in EGR On Engine Power and Combustion Characteristics in a Stoichiometric Dual Fuel Heavy-Duty Natural Gas Engine Ignited with Diesel. Applied Thermal Engineering. 180: p. 115860. DOI: https://doi.org/10.1016/j.applthermaleng.2020.115860.

21. Naber, J.D., (2020) High Brake Mean Effective Pressure and High Efficiency Micro Pilot Ignition Natural Gas Engine: United States. p. Final Report. DOI: https://doi.org/10.2172/1605097.

22. Taylor, B.N. and C.E. Kuyatt, (1994) Guidelines for Evaluating and Expressing the Encertainty of NIST Measurement Results. NIST Technical Note 1297. DOI: https://doi.org/10.6028/nist.tn.1297

23. "Wärtsilä Methane Number Calculator". 2021 [Accessed on 06/09 2021]; Available from: https://www.wartsila.com/marine/build/gas-solutions/methane-number-calculator.

24. Bonfochi Vinhaes, V., X. Yang, B. Eggart, G. McTaggart-Cowan, S.R. Munshi, J.D. Naber, and M. Shahbakhti, (2022) Multi-Variable Sensitivity Analysis and Ranking of Control Factors Impact in a Stoichiometric Micro-Pilot Natural Gas Engine at Medium Loads. SAE Technical Paper: 22PFL-0539 ,2022 SAE World Congress.

25. Ayala, F.A., M.D. Gerty, and J.B. Heywood, (2006) Effects of Combustion Phasing, Relative Air-Fuel Ratio, Compression Ratio, and Load on SI Engine Efficiency. SAE2006-01-0229: p. 177-195. DOI: https://doi.org/10.4271/2006-01-0229.

26. Khosravi, M., J. Rochussen, J. Yeo, P. Kirchen, G. McTaggart-Cowan, and N. Wu. Effect of Fuelling Control Parameters on Combustion Characteristics of Diesel-Ignited Natural Gas Dual-Fuel Combustion in an Optical Engine. in ASME 2016 Internal Combustion Engine Division Fall Technical Conference. 2016. DOI: https://doi.org/10.1115/icef2016-9399.

27. Abd Alla, G.H., H.A. Soliman, O.A. Badr, and M.F. Abd Rabbo, (1999) Effect of Pilot Fuel Quantity on the Performance of a Dual Fuel Engine. SAE1999-01-3597. DOI: https://doi.org/10.4271/1999-01-3597.

28. Liu, J., F. Yang, H. Wang, M. Ouyang, and S. Hao, (2013) Effects of Pilot Fuel Quantity on the Emissions Characteristics of a CNG/Diesel Dual Fuel Engine with Optimized Pilot Injection Timing. Applied Energy. 110: p. 201-206. DOI: https://doi.org/10.1016/j.apenergy.2013.03.024.

29. Papagiannakis, R., D. Hountalas, and C. Rakopoulos, (2007) Theoretical Study of the Effects of Pilot Fuel Quantity and its Injection Timing on the Performance and Emissions of a Dual Fuel Diesel Engine. Energy Conversion and Management. 48(11): p. 2951-2961. DOI: https://doi.org/10.1016/j.enconman.2007.07.003.

30. Zirngibl, S. and G. Wachtmeister, (2016) Extensive Investigation of a Common Rail Diesel Injector Regarding Injection Characteristics and the Resulting Influences on the Dual Fuel Pilot Injection Combustion Process. SAE2016-01-0780. DOI: https://doi.org/10.4271/2016-01-0780.

31. Heywood, J.B., (2018) Internal Combustion Engine Fundamentals. McGraw-Hill Education. Chapters: 4 and 11. ISBN: 1260116107.

32. Smith, I., J. Chiu, G. Bartley, E. Jimenez, T. Briggs, and C. Sharp, (2018) Achieving Fast Catalyst Light-Off from a Heavy-Duty Stoichiometric Natural Gas Engine Capable of 0.02 g/bhp-hr NO X Emissions. SAE2018-01-1136. DOI: https://doi.org/10.4271/2018-01-1136.

7 SUMMARY AND CONCLUSIONS

This dissertation focused on understanding the potential of a combustion system that combines a diesel micro-pilot ignition with a globally stoichiometric NG premixed charge in medium/heavy duty engines to benefit from both dedicated SI NG and lean-burn diesel piloted NG technologies. The study involved developing the micro-pilot engine testbed, including the compression ratio reduction, the air handling system (i.e., air-fuel-EGR mixer, selection of a controllable wastegate turbocharger, and the addition of a throttle valve), the fuel system (i.e., NG fueling rail and diesel injector), the installation of a TWC, and the development of a custom control strategy, followed by extensive experimental investigation of the micro-pilot concept at low, medium and high load operating condition.

A peak BMEP of 23 bar with 41% BTE was achieved for maximum load investigation. The peak BMEP was limited by pre-ignition and turbine inlet temperature. At medium load conditions representative of loaded cruising, the micro-pilot engine achieved a BTE of 40%, nearly equivalent to the efficiency of the base diesel engine. This also resulted in CO_2 emissions 20% lower than the base diesel engine.

The micro-pilot engine was observed to have equivalent BTE to the SI engine under low-load conditions (29% for Micro-Pilot; 29% for NG-SI; 35% for Diesel). This is due to SI-like performance, including intake air throttling losses due to the stoichiometric operation.

An experimental study described in Appendix 9C investigated the effect of cooled EGR on the combustion and emissions characteristics of the micro-pilot engine. The engine was operated at medium loads (11 bar BMEP @ 1620 RPM) with levels of EGR from 0% to 15% while keeping load and combustion phasing constant. At 15% EGR, the ignition delay was 31% longer, with a 56% longer combustion duration than the condition with no EGR. Moreover, engine-out NOx emissions were reduced by 84%, while UHC doubled. It was observed that the cyclic variability of the ignition delay and combustion duration was below 1% and 10%, respectively, with stable combustion. Additional investigation is

required to assess the EGR tolerance over a range of loads and speeds in the micro-pilot engine, and it is part of the future work discussed in Chapter 8.

The stoichiometric operation was maintained under all operating conditions investigated. This enables the employment of a TWC to achieve low tailpipe emissions. Exhaust gas temperatures on the order of 650°C were observed even at the lowest load achieved, well above the temperature required for TWC operation (including methane oxidation).

The conclusions from the study relating back to the specific objectives of the dissertation are outlined as follows:

Objective 1: Identify the dominant factors and their impact on maximizing the thermal efficiency at medium loads. This provides the basis for understanding the primary factors that control engine performance and a path forward for developing a high-efficiency engine with an optimized fuel and air handling system.

- A Taguchi Orthogonal approach was carried out to systematically study, quantify, and rank the controlling factors for the combustion and performance of the micro-pilot engine operating at medium load. This design of experiments strategy is employed to reduce the cost and the total number of required tests to investigate engine performance.
- A literature review revealed that the most common combustion control factors studied include the diesel pilot start of injection and injection pressure, charge dilution, substitution ratio of diesel to total fuel, boost pressure, and intake manifold air temperature.
- The identified control factors were systematically studied, and their impact on common combustion and performance metrics (e.g., BTE, combustion knock, combustion stability, combustion phasing, combustion duration, load, and ignition delay). It was observed that, while keeping the equivalence ratio constrained to stoichiometric operation, the diesel pilot injection timing and EGR are the most influential factors in maximizing BTE. Of these, advancing the pilot start of

injection and reducing EGR is the desired strategy to achieve the highest possible efficiency.

- Across the various performance measures evaluated in this study, EGR and diesel pilot start of injection were the most prominent control factors for controlling combustion and performance in this operating regime. Intake temperature and diesel pilot injection pressure, on the other hand, were shown to be the least sensitive.
- These findings provide an improved understanding of the primary governing elements and their responses in the stoichiometric micro-pilot engine operation at medium loads and an overall guideline for combustion development and control.

Objective 2: Determine the factors that positively and negatively impact combustion stability at low load. The results provide a quantitative assessment of the individual factors and their impact on combustion stability. This investigation also provides insights on how to best overcome the limitations of this operating condition.

- By utilizing the results from the Taguchi Orthogonal Matrix investigation at medium loads as guidance, an experimental program was undertaken to study the limits of low load operation and the effect of control parameters, including the diesel pilot start of injection, dilution with cooled EGR, pilot injection pressure, injection quantity, and reducing the compression ratio. The lowest load achieved while operating stoichiometric was 6.2 bar NMEP at the reduced compression ratio (CR 15.0) and 5.0 bar NMEP at the original compression ratio (CR 17.3).
- The compression ratio influenced the minimal intake manifold pressure that keeps combustion stable. The intake manifold pressure had to be increased from 80 kPa to 85 kPa when the compression ratio was modified from 17.3:1 to 15.0:1, respectively. Due to the extra premix fuel required to maintain a globally stoichiometric mixture, the lowest load attainable was increased by 1 bar NMEP.
- Lower loads can be achieved by delaying combustion phasing, controlled by the diesel micro-pilot start of injection. This is one of the techniques used in spark-ignited engines to reduce load, as it shifts the combustion process to the expansion

stroke. This research proposes a modified version of the SI engine correlation found in the literature to fit the diesel micro-pilot natural gas combustion system. It was observed that the micro-pilot engine combustion phasing retard has a slightly stronger impact on the minimum possible load than an SI engine. For CA50s of up to 10° more retarded than $CA50_{MBT}$, the micro-pilot engine has the same load reduction seen in the SI engine. However, for CA50s that occur later than 10° more than $CA50_{MBT}$, a 0.2% load reduction per degree was observed relative to the SI engine correlation. This highlights the importance of optimum combustion phasing in the micro-pilot engine.

- The reduction of pilot injection pressure improves combustion stability by the observed shortening of ignition delay. The lower injection pressure helps keep the pilot fuel-rich zones near the injector tip, facilitating the flame to initiate and spread inside the combustion chamber. The effect of diesel injection pressure was observed to be more dominant in low-load operating conditions due to the lower in-cylinder temperature caused by the low intake manifold pressure. As the in-cylinder charge temperature is near the diesel auto-ignition limit, the lower injection pressure can improve flame development and combustion stability. This effect becomes negligible as the in-cylinder temperature increases.
- Adding exhaust gas to the intake can reduce the total fuel ingested at a fixed intake manifold pressure while maintaining a stoichiometric mixture, leading to longer diesel pilot ignition delays. The exhaust gas recirculation limit at low load was found to be 12%, as increasing delay in ignition results in unstable combustion beyond this limit, independent of injection pressure and timing.
- Increasing the diesel pilot quantity can improve the combustion stability at a given operating condition by providing a higher ignition energy source. This comes at the cost of reducing the total diesel substitution ratio.
- Lean operations enabled lower loads by reducing the total fuel quantity in the intake premix for a given intake pressure. Reducing the EQR by 20% enabled the minimum load to be reduced by 12%, with the tradeoff of an increase in engine-out unburned hydrocarbons by 160%. At this condition, engine-out NOx emission

increased by 40% compared to the stoichiometric operation. However, the lean operation precludes using a TWC to control NOx emissions.

- Other strategies, such as variable valve timing, cylinder deactivation, lower intake manifold pressure, and hot EGR are potential solutions to further reduce the low-load limit below this limit. However, their implications for the aftertreatment system will need to be investigated further. Low load and idle situations may eventually be run in diesel-only mode, with NOx managed by charge dilution and combustion phasing optimization.

Objective 3: Specify the positive and negative factors for reducing combustion knock impact via a medium load sensitivity study. As discussed later in this dissertation, pre-ignition and high injector tip temperatures due to the reduced diesel flow are limiting factors for high load operation. However, understanding the impact of the controlling factors that can be used towards minimizing combustion knock occurrence is critical. The results obtained in the medium load investigation provided insights for achieving high load output at the limit of combustion knock.

- An experimental study was conducted to identify the micro-pilot system's maximum load output. While it was possible to achieve 24 bar BMEP, the high load operation was limited by severe abnormal combustions (combustion knock and pre-ignition) and exhaust (turbocharger inlet) temperature. At this condition, the diesel micro-pilot injection contributed to only 3% of the total fuel energy.
- An inspection of the diesel injectors carried out post high load investigations revealed signs of internal carbon build-up inside the injector, likely due to diesel pyrolyzing under high temperatures. Additionally, the injector needle showed a significant amount of black residue, likely caused by the evaporation of lighter compounds. Despite the absence of direct validation, it is safe to conclude that the residue was created by high temperatures inside the nozzle due to lower diesel flow, which resulted in less cooling. Anti-coking additives (Powerzol 9040 series) successfully prevented injector coking for the remainder of the experimental investigations with no signs of cetane enhancement.

- A combustion control parameter sensitivity analysis (including pilot SOI, pilot injection pressure, pilot injection quantity, intake temperature, and EGR) was conducted to identify knock control parameters at medium load and avoid diesel injector fouling due to high tip temperature. It was observed that combustion knock was primarily controlled by EGR, pilot pulse width, and the diesel pilot SOI. These findings are consistent with what has been reported in the literature. EGR increases the in-cylinder charge heat capacity and reduces overall end gas temperature and combustion knock propensity. The pilot pulse width determines the diesel pilot quantity influencing the ignition delay and combustion duration. Pilot SOI affects the start of combustion and combustion phasing, which, similar to SI engines, leads to higher in-cylinder temperatures and increases combustion knock propensity.
- The results of experimental studies at high load conditions (i.e., 16 bar and 23 bar BMEP) can be found in Appendix 9A; a strong correlation between pilot SOI and combustion knock peak-to-peak was observed at 16 bar BMEP, confirming the effect seen at the medium load study. The addition of EGR and pilot SOI control enabled 23 bar BMEP to be operated with no combustion knock. At this condition, turbocharger inlet temperature and combustion knock constrained operations at different diesel pilot SOIs. It is expected that the controlling factors observed to impact combustion knock at medium loads are similar at high load operation that is not limited by pre-ignition.
- The high injector tip temperature at high loads is still a challenge, and optimizing low flow injectors with enhanced cooling is required.

Objective 4: Investigate the ability of a TWC to effectively minimize emissions (i.e., UHC, CO, NOx) and its sensitivity to equivalence ratio. This helps determine if the application of a TWC is feasible and provides a path forward to optimize the design of components (i.e., piston).

- An EQR study to determine the TWC sensitivity and efficiency at medium loads was carried out. The engine was operated at a steady-state condition of 1200 RPM and 8 bar BMEP with no EGR and micro-pilot DSR. Equivalence ratio was varied

from 0.94 (lean) to 1.06 (rich). It was shown that a high conversion efficiency (>99%) of CO, NOx, and UHC can be achieved at EQR=1.01.

- The system was sensitive to EQR, consistent with TWC operation. In a production scenario, oxygen storage would be required, and a control system similar to that used in today's stoichiometric on-road engines for controlling lambda biasing via upstream and downstream oxygen sensors. Because the exhaust temperature is within the operating range for high conversion without excessive catalyst aging, very low emissions are expected with this management.
- These findings are an indication that very low NOx, UHC, and CO can be achieved while avoiding the complicated system integration and controls required by multi-component aftertreatment systems utilized in modern diesel engines. Further investigation is required to determine if such an approach is a viable solution to meet current EPA ultra-low NOx (0.02 g/bhp) emissions standards.

In summary, these results demonstrated that the stoichiometric micro-pilot concept can achieve efficiencies that approach those of an equivalent diesel engine with diesel-like BMEPs, with a CO_2 emissions reduction potential of up to 25%, and the possibility to employ a TWC to target very low NOx levels that meet the California ultra-low NOx standard (0.02 g/bhph).

8 FUTURE WORK

With the conclusions outlined in Chapter 7, several aspects of the combustion and engine system require further research to increase the understanding of micro-pilot technology from practical and fundamental perspectives. The utilization of an optically accessible vessel and/or engine, coupled with 1-D and 3-D simulation, can provide further improvement to engine development. The key areas that can be explored further include:

- Diesel fuel system optimization and thermal management: Evaluate injectors with a smaller number of holes to provide better ignition/control stability at low loads. Develop approaches for controlling injector temperature to avoid fouling.

- Impact of Natural Gas composition: Investigate the impact of different natural gas compositions on the performance of the micro-pilot engine, including the limits of combustion (e.g., low load combustion stability and combustion knock).

- Exhaust Gas Recirculation tolerance: Investigate the micro-pilot engine dilution tolerance using EGR at different operating conditions (i.e., Low-load, Medium-load, and High-load) and how it compares to an SI-NG and CI-diesel counterparts. Develop strategies to extend the dilution limit.

- Air handling system optimization: Sizing and control of turbocharger, wastegate, intake throttle, and air and EGR coolers to improve overall system performance.

- Base engine thermal management: Investigate thermal impacts of stoichiometric micro-pilot combustion approach on engine components (piston, cylinder head, valves, manifolds); identify components that are at risk.

- Low-load lean diesel combustion process development: Develop a lean, dilute diesel-only combustion process to enable engine operation at low loads within PM and NOx emissions constraints.

- Control system development: Develop a control system module, develop closed-loop air and fueling control, and initiate preliminary development of combustion knock control and transient control approaches to maintain ignition at low loads.

9 BIBLIOGRAPHY

1. Reitz R, Ogawa H, Payri R, et al. IJER Editorial: The Future of the Internal Combustion Engine. 2020. DOI: https://doi.org/10.1177/1468087419877990.
2. Manns HJ, Brauer M, Dyja H, et al. Diesel CNG-The Potential of a Dual Fuel Combustion Concept for Lower CO2 and Emissions. *SAE2015-26-0048* 2015. DOI: https://doi.org/10.4271/2015-26-0048.
3. Andruleit H. BA, et al. BGR (2013): Energy Study 2013. Reserves, resources and availability of energy resources. 2013: 112.
4. Nalley S and LaRose A. Annual energy outlook 2022. *United States Energy Information Administration: Washington DC* 2022.
5. Ou X and Zhang X. Life-Cycle Analyses of Energy Consumption and GHG Emissions of Natural Gas-Based Alternative Vehicle Fuels in China. *Journal of Energy* 2013; 2013: 268263. DOI: https://doi.org/10.1155/2013/268263.
6. Moniz EJ, Jacoby HD, Meggs AJ, et al. The future of natural gas. *Cambridge, MA: Massachusetts Institute of Technology* 2011. DOI: ISBN: 9780982800836.
7. FMI. Automotive Natural Gas Vehicle Market, (2022, accessed 03/21 2022).
8. Intelligence M. Heavy-Duty Truckes Market - Growth, Trends, COVID-19 Impact, and Forecast, (2022, accessed 03/20 2022).
9. Karim GA. *Dual-Fuel Diesel Engines*. CRC Press: Boca Raton, FL, USA, 2015, p.Chapters: 3, 5, and 6.
10. Hesterberg T, Bunn W and Lapin C. An evaluation of criteria for selecting vehicles fueled with diesel or compressed natural gas. *Sustainability: Science, Practice and Policy* 2009; 5: 20-30. DOI: https://doi.org/10.1080/15487733.2009.11908025.
11. Xian H, Karali B, Colson G, et al. Diesel or compressed natural gas? A real options evaluation of the US natural gas boom on fuel choice for trucking fleets. *Energy* 2015; 90: 1342-1348. DOI: https://doi.org/10.1016/j.energy.2015.06.080.
12. Curran SJ, Wagner RM, Graves RL, et al. Well-to-wheel analysis of direct and indirect use of natural gas in passenger vehicles. *Energy* 2014; 75: 194-203. DOI: https://doi.org/10.1016/j.energy.2014.07.035.
13. Chala GT, Abd Aziz AR and Hagos FY. Natural gas engine technologies: challenges and energy sustainability issue. *Energies* 2018; 11: 2934. DOI: https://doi.org/10.3390/en11112934.
14. Salman CA, Schwede S, Thorin E, et al. Enhancing biomethane production by integrating pyrolysis and anaerobic digestion processes. *Applied Energy* 2017; 204: 1074-1083. DOI: https://doi.org/10.1016/j.apenergy.2017.05.006.
15. Görling M, Larsson M and Alvfors P. Bio-methane via fast pyrolysis of biomass. *Applied energy* 2013; 112: 440-447. DOI: https://doi.org/10.1016/j.apenergy.2013.01.002.
16. CARB LCFS Pathway Certified Carbon Intensities, (2022, accessed 03/08 2022).
17. Semin RAB. A technical review of compressed natural gas as an alternative fuel for internal combustion engines. *Am J Eng Appl Sci* 2008; 1: 302-311.

18. Heywood JB. *Internal Combustion Engine Fundamentals*. McGraw-Hill Education, 2018, p.Chapters: 4 and 11.
19. Willems H and Sierens R. Modeling the initial growth of the plasma and flame kernel in SI engines. *J Eng Gas Turbines Power* 2003; 125: 479-484. DOI: https://doi.org/10.1115/1.1501912.
20. Arcoumanis C and Kamimoto T. *Flow and combustion in reciprocating engines*. Springer Science & Business Media, 2009.
21. Aleiferis PG, Taylor AM, Whitelaw JH, et al. Cyclic variations of initial flame kernel growth in a Honda VTEC-E lean-burn spark-ignition engine. *SAE transactions* 2000: 1340-1380. DOI: https://doi.org/10.4271/2000-01-1207.
22. Cho HM and He B-Q. Spark ignition natural gas engines—A review. *Energy conversion and management* 2007; 48: 608-618. DOI: https://doi.org/10.1016/j.enconman.2006.05.023.
23. Hassan MH, Kalam MA, Mahlia TI, et al. Experimental test of a new compressed natural gas direct injection engine. *Energy & fuels* 2009; 23: 4981-4987. DOI: https://doi.org/10.1021/ef8011382.
24. Kalam M and Masjuki H. An experimental investigation of high performance natural gas engine with direct injection. *Energy* 2011; 36: 3563-3571. DOI: https://doi.org/10.1016/j.energy.2011.03.066.
25. Nijboer M. The contribution of natural gas vehicles to sustainable transport. *International Energy Agency: Paris, France* 2010; 2079-2581.
26. Hagos FY, Aziz ARA and Sulaiman SA. Combustion characteristics of late injected CNG in a spark ignition engine under lean operating condition. *Journal of Applied Sciences* 2012; 12: 2368-2375. DOI: https://doi.org/10.3923/jas.2012.2368.2375.
27. Karim GA. Combustion in Gas Fueled Compression Ignition Engines of the Dual Fuel Type. *Journal of engineering for gas turbines and power* 2003; 125: 827-836. DOI: https://doi.org/10.1115/1.1581894.
28. Di Iorio S, Magno A, Mancaruso E, et al. Diesel/methane dual fuel strategy to improve environmental performance of energy power systems. *International Journal of Heat and Technology* 2016; 34: 581-588. DOI: https://doi.org/10.18280/ijht.34S254.
29. Kubesh J and Brehob DD. Analysis of Knock in a Dual-Fuel Engine. SAE International, 1992.
30. Weaver CS and Turner SH. Dual Fuel Natural Gas/Diesel Engines: Technology, Performance, and Emissions. *SAE 940548* 1994. DOI: https://doi.org/10.4271/940548.
31. Daisho Y, Yaeo T, Koseki T, et al. *Combustion and Exhaust Emissions in a Direct-injection Diesel Engine Dual-Fueled with Natural Gas*. 1995. United States.
32. Chen H, He J and Zhong X. Engine combustion and emission fuelled with natural gas: a review. *Journal of the Energy Institute* 2019; 92: 1123-1136. DOI: https://doi.org/10.1016/j.joei.2018.06.005.
33. Li M, Wu H, Zhang T, et al. A comprehensive review of pilot ignited high pressure direct injection natural gas engines: Factors affecting combustion, emissions and performance. *Renewable and Sustainable Energy Reviews* 2020; 119: 109653. DOI: https://doi.org/10.1016/j.rser.2019.109653.
34. Korakianitis T, Namasivayam A and Crookes R. Natural-gas fueled spark-ignition (SI) and compression-ignition (CI) engine performance and emissions. *Progress in energy*

and combustion science 2011; 37: 89-112. DOI: https://doi.org/10.1016/j.pecs.2010.04.002.
35. Umierski M and Stommel P. Fuel Efficient Natural Gas Engine with Common-Rail Micro-Pilot Injection. 2000. DOI: https://doi.org/10.4271/2000-01-3080.
36. Mitchell R and Kocsis M. Performance Evaluation of Dedicated EGR on a 12 L Natural Gas Engine. *SAE20190-01-1143* 2019. DOI: https://doi.org/10.4271/2019-01-1143.
37. Joshi S, Dahodwala M, Koehler EW, et al. Trade-Off Analysis and Systematic Optimization of a Heavy-Duty Diesel Hybrid Powertrain. *SAE2020-01-0847* 2020. DOI: https://doi.org/10.4271/2020-01-0847.
38. Naber J and Johnson J. Internal combustion engine cycles and concepts. Alternative Fuels and Advanced Vehicle Technologies for Improved Environmental Performance. 2014: 197-224. DOI: https://doi.org/10.1533/9780857097422.2.197.
39. Karim GA. The Dual Fuel Engine. *In: Evans RL (eds) Automotive Engine Alternatives Springer, Boston, MA* 1987: 83-104. DOI: https://doi.org/10.1007/978-1-4757-9348-2_3.
40. Hodgins KB, Hill PG, Ouellette P, et al. Directly injected natural gas fueling of diesel engines. 1996. DOI: https://doi.org/10.4271/961671.
41. Goudie D, Dunn M, Munshi S, et al. *Development of a compression ignition heavy duty pilot-ignited natural gas fuelled engine for low NOx emissions*. Report no. 0148-7191, 2004. SAE Technical Paper 2004-01-2954.
42. Munshi S, McTaggart-Cowan G, Huang J, et al. Development of a partially-premixed combustion strategy for a low-emission, direct injection high efficiency natural gas engine. *ASME 2011 Internal Combustion Engine Division Fall Technical Conference* 2011: 515-528. DOI: https://doi.org/10.1115/ICEF2011-60181.
43. Faghani E, Kheirkhah P, Mabson CW, et al. Effect of injection strategies on emissions from a pilot-ignited direct-injection natural-gas engine-part ii: slightly premixed combustion. 2017. DOI: https://doi.org/10.4271/2017-01-0763.
44. Shah A, Thipse SS, Tyagi A, et al. Literature Review and Simulation of Dual Fuel Diesel-CNG Engines. 2011. DOI: https://doi.org/10.4271/2011-26-0001.
45. McTaggart-Cowan G, Jones H, Rogak S, et al. The effects of high-pressure injection on a compression-ignition, direct injection of natural gas engine. *ASME 2005 Internal Combustion Engine Division Fall Technical Conference* 2005: 161-173. DOI: https://doi.org/10.1115/ICEF2005-1213.
46. McTaggart-Cowan G, Bushe W, Hill P, et al. Nox. reduction from a heavy-duty diesel engine with direct injection of natural gas and cooled exhaust gas recirculation. *International Journal of Engine Research* 2004; 5: 175-191. DOI: https://doi.org/10.1243/146808704773564578.
47. Lin Z and Su W. A Study On the Determination of the Amount of Pilot Injection and Rich and Lean Boundaries of the Pre-Mixed CNG/Air Mixture for a CNG/Diesel Dual-Fuel Engine. SAE International, 2003.
48. Uma R, Kandpal T and Kishore V. Emission characteristics of an electricity generation system in diesel alone and dual fuel modes. *Biomass and bioenergy* 2004; 27: 195-203. DOI: https://doi.org/10.1016/j.biombioe.2004.01.003.

49. Liu J, Yang F, Wang H, et al. Effects of Pilot Fuel Quantity on the Emissions Characteristics of a CNG/Diesel Dual Fuel Engine with Optimized Pilot Injection Timing. *Applied Energy* 2013; 110: 201-206. DOI: https://doi.org/10.1016/j.apenergy.2013.03.024.
50. Gebert K, Beck NJ, Barkhimer RL, et al. Strategies to improve combustion and emission characteristics of dual-fuel pilot ignited natural gas engines. 1997. DOI: https://doi.org/10.4271/971712.
51. Danyluk PR. Development of a high-output dual-fuel engine. *Journal of engineering for gas turbines and power* 1993; 115: 728-733. DOI: https://doi.org/10.1115/1.2906766.
52. Munshi SR, McTaggart-Cowan GP, Bushe WK, et al. Injection Parameter Effects on a Direct Injected, Pilot Ignited, Heavy Duty Natural Gas Engine with EGR. SAE International, 2003.
53. Munshi SR, McTaggart-Cowan GP, Bushe WK, et al. The Effects of Varying EGR Test Conditions on a Direct Injection of Natural Gas Heavy-Duty Engine with High EGR Levels. SAE International, 2004.
54. Rochussen J, McTaggart-Cowan G and Kirchen P. Parametric study of pilot-ignited direct-injection natural gas combustion in an optically accessible heavy-duty engine. *International Journal of Engine Research* 2020; 21: 497-513. DOI: https://doi.org/10.1177/1468087419836877.
55. Zheng J, Wang J, Zhao Z, et al. Effect of Equivalence Ratio on Combustion and Emissions of a Dual-Fuel Natural Gas Engine Ignited with Diesel. *Applied Thermal Engineering* 2019; 146: 738-751. DOI: https://doi.org/10.1016/j.applthermaleng.2018.10.045.
56. Yousefi A, Birouk M and Guo H. An Experimental and Numerical Study of the Effect of Diesel Injection Timing on Natural Gas/Diesel Dual-Fuel Combustion at Low Load. *Fuel* 2017; 203: 642-657. DOI: https://doi.org/10.1016/j.fuel.2017.05.009.
57. Zhou H, Zhao H-W, Huang Y-P, et al. Effects of Injection Timing on Combustion and Emission Performance of Dual-Fuel Diesel Engine under Low to Medium Load Conditions. *Energies* 2019; 12: 2349. DOI: https://doi.org/10.3390/en12122349.
58. Papagiannakis R, Hountalas D and Rakopoulos C. Theoretical Study of the Effects of Pilot Fuel Quantity and its Injection Timing on the Performance and Emissions of a Dual Fuel Diesel Engine. *Energy Conversion and Management* 2007; 48: 2951-2961. DOI: https://doi.org/10.1016/j.enconman.2007.07.003.
59. Papagiannakis R and Hountalas D. Combustion and Exhaust Emission Characteristics of a Dual Fuel Compression Ignition Engine Operated with Pilot Diesel Fuel And Natural Gas. *Energy conversion and management* 2004; 45: 2971-2987. DOI: https://doi.org/10.1016/j.enconman.2004.01.013.
60. Papagiannakis RG, Hountalas DT, Rakopoulos CD, et al. Combustion and Performance Characteristics of a DI Diesel Engine Operating from Low to High Natural Gas Supplement Ratios at Various Operating Conditions. SAE2008-01-1392, 2008.
61. Guo H, Neill WS and Liko B. An Experimental Investigation on the Combustion and Emissions Performance of a Natural Gas–Diesel Dual Fuel Engine at Low and Medium Loads. *ASME 2015 Internal Combustion Engine Division Fall Technical Conference* 2015: V001T003A005-V001T003A005. DOI: https://doi.org/10.1115/ICEF2015-1041.

62. Liu J, Guo Q, Guo J, et al. Optimization of a Diesel/Natural Gas Dual Fuel Engine Under Different Diesel Substitution Ratios. *Fuel* 2021; 305: 121522. DOI: https://doi.org/10.1016/j.fuel.2021.121522.
63. Rochussen J, Yeo J and Kirchen P. Effect of Fueling Control Parameters on Combustion and Emissions Characteristics of Diesel-Ignited Methane Dual-Fuel Combustion. 2016. DOI: https://doi.org/10.4271/2016-01-0792.
64. Azimov U, Tomita E and Kawahara N. Ignition, Combustion and Exhaust Emission Characteristics of Micro-pilot Ignited Dual-fuel Engine Operated under PREMIER Combustion Mode. *SAE2011-01-1764* 2011. DOI: https://doi.org/10.4271/2011-01-1764.
65. Valladolid PG and Tunestal P. Effects of Intake Manifold Conditions on Dual-Fuel CNG-Diesel Combustion in a Light Duty Diesel Engine Operated at Low Loads. *SAE2016-01-0805* 2016. DOI: https://doi.org/10.4271/2016-01-0805.
66. Krishnan SR, Srinivasan KK and Midkiff KC. Ignition in pilot-ignited natural gas low temperature combustion: multi-zone modeling and experimental results. *Internal Combustion Engine Division Spring Technical Conference* 2009; 43406: 625-634. DOI: https://doi.org/10.1115/ICES2009-76145.
67. Qi Y, Srinivasan K, Krishnan S, et al. Effect of hot exhaust gas recirculation on the performance and emissions of an advanced injection low pilot-ignited natural gas engine. *International Journal of Engine Research* 2007; 8: 289-303. DOI: https://doi.org/10.1243/14680874JER02306.
68. Vávra J, Bortel I, Takáts M, et al. Emissions and Performance of Diesel–Natural Gas Dual-Fuel Engine Operated With Stoichiometric Mixture. *Fuel* 2017; 208: 722-733. DOI: https://doi.org/10.1016/j.fuel.2017.07.057.
69. Taniguchi S, Masubuchi M, Kitano K, et al. Feasibility Study of Exhaust Emissions in a Natural Gas Diesel Dual Fuel (DDF) Engine. *SAE2012-01-1649* 2012. DOI: https://doi.org/10.4271/2012-01-1649.
70. Yang X, Bonfochi Vinhaes V, Turcios M, et al. Process for Study of Micro-pilot Diesel-NG Dual Fuel Combustion in a Constant Volume Combustion Vessel Utilizing the Premixed Pre-burn Procedure. *SAE2019-01-1160* 2019; 1. DOI: https://doi.org/10.4271/2019-01-1160.
71. Zirngibl S and Wachtmeister G. Extensive Investigation of a Common Rail Diesel Injector Regarding Injection Characteristics and the Resulting Influences on the Dual Fuel Pilot Injection Combustion Process. *SAE2016-01-0780* 2016. DOI: https://doi.org/10.4271/2016-01-0780.
72. Choi M, Mohiuddin K and Park S. Effects of methane ratio on MPDF (micro-pilot dual-fuel) combustion characteristic in a heavy-duty single cylinder engine. *Scientific reports* 2021; 11: 1-16. DOI: https://doi.org/10.1038/s41598-021-89161-z.
73. Jamrozik A, Tutak W and Grab-Rogaliński K. An Experimental Study on the Performance and Emission of the diesel/CNG Dual-Fuel Combustion Mode in a Stationary CI Engine. *Energies* 2019; 12: 3857. DOI: https://doi.org/10.3390/en12203857.
74. You J, Liu Z, Wang Z, et al. Experimental Analysis of Inert Gases in EGR On Engine Power and Combustion Characteristics in a Stoichiometric Dual Fuel Heavy-Duty Natural Gas Engine Ignited with Diesel. *Applied Thermal Engineering* 2020; 180: 115860. DOI: https://doi.org/10.1016/j.applthermaleng.2020.115860.

75. Bonfochi Vinhaes V, McTaggart-Cowan G, Munshi S, et al. Experimental Studies of Low-Load Limit in a Stoichiometric Micro-Pilot Diesel Natural Gas Engine. *Energies* 2022; 15: 728. DOI: https://doi.org/10.3390/en15030728.
76. Bonfochi Vinhaes V, Yang X, McTaggart-Cowan G, et al. Multi-Variable Sensitivity Analysis and Ranking of Control Factors Impact in a Stoichiometric Micro-Pilot Natural Gas Engine at Medium Loads. 2022. DOI: https://doi.org/10.4271/2022-01-0463.
77. Bonfochi Vinhaes V, Yang X, McTaggart-Cowan G, et al. Development of a Medium-Duty Stoichiometric Diesel Micro-Pilot Natural Gas Engine. *International Journal of Engine Research: Accepted for publication* 2022.
78. Wang Z, Ding H, Ma X, et al. Ultra-High Speed Imaging Study of the Diesel Spray Close to the Injector Tip at the Initial Opening Stage with Single Injection. *Applied energy* 2016; 165: 335-344. DOI: https://doi.org/10.1016/j.apenergy.2015.12.046.
79. Wang Z, Zhao Z, Wang D, et al. Impact of Pilot Diesel Ignition Mode on Combustion and Emissions Characteristics of a Diesel/Natural Gas Dual Fuel Heavy-Duty Engine. *Fuel* 2016; 167: 248-256. DOI: https://doi.org/10.1016/j.fuel.2015.11.077.
80. Dronniou N, Kashdan J, Lecointe B, et al. Optical Investigation of Dual-fuel CNG/Diesel Combustion Strategies to Reduce CO_2 Emissions. *SAE2014-01-1313* 2014; 7: 873-887. DOI: https://doi.org/10.4271/2014-01-1313.
81. "Wärtsilä Methane Number Calculator", https://www.wartsila.com/marine/build/gas-solutions/methane-number-calculator (2021, accessed 06/09 2021).

A HIGH LOAD EXPERIMENTAL RESULTS

This section discusses the results of the high load (16 bar and 23 bar BMEP) experimental studies. These experiments were conducted after the medium load sensitivity analysis described in Chapter 5, utilizing the investigation results as guidance for the engine operating at high load conditions.

A.1 23 bar BMEP w/ EGR: Knock Free Operation

In this investigation, the engine was initially operated at 1620 rpm and 25 bar BMEP. At this condition, severe combustion knock (12 bar Peak-Peak 95th Percentile) and pre-ignition were observed and are shown in Figure A-1(a). The diesel pilot SOI could not be retarded because the turbocharger inlet temperature was near the maximum limit of 870°C, and the turbocharger shaft speed was observed near the maximum limit of 140kRPM.

Figure 1-1(b) shows 100 logged cycles with no signs of pre-ignition and a low level of combustion knock (4 bar Peak-Peak 95th Percentile). In this condition, 2.5% EGR was added, confirming that EGR is a viable strategy to control combustion knock, as observed in the medium load sensitivity study.

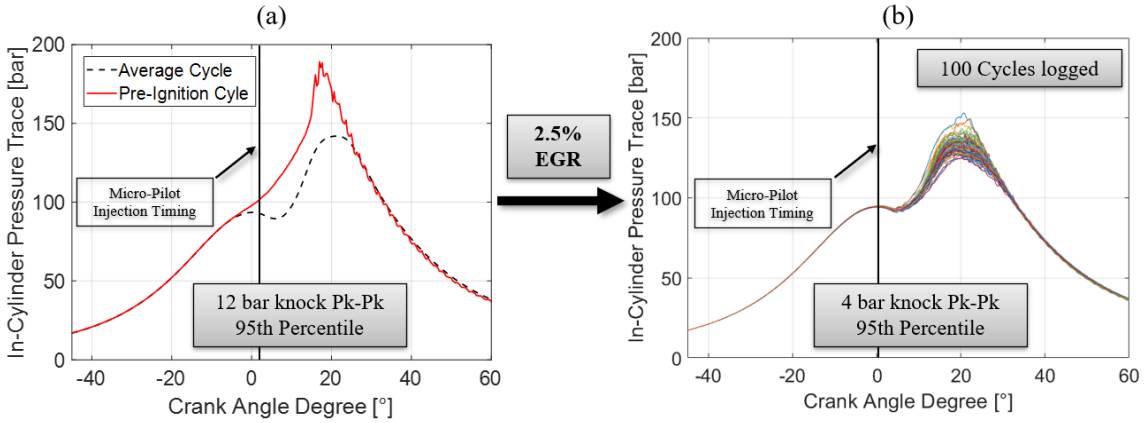

Figure A-1. In-cylinder pressure curves at high load. (a) Operation with signs of pre-ignition; Engine operated at 25 bar BMEP; 1620 RPM; EQR 1; 0% EGR; 1000bar Pilot

Inj. Pressure; 97% DSR; (b) Operation with no sign of pre-ignition and controlled combustion knock; Engine operated at 23 bar BMEP; 1620 RPM; EQR 1; 2.5% EGR; 1000bar Pilot Inj. Pressure;

As seen in Table A-1, for the non-knocking condition, the diesel pilot SOI could be advanced for load output recovery as the knock peak-peak 95th percentile is 4 bar. However, the experimental studies in this operating condition were limited due to the turbocharger inlet temperature and shaft speed (for the 25 bar BMEP operation) and the high injector tip temperature (for both 25 bar and 23 bar BMEP operation). Additional investigation is needed. However, to further determine if the medium load sensitivity study observations can be applied at high loads, a diesel pilot SOI study was conducted at 16 bar BMEP and is shown in Chapter A.2.

Table A-1. High load detailed operating condition

Speed: 1620 RPM	Combustion Knock + Pre-Ignition	Non-knocking condition
BMEP [bar]	25.0	23.0
Brake Thermal Efficiency [%]	41.0	41.0
EGR [%]	0.00	2.50
Substitution Ratio [%]	97.0	97.0
MAP [kPa]	245	247
IMT [°C]	38.0	38.0
P. Pre-Turbine [kPa]	307	274
Turbine Inlet Temp. [°C]	820	790
CA50 [CAD]	17.0	17.3
Knock pk2pk 95 pct [bar]	12.0	4.50

Peak Cylinder Pressure [bar]	144	130
NOx [ppm]	2076	1130

A.2 16 bar BMEP: Diesel Pilot Injection Timing Study

In this investigation, the engine was operated at 16 bar BMEP, 1620 RPM with 0% EGR, at a global EQR of 1 and 96% diesel substitution ratio. The pilot SOI was retarded from borderline knocking condition (near the 10 bar Peak-Peak limit), as seen in Figure A-2. The result shows a strong correlation between pilot SOI and combustion knock peak-peak, confirming the trend seen in the medium load study. This indicates that, for EGR and diesel pilot SOI, the expected effects on combustion knock could be extrapolated from the investigation performed at medium load.

As previously mentioned, the high load investigation at 16 bar BMEP was limited due to high injector tip temperature to avoid injector damage. Therefore, additional experiments are needed to investigate the effects of other parameters on combustion knock, including the diesel pilot injection pressure, diesel pilot quantity, equivalence ratio, substitution ratio, intake temperature, and dilution.

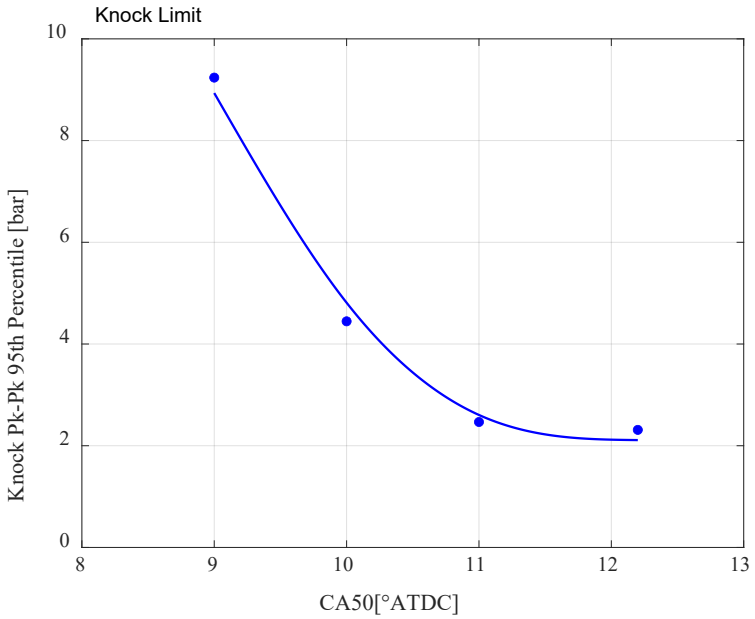

Figure A-2. Diesel Pilot SOI vs. Combustion Knock. Engine operated at 16 bar BMEP; 1620 RPM; EQR 1; 0% EGR; 1000bar Pilot Inj. Pressure; 96% DSR;

B NATURAL GAS COMPOSITION LOGS

The local CNG supplier provided a detailed CNG composition log for the first ten months of the experimental investigations undertaken for fifteen months. The daily composition log is shown in Table B-2, and it is divided by month. The reports consisted of the %vol of the CNG constituents, including CO_2, N_2, CH_4 (Methane), Ethane, Propane, Iso-Butane, N-Butane, Iso-Pentane, and N-Pentane. The density, heating value, AFR, and hydrogen to carbon ratio are provided at the bottom of each month and calculated using a code developed to run in the Engineering Equation Software (EES). The code is provided at the end of this Appendix. For the Methane Number, the online calculator provided by Wärtsilä [81] was utilized. Additional investigation is required to asses the impact of natural gas composition in the micro-pilot engine combustion, and it is part of future work.

Table B-2. CNG composition and properties by month

Month 1	CO_2	N_2	CH_4	Ethane	Propane	IButane	NButane	IPentane	NPentane
	%vol	%vol	%vol	%vol	%vol	%vol	%vol	%vol	%vol
	0.796	1.58	85.8	11.0	0.704	0.024	0.036	0.002	0.002
	0.799	1.59	86.1	10.8	0.670	0.018	0.034	0.002	0.002
	0.814	1.62	85.6	11.2	0.758	0.020	0.039	0.003	0.003
	0.817	1.64	85.2	11.4	0.852	0.022	0.043	0.003	0.004
	0.817	1.67	84.9	11.6	0.913	0.021	0.038	0.002	0.003
	0.824	1.71	84.4	12.1	0.917	0.020	0.037	0.002	0.003
	0.826	1.69	84.0	12.4	1.001	0.024	0.040	0.003	0.003
	0.821	1.68	84.4	12.1	0.947	0.018	0.031	0.001	0.001
	0.793	1.68	84.8	11.7	0.983	0.017	0.029	0.001	0.001
	0.802	1.70	84.7	11.8	0.968	0.019	0.033	0.002	0.001
	0.793	1.67	85.2	11.5	0.804	0.017	0.030	0.002	0.001
	0.802	1.67	84.7	11.8	1.021	0.019	0.032	0.002	0.002
	0.836	1.64	84.7	11.9	0.814	0.020	0.039	0.002	0.003
	0.729	1.64	84.7	11.9	0.967	0.021	0.034	0.001	0.002
	0.799	1.53	86.2	10.5	0.832	0.017	0.033	0.002	0.002
	0.844	1.47	87.8	9.3	0.527	0.015	0.032	0.002	0.002
	1.000	1.54	87.1	9.8	0.558	0.014	0.036	0.002	0.002

	1.000	1.67	85.6	11.0	0.671	0.020	0.048	0.003	0.004
	0.967	1.57	87.0	9.7	0.618	0.014	0.034	0.002	0.002
	1.032	1.36	90.0	7.1	0.445	0.011	0.027	0.002	0.002
	1.057	1.64	87.2	9.5	0.584	0.013	0.034	0.002	0.002
	0.964	1.73	85.1	11.2	0.880	0.022	0.050	0.002	0.003
	0.908	1.74	85.9	10.7	0.733	0.020	0.043	0.002	0.002
	0.983	1.69	86.3	10.4	0.619	0.016	0.039	0.002	0.003
	0.913	1.73	86.0	10.7	0.647	0.017	0.038	0.002	0.003
	0.950	1.73	86.3	10.3	0.635	0.017	0.037	0.002	0.002
	0.741	1.30	87.6	9.8	0.569	0.017	0.025	0.002	0.001
	0.877	1.70	86.2	10.5	0.604	0.015	0.033	0.002	0.002
	1.023	1.71	85.1	11.4	0.666	0.016	0.035	0.002	0.002
	1.001	1.74	85.5	11.0	0.663	0.017	0.038	0.002	0.003
	0.796	1.58	85.8	11.0	0.704	0.024	0.036	0.002	0.002
Average	**0.878**	**1.63**	**85.8**	**10.9**	**0.752**	**0.018**	**0.036**	**0.002**	**0.002**
Standard Dev.	**0.096**	**0.11**	**1.3**	**1.1**	**0.163**	**0.003**	**0.006**	**0.000**	**0.001**

Density (kg/m3) @ 20°C, 1 atm	**Heating value (MJ/kg)**	**AFR**	**H/C**	**Methane Number**
0.768±0.006	47.25±0.04	16.20±0.01	3.74±0.01	76

Month 2	CO_2	N_2	CH_4	Ethane	Propane	IButane	NButane	IPentane	NPentane
	%vol	%vol	%vol	%vol	%vol	%vol	%vol	%vol	%vol
	0.796	1.58	85.8	11.0	0.704	0.024	0.036	0.002	0.002
	0.799	1.59	86.1	10.8	0.670	0.018	0.034	0.002	0.002
	0.814	1.62	85.6	11.2	0.758	0.020	0.039	0.003	0.003
	0.817	1.64	85.2	11.4	0.852	0.022	0.043	0.003	0.004
	0.817	1.67	84.9	11.6	0.913	0.021	0.038	0.002	0.003
	0.824	1.71	84.4	12.1	0.917	0.020	0.037	0.002	0.003
	0.826	1.69	84.0	12.4	1.001	0.024	0.040	0.003	0.003
	0.821	1.68	84.4	12.1	0.947	0.018	0.031	0.001	0.001
	0.793	1.68	84.8	11.7	0.983	0.017	0.029	0.001	0.001
	0.802	1.70	84.7	11.8	0.968	0.019	0.033	0.002	0.001
	0.793	1.67	85.2	11.5	0.804	0.017	0.030	0.002	0.001

	0.802	1.67	84.7	11.8	1.021	0.019	0.032	0.002	0.002
	0.836	1.64	84.7	11.9	0.814	0.020	0.039	0.002	0.003
	0.729	1.64	84.7	11.9	0.967	0.021	0.034	0.001	0.002
	0.799	1.53	86.2	10.5	0.832	0.017	0.033	0.002	0.002
	0.844	1.47	87.8	9.3	0.527	0.015	0.032	0.002	0.002
	1.000	1.54	87.1	9.8	0.558	0.014	0.036	0.002	0.002
	1.000	1.67	85.6	11.0	0.671	0.020	0.048	0.003	0.004
	0.967	1.57	87.0	9.7	0.618	0.014	0.034	0.002	0.002
	1.032	1.36	90.0	7.1	0.445	0.011	0.027	0.002	0.002
	1.057	1.64	87.2	9.5	0.584	0.013	0.034	0.002	0.002
	0.964	1.73	85.1	11.2	0.880	0.022	0.050	0.002	0.003
	0.908	1.74	85.9	10.7	0.733	0.020	0.043	0.002	0.002
	0.983	1.69	86.3	10.4	0.619	0.016	0.039	0.002	0.003
	0.913	1.73	86.0	10.7	0.647	0.017	0.038	0.002	0.003
	0.950	1.73	86.3	10.3	0.635	0.017	0.037	0.002	0.002
	0.741	1.30	87.6	9.8	0.569	0.017	0.025	0.002	0.001
	0.877	1.70	86.2	10.5	0.604	0.015	0.033	0.002	0.002
	1.023	1.71	85.1	11.4	0.666	0.016	0.035	0.002	0.002
	1.001	1.74	85.5	11.0	0.663	0.017	0.038	0.002	0.003
Average	**0.878**	**1.63**	**85.8**	**10.9**	**0.752**	**0.018**	**0.036**	**0.002**	**0.002**
Standard Dev.	**0.096**	**0.11**	**1.3**	**1.1**	**0.163**	**0.003**	**0.006**	**0.000**	**0.001**

Density (kg/m3) @ 20°C, 1 atm	Heating value (MJ/kg)	AFR	H/C	Methane Number
0.760±0.003	47.20±0.14	16.20±0.06	3.74±0.019	77

Month 3	CO_2	N_2	CH_4	Ethane	Propane	IButane	NButane	IPentane	NPentane
	%vol	%vol	%vol	%vol	%vol	%vol	%vol	%vol	%vol
	1.010	1.81	84.9	11.5	0.722	0.019	0.047	0.003	0.004
	1.009	1.79	85.0	11.4	0.678	0.019	0.045	0.002	0.003
	0.988	1.79	85.5	11.0	0.656	0.017	0.042	0.002	0.004
	0.994	1.82	85.0	11.5	0.635	0.016	0.040	0.002	0.003
	1.021	1.69	85.7	10.9	0.659	0.016	0.037	0.002	0.002
	1.001	1.70	86.1	10.5	0.653	0.019	0.043	0.003	0.003
	1.083	1.71	85.3	11.1	0.701	0.022	0.055	0.003	0.004

	1.019	1.72	85.6	10.9	0.623	0.016	0.039	0.002	0.003
	1.018	1.73	85.6	10.9	0.663	0.015	0.036	0.002	0.002
	0.973	1.77	85.6	10.9	0.653	0.015	0.032	0.002	0.002
	0.908	1.84	85.4	11.1	0.704	0.016	0.036	0.002	0.003
	1.042	1.81	84.9	11.5	0.685	0.016	0.038	0.002	0.003
	1.024	1.78	85.2	11.2	0.677	0.016	0.039	0.002	0.003
	1.055	1.90	84.9	11.3	0.745	0.019	0.049	0.002	0.004
	0.924	1.83	85.5	10.9	0.801	0.022	0.050	0.004	0.006
	0.971	1.74	86.2	10.3	0.691	0.018	0.043	0.003	0.005
	1.006	1.78	85.5	10.9	0.728	0.019	0.047	0.003	0.005
	1.043	1.70	85.7	10.8	0.721	0.017	0.042	0.002	0.004
	1.012	1.73	86.0	10.5	0.668	0.017	0.041	0.003	0.004
	1.043	1.83	85.6	10.7	0.743	0.018	0.044	0.002	0.004
	1.064	1.79	85.0	11.2	0.850	0.024	0.056	0.003	0.004
	1.015	1.83	85.5	10.9	0.731	0.019	0.046	0.003	0.004
	1.017	1.86	84.8	11.5	0.779	0.021	0.049	0.003	0.004
	1.011	1.85	84.8	11.3	0.904	0.026	0.061	0.003	0.004
	1.020	1.93	84.9	11.3	0.717	0.019	0.045	0.002	0.003
	1.038	1.93	84.8	11.4	0.737	0.020	0.050	0.003	0.005
	1.027	1.85	85.4	10.9	0.700	0.020	0.049	0.003	0.004
	1.051	1.87	85.8	10.5	0.723	0.022	0.055	0.004	0.005
	1.014	1.89	85.7	10.7	0.692	0.020	0.051	0.003	0.005
	1.002	1.89	85.5	10.7	0.817	0.025	0.064	0.005	0.008
	0.997	1.89	85.3	11.0	0.744	0.021	0.052	0.004	0.006
Average	**1.013**	**1.81**	**85.4**	**11.0**	**0.716**	**0.019**	**0.046**	**0.003**	**0.004**
Standard Dev.	**0.036**	**0.07**	**0.4**	**0.3**	**0.063**	**0.003**	**0.008**	**0.001**	**0.001**

Density (kg/m3) @ 20°C, 1 atm	**Heating value (MJ/kg)**	**AFR**	**H/C**	**Methane Number**
0.760±0.003	46.90±0.07	16.10±0.03	3.74±0.01	77

Month 4	CO_2	N_2	CH_4	Ethane	Propane	IButane	NButane	IPentane	NPentane
	%vol	%vol	%vol	%vol	%vol	%vol	%vol	%vol	%vol
	0.998	1.90	85.3	10.9	0.788	0.030	0.065	0.006	0.008
	0.901	1.71	86.3	10.4	0.697	0.024	0.051	0.004	0.005

	1.001	1.89	85.7	10.5	0.737	0.021	0.051	0.004	0.005
	0.961	1.84	85.6	10.8	0.700	0.022	0.052	0.004	0.005
	0.992	1.85	85.2	11.2	0.679	0.022	0.051	0.004	0.005
	0.943	1.82	85.4	11.0	0.744	0.028	0.054	0.004	0.005
	1.013	1.99	86.1	10.2	0.671	0.023	0.057	0.005	0.006
	0.949	1.35	90.2	7.0	0.495	0.020	0.036	0.004	0.004
	0.549	0.71	93.6	4.8	0.294	0.011	0.003	0.002	0.000
	0.800	0.86	95.9	2.3	0.089	0.003	0.003	0.000	0.000
	0.782	0.96	95.8	2.4	0.093	0.003	0.003	0.000	0.000
	0.789	0.98	95.6	2.5	0.110	0.003	0.004	0.000	0.000
	0.784	0.93	95.6	2.5	0.111	0.003	0.004	0.000	0.000
	0.762	0.94	95.7	2.5	0.100	0.003	0.004	0.000	0.000
	0.846	1.09	94.9	3.0	0.138	0.004	0.007	0.001	0.000
	0.937	1.53	90.4	6.8	0.337	0.011	0.024	0.002	0.002
	1.006	1.61	89.0	8.0	0.389	0.012	0.029	0.002	0.003
	1.021	1.67	88.8	8.1	0.384	0.011	0.026	0.002	0.002
	0.991	1.61	89.6	7.4	0.353	0.012	0.027	0.002	0.003
	1.003	1.61	89.4	7.5	0.378	0.014	0.029	0.003	0.003
	0.734	1.42	89.8	7.6	0.417	0.016	0.025	0.003	0.003
	0.986	1.71	88.5	8.3	0.459	0.019	0.043	0.004	0.005
	0.993	1.83	87.3	9.2	0.528	0.019	0.046	0.004	0.006
	0.994	2.12	86.0	10.2	0.586	0.019	0.051	0.004	0.006
	1.039	1.85	86.3	10.0	0.635	0.023	0.055	0.004	0.006
	1.016	1.54	87.3	9.3	0.706	0.036	0.066	0.007	0.007
	0.786	1.26	89.0	8.2	0.612	0.027	0.044	0.005	0.005
	0.853	0.91	94.2	3.8	0.205	0.007	0.011	0.001	0.001
	0.862	1.01	93.7	4.2	0.228	0.008	0.011	0.001	0.001
	0.932	1.38	89.9	7.3	0.468	0.015	0.031	0.002	0.003
Average	**0.907**	**1.46**	**89.9**	**7.3**	**0.438**	**0.016**	**0.032**	**0.003**	**0.003**
Standard Dev.	**0.116**	**0.40**	**3.8**	**3.1**	**0.230**	**0.009**	**0.021**	**0.002**	**0.002**

Density (kg/m3) @ 20°C, 1 atm	**Heating value (MJ/kg)**	**AFR**	**H/C**	**Methane Number**
0.722±0.025	47.40±0.32	16.30±0.12	3.74±0.01	81

Month 5	CO_2	N_2	CH_4	Ethane	Propane	IButane	NButane	IPentane	NPentane
	%vol	%vol	%vol	%vol	%vol	%vol	%vol	%vol	%vol
	0.991	1.52	89.1	7.9	0.435	0.014	0.033	0.002	0.003
	1.071	1.66	89.2	7.6	0.390	0.013	0.032	0.002	0.002
	0.993	1.50	89.3	7.6	0.510	0.024	0.048	0.004	0.005
	0.959	1.43	90.6	6.6	0.391	0.014	0.033	0.003	0.004
	0.849	1.15	93.5	4.2	0.235	0.008	0.017	0.002	0.002
	0.674	0.93	95.3	2.9	0.141	0.005	0.007	0.000	0.000
	0.610	0.78	96.1	2.4	0.096	0.003	0.003	0.000	0.000
	0.641	0.74	96.1	2.4	0.090	0.004	0.003	0.000	0.000
	0.650	0.77	96.0	2.5	0.089	0.003	0.003	0.000	0.000
	0.681	1.16	93.0	4.8	0.287	0.012	0.018	0.002	0.002
	0.804	1.25	92.1	5.4	0.346	0.017	0.029	0.004	0.003
	0.820	1.36	91.1	6.3	0.397	0.017	0.033	0.004	0.004
	0.892	1.49	90.1	7.0	0.473	0.020	0.042	0.004	0.005
Average	**0.818**	**1.21**	**92.4**	**5.2**	**0.298**	**0.012**	**0.023**	**0.002**	**0.002**
Standard Dev.	**0.156**	**0.32**	**2.8**	**2.1**	**0.153**	**0.007**	**0.016**	**0.002**	**0.002**

Density (kg/m3) @ 20°C, 1 atm	Heating value (MJ/kg)	AFR	H/C	Methane Number
0.702±0.018	47.70±0.36	16.40±0.14	3.86±0.04	84

Month 6	CO_2	N_2	CH_4	Ethane	Propane	IButane	NButane	IPentane	NPentane
	%vol	%vol	%vol	%vol	%vol	%vol	%vol	%vol	%vol
	0.769	0.85	94.6	3.7	0.070	0.003	0.004	0.000	0.000
	0.785	0.78	94.6	3.8	0.074	0.003	0.004	0.000	0.000
	0.640	0.82	94.6	3.9	0.073	0.004	0.004	0.000	0.000
	0.645	0.84	94.7	3.8	0.071	0.004	0.003	0.000	0.000
	0.618	0.92	94.7	3.6	0.075	0.004	0.004	0.000	0.000
	0.718	1.10	91.4	6.5	0.279	0.008	0.013	0.001	0.000
	0.744	1.33	89.6	7.9	0.389	0.010	0.017	0.001	0.001
	0.746	1.41	89.4	8.0	0.408	0.011	0.019	0.001	0.001
	0.715	1.15	91.2	6.6	0.292	0.009	0.015	0.002	0.001
	0.480	0.78	92.1	6.3	0.314	0.011	0.009	0.002	0.001

	0.672	1.02	92.3	5.7	0.264	0.010	0.017	0.002	0.002
	0.664	1.15	91.8	6.1	0.285	0.011	0.018	0.003	0.002
	0.697	1.20	91.4	6.3	0.284	0.011	0.020	0.003	0.003
	0.696	1.23	91.3	6.4	0.326	0.012	0.022	0.003	0.003
	0.415	0.83	91.2	7.2	0.405	0.015	0.011	0.003	0.001
	0.686	1.08	92.0	6.0	0.229	0.007	0.011	0.001	0.001
	0.655	0.80	94.0	4.4	0.103	0.004	0.005	0.000	0.000
	0.660	0.95	93.1	5.1	0.166	0.006	0.009	0.001	0.001
	0.651	0.76	94.2	4.3	0.094	0.005	0.005	0.001	0.000
	0.614	0.77	95.4	3.2	0.067	0.004	0.003	0.000	0.000
	0.408	0.60	93.9	4.8	0.234	0.010	0.003	0.001	0.000
	0.121	0.37	91.4	7.6	0.482	0.019	0.002	0.003	0.000
	0.630	0.78	95.1	3.4	0.063	0.003	0.003	0.000	0.000
	0.631	0.80	95.1	3.4	0.062	0.003	0.003	0.000	0.000
	0.668	0.80	95.0	3.4	0.072	0.004	0.004	0.000	0.000
	0.707	0.76	94.7	3.7	0.139	0.013	0.017	0.003	0.002
	0.736	0.75	95.0	3.4	0.072	0.004	0.005	0.000	0.000
	0.767	0.75	94.9	3.5	0.070	0.004	0.005	0.000	0.000
	0.740	0.78	95.0	3.4	0.068	0.003	0.004	0.000	0.000
	0.532	0.63	93.4	5.2	0.251	0.010	0.003	0.002	0.000
	0.154	0.35	91.1	7.9	0.518	0.020	0.002	0.003	0.000
Average	**0.625**	**0.88**	**93.2**	**5.1**	**0.203**	**0.008**	**0.008**	**0.001**	**0.001**
Standard Dev.	**0.160**	**0.24**	**1.8**	**1.6**	**0.141**	**0.005**	**0.006**	**0.001**	**0.001**

Density (kg/m3) @ 20°C, 1 atm	**Heating value (MJ/kg)**	**AFR**	**H/C**	**Methane Number**
0.704±0.013	48.25±0.37	16.60±0.14	3.90±0.03	85

Month 7	CO_2	N_2	CH_4	Ethane	Propane	IButane	NButane	IPentane	NPentane
	%vol	%vol	%vol	%vol	%vol	%vol	%vol	%vol	%vol
	0.410	0.54	92.6	6.1	0.333	0.013	0.003	0.002	0.000
	0.740	0.86	95.4	2.9	0.075	0.003	0.004	0.000	0.000
	0.766	0.97	95.3	2.9	0.095	0.004	0.005	0.000	0.000
	0.804	1.17	91.7	6.1	0.235	0.008	0.014	0.002	0.001
	0.421	0.63	91.3	7.2	0.404	0.015	0.008	0.002	0.001

	0.210	0.38	91.5	7.4	0.449	0.018	0.003	0.003	0.000
	0.805	0.84	94.4	3.8	0.084	0.005	0.007	0.001	0.001
	0.774	0.86	95.0	3.3	0.066	0.003	0.004	0.000	0.000
	0.710	0.84	95.0	3.4	0.075	0.004	0.004	0.000	0.000
	0.747	0.88	95.0	3.3	0.063	0.003	0.004	0.000	0.000
	0.728	0.95	95.2	3.1	0.067	0.004	0.005	0.000	0.000
	0.763	0.93	95.2	3.0	0.071	0.003	0.004	0.000	0.000
	0.732	0.95	95.3	2.9	0.078	0.003	0.003	0.000	0.000
	0.764	0.85	95.6	2.7	0.068	0.003	0.004	0.000	0.000
	0.749	0.88	95.7	2.6	0.067	0.003	0.004	0.000	0.000
	0.759	0.82	95.5	2.9	0.082	0.004	0.005	0.000	0.000
	0.769	0.82	95.4	2.9	0.090	0.004	0.006	0.000	0.000
	0.708	0.84	95.5	2.8	0.087	0.004	0.005	0.000	0.000
	0.760	0.80	95.3	3.1	0.081	0.003	0.005	0.000	0.000
	0.769	0.79	95.2	3.2	0.078	0.003	0.004	0.000	0.000
	0.731	0.90	95.0	3.3	0.100	0.004	0.005	0.000	0.000
	0.759	0.77	94.9	3.5	0.096	0.004	0.005	0.000	0.000
	0.607	0.66	93.9	4.6	0.208	0.008	0.005	0.001	0.000
	0.778	0.89	94.8	3.4	0.107	0.004	0.006	0.000	0.000
	0.762	0.87	94.7	3.5	0.104	0.004	0.006	0.000	0.000
	0.197	0.32	92.0	7.0	0.421	0.016	0.002	0.003	0.000
	0.370	0.48	92.8	6.0	0.332	0.013	0.003	0.002	0.000
	0.853	0.82	94.2	3.7	0.247	0.034	0.042	0.018	0.011
Average	**0.676**	**0.80**	**94.4**	**3.9**	**0.152**	**0.007**	**0.006**	**0.001**	**0.000**
Standard Dev.	**0.178**	**0.18**	**1.4**	**1.5**	**0.123**	**0.007**	**0.007**	**0.003**	**0.002**

Density (kg/m3) @ 20°C, 1 atm	Heating value (MJ/kg)	AFR	H/C	Methane Number
0.691±0.014	48.30±0.36	16.60±0.14	3.90±0.04	88

Month 8	CO_2	N_2	CH_4	Ethane	Propane	IButane	NButane	IPentane	NPentane
	%vol	%vol	%vol	%vol	%vol	%vol	%vol	%vol	%vol
	0.793	0.92	94.6	3.5	0.140	0.015	0.020	0.008	0.005
	0.834	0.89	94.4	3.5	0.219	0.029	0.037	0.016	0.010
	0.866	0.90	94.2	3.6	0.260	0.038	0.049	0.020	0.013

	0.808	0.90	94.3	3.7	0.183	0.020	0.029	0.010	0.007
	0.780	0.95	95.2	3.0	0.068	0.003	0.004	0.000	0.000
	0.791	0.89	95.4	2.9	0.074	0.004	0.005	0.001	0.001
	0.780	0.85	95.9	2.3	0.071	0.003	0.003	0.000	0.000
	0.753	0.87	95.7	2.6	0.079	0.003	0.004	0.000	0.000
	0.827	0.87	95.7	2.5	0.097	0.003	0.004	0.000	0.000
	0.793	0.96	95.6	2.6	0.097	0.004	0.005	0.000	0.000
	0.829	0.94	95.2	2.9	0.108	0.005	0.007	0.001	0.000
	0.938	1.07	92.8	5.0	0.225	0.010	0.020	0.002	0.002
	0.849	0.88	94.7	3.5	0.096	0.005	0.008	0.001	0.001
	0.848	1.05	94.0	3.9	0.129	0.006	0.012	0.001	0.001
	0.949	1.29	91.7	5.8	0.251	0.010	0.026	0.003	0.004
	0.915	0.96	92.5	5.3	0.220	0.011	0.025	0.003	0.003
	0.908	1.15	91.7	5.9	0.256	0.010	0.026	0.003	0.003
	0.863	1.15	92.0	5.7	0.225	0.008	0.018	0.002	0.002
	0.858	1.18	92.2	5.5	0.226	0.009	0.020	0.002	0.003
	0.863	1.13	92.7	5.1	0.205	0.008	0.018	0.002	0.002
	0.853	1.20	92.2	5.5	0.233	0.009	0.019	0.002	0.002
	0.928	1.41	89.9	7.3	0.344	0.013	0.032	0.003	0.004
	0.940	1.51	89.1	8.0	0.409	0.015	0.038	0.004	0.005
	0.961	1.51	89.2	7.8	0.438	0.017	0.044	0.004	0.006
	1.011	1.55	88.0	8.9	0.507	0.023	0.051	0.005	0.007
	0.848	1.37	89.0	8.2	0.496	0.025	0.052	0.006	0.007
	2.097	1.66	88.2	7.3	0.530	0.031	0.134	0.012	0.017
	0.827	1.63	87.1	9.9	0.533	0.017	0.032	0.004	0.004
	1.004	1.58	88.0	8.9	0.487	0.018	0.042	0.004	0.005
	0.961	1.38	90.4	6.7	0.457	0.022	0.060	0.007	0.009
	0.631	0.90	90.9	7.1	0.463	0.022	0.039	0.006	0.006
Average	**0.900**	**1.15**	**92.3**	**5.3**	**0.262**	**0.013**	**0.028**	**0.004**	**0.004**
Standard Dev.	**0.236**	**0.27**	**2.7**	**2.2**	**0.158**	**0.009**	**0.026**	**0.005**	**0.004**

Density (kg/m3) @ 20°C, 1 atm	Heating value (MJ/kg)	AFR	H/C	Methane Number
0.702±0.019	47.70±0.42	16.40±0.15	3.85±0.05	86

Month 9	CO_2	N_2	CH_4	Ethane	Propane	IButane	NButane	IPentane	NPentane
	%vol	%vol	%vol	%vol	%vol	%vol	%vol	%vol	%vol
	0.021	0.28	92.0	7.2	0.443	0.019	0.001	0.004	0.000
	0.436	0.62	93.2	5.4	0.288	0.012	0.006	0.003	0.000
	0.959	1.62	87.7	9.0	0.611	0.029	0.068	0.008	0.011
	0.930	1.34	89.3	7.9	0.472	0.020	0.048	0.005	0.007
	0.917	1.35	89.5	7.7	0.480	0.021	0.048	0.005	0.007
	0.887	1.27	90.0	7.3	0.461	0.019	0.044	0.005	0.006
	0.905	1.24	90.6	6.8	0.416	0.018	0.044	0.005	0.006
	0.857	1.17	91.9	5.7	0.302	0.011	0.025	0.003	0.003
	0.844	1.06	91.8	5.9	0.275	0.010	0.021	0.002	0.002
	0.899	1.31	90.1	7.2	0.422	0.018	0.043	0.005	0.006
	0.941	1.16	90.4	7.0	0.418	0.022	0.052	0.007	0.009
	0.892	1.12	91.6	6.0	0.329	0.016	0.038	0.005	0.006
	0.873	1.20	91.1	6.5	0.343	0.014	0.034	0.004	0.005
	0.863	1.08	91.7	6.0	0.301	0.014	0.032	0.004	0.004
	0.857	1.03	92.2	5.6	0.261	0.011	0.026	0.003	0.003
	0.919	1.02	92.0	5.7	0.276	0.009	0.019	0.002	0.002
	0.825	0.84	94.2	3.9	0.132	0.006	0.011	0.001	0.001
	0.819	1.02	93.4	4.6	0.193	0.007	0.015	0.002	0.002
	0.837	1.01	92.7	5.1	0.236	0.009	0.019	0.002	0.002
	0.847	1.13	91.5	6.2	0.330	0.011	0.023	0.002	0.003
	0.845	1.09	92.1	5.6	0.317	0.011	0.024	0.002	0.002
	0.840	0.98	92.7	5.2	0.235	0.008	0.017	0.002	0.002
	0.869	1.20	90.8	6.7	0.351	0.013	0.029	0.003	0.004
	0.830	1.25	90.2	7.3	0.386	0.013	0.028	0.003	0.003
	0.780	0.99	93.1	4.9	0.209	0.009	0.017	0.002	0.002
	0.805	1.01	93.1	4.9	0.219	0.009	0.020	0.002	0.002
	0.904	1.24	89.7	7.7	0.445	0.016	0.037	0.004	0.004
	0.956	1.39	88.4	8.7	0.513	0.017	0.043	0.005	0.006
	0.941	1.37	89.4	7.7	0.462	0.017	0.041	0.004	0.005
	0.943	1.38	88.7	8.4	0.520	0.019	0.046	0.005	0.006
Average	**0.835**	**1.12**	**91.2**	**6.5**	**0.355**	**0.014**	**0.031**	**0.004**	**0.004**
Standard Dev.	**0.180**	**0.25**	**1.6**	**1.3**	**0.114**	**0.005**	**0.015**	**0.002**	**0.003**

Density (kg/m3) @ 20°C, 1 atm	Heating value (MJ/kg)	AFR	H/C	Methane Number
0.717±0.009	47.74±0.36	16.40±0.13	3.83±0.03	82

Month 10	CO_2	N_2	CH_4	Ethane	Propane	IButane	NButane	IPentane	NPentane
	%vol	%vol	%vol	%vol	%vol	%vol	%vol	%vol	%vol
	0.559	1.06	88.6	9.1	0.582	0.021	0.030	0.004	0.004
	0.519	0.86	90.5	7.5	0.545	0.030	0.037	0.006	0.004
	0.912	1.33	89.0	7.9	0.725	0.050	0.079	0.010	0.010
	0.932	1.49	89.9	7.0	0.537	0.031	0.060	0.007	0.007
	0.978	1.64	85.8	10.5	0.900	0.059	0.095	0.013	0.012
	0.953	1.53	87.5	9.4	0.544	0.024	0.047	0.005	0.005
	0.960	1.57	87.9	9.0	0.547	0.019	0.041	0.004	0.005
	1.051	1.83	86.0	10.3	0.692	0.022	0.053	0.005	0.007
	0.946	1.38	89.9	7.3	0.434	0.015	0.037	0.004	0.004
	0.899	1.42	89.6	7.6	0.433	0.015	0.032	0.003	0.003
	0.866	1.33	90.6	6.8	0.349	0.011	0.025	0.002	0.003
	0.936	1.48	89.7	7.4	0.436	0.013	0.030	0.003	0.003
	1.012	1.68	88.3	8.5	0.455	0.012	0.034	0.002	0.004
	0.950	1.81	87.6	9.0	0.556	0.017	0.041	0.004	0.004
	0.960	1.80	88.5	8.1	0.519	0.019	0.048	0.005	0.006
	0.944	1.57	89.4	7.5	0.456	0.016	0.037	0.004	0.004
	0.936	1.69	88.1	8.8	0.504	0.015	0.035	0.003	0.004
	1.000	1.81	86.0	10.4	0.683	0.024	0.058	0.006	0.008
	1.029	1.62	87.9	8.8	0.545	0.022	0.058	0.007	0.009
	1.127	1.66	86.2	10.2	0.728	0.034	0.083	0.010	0.014
	1.062	1.76	85.7	10.6	0.751	0.031	0.075	0.009	0.011
	0.699	1.33	91.4	6.3	0.276	0.010	0.018	0.002	0.002
	0.718	1.28	91.1	6.6	0.319	0.012	0.022	0.002	0.003
	0.761	1.35	89.1	8.3	0.434	0.016	0.030	0.003	0.004
	0.774	1.47	88.4	8.8	0.498	0.020	0.038	0.004	0.005
	0.779	1.37	88.9	8.4	0.508	0.022	0.044	0.005	0.006
	0.748	1.40	89.1	8.3	0.424	0.016	0.029	0.003	0.003
	0.777	1.44	88.0	9.2	0.497	0.017	0.032	0.003	0.003
	0.856	1.83	84.8	11.7	0.764	0.027	0.056	0.006	0.007

	0.838	1.92	84.9	11.4	0.814	0.032	0.067	0.008	0.009
	0.813	1.65	86.2	10.5	0.751	0.028	0.057	0.007	0.008
Average	**0.880**	**1.53**	**88.2**	**8.7**	**0.555**	**0.022**	**0.046**	**0.005**	**0.006**
Standard Dev.	**0.140**	**0.24**	**1.8**	**1.4**	**0.151**	**0.011**	**0.019**	**0.003**	**0.003**

Density (kg/m3) @ 20°C, 1 atm	**Heating value (MJ/kg)**	**AFR**	**H/C**	**Methane Number**
0.741±0.011	47.30±0.28	16.25±0.10	3.80±0.03	79

The EES code utilized to calculate the density, heating value, AFR, H/C and Methane Number is as follows:

```
"! - CNG Fuel Composition (From Composition Report)  "

"For Parametric Table use: "

y_Methane = y_Methane_mol%                    {mol%}
y_Ethane = y_Ethane_mol%                      {mol%}
y_Propane = y_Propane_mol%                    {mol%}
y_isobutane = y_isobutane_mol%                {mol%}
y_nbutane = y_nbutane_mol%                    {mol%}
y_IPentane = y_IPentane_mol%                  {mol%}
y_NPentane = y_NPentane_mol%                  {mol%}
y_CO_2 = y_CO_2_mol%                          {mol%}
y_Nitrogen = y_Nitrogen_mol%                  {mol%}


MW_CNG = (y_Methane * molarmass(Methane) + y_Ethane * molarmass (Ethane) + y_Propane
* molarmass(Propane) + y_isobutane*molarmass(isobutane) + y_nbutane*molarmass(n-
butane)+y_IPentane*molarmass(n-pentane)+ y_NPentane*molarmass(n-
pentane)+y_CO_2*molarmass(CO2)+y_Nitrogen*molarmass(N2))/100;
    {g/mol}

"  Fuel Atomic Ratio used to describe C1 fuel model "

n_C = (y_Methane*1 +  y_Ethane * 2 + y_Propane * 3 +  y_isobutane * 4 +  y_nbutane * 4 +
y_IPentane * 5+y_NPentane*5 + y_CO_2) {Sum of carbon from each component}

n_H = (y_Methane*4 +  y_Ethane * 6 + y_Propane * 8 +  y_isobutane * 10 +  y_nbutane * 10 +
y_IPentane * 12+y_NPentane*12)  {Sum of hydrogen from each component}

n_O = y_CO_2*2;

n_N = y_Nitrogen * 2;
```

```
HCR_CNG =  n_H / n_C;

OCR = n_O / n_C;

NCR = n_N / n_C;

 "Thermochemistry reaction coefficient for C1 fuel          "

 R_CNG = 1  + HCR_CNG /4 - OCR/2

  "  Molecular Weight of C1_Fuel                              "

  MW_CNG_C1 = molarmass(C) + molarmass(H)*HCR_CNG + molarmass(O) * OCR +
molarmass(N)*NCR  ; {g/mol}

MW_CNG_total = MW_CNG_C1 * n_C/100;

"Stoichiomeric AFR"

AFR_stoich_CNG = R_CNG*(4.773*28.96)/MW_CNG_C1;

"Heating Value"

"Assume 100 mols base"

x_Methane = (y_Methane * molarmass(Methane))/MW_CNG;
x_Ethane =  y_Ethane * molarmass (Ethane)/MW_CNG;
x_Propane = y_Propane * molarmass(Propane)/MW_CNG;
x_isobutane = y_isobutane*molarmass(isobutane) / MW_CNG;
x_nbutane = y_nbutane*molarmass(n-butane)/MW_CNG;
x_ipentane = y_IPentane*molarmass(n-pentane)/MW_CNG;
x_npentane = y_NPentane*molarmass(n-pentane)/MW_CNG;
x_CO_2 = y_CO_2*molarmass(CO2)/MW_CNG;
x_Nitrogen = y_Nitrogen*molarmass(N2)/MW_CNG;

QLH = (x_Methane*lowerheatingvalue(CH4) + x_Ethane*lowerheatingvalue(C2H6) + x_Propane
* lowerheatingvalue(C3H8) + x_isobutane * lowerheatingvalue(C4H10) + x_nbutane *
lowerheatingvalue(C4H10) + x_ipentane * lowerheatingvalue(C5H12) + x_npentane *
lowerheatingvalue(C5H12))/100000;

T = 20; {°C}
P= 101; {kPa}

rho_CNG = (x_Methane*Density(CH4,T=T,P=P)+ x_Ethane*Density(C2H6,T=T,P=P) +
x_Propane *Density(C3H8,T=T,P=P) + x_isobutane * Density(C4H10,T=T,P=P) + x_nbutane *
Density(C4H10,T=T,P=P) + x_ipentane * Density(C5H12,T=T,P=P) + x_npentane
*Density(C5H12,T=T,P=P))/100;
```

C COOLED EGR IMPACT ON COMBUSTION AND EMISSIONS OF THE MEDIUM LOAD OPERATION

This experimental study focused on the effects of cooled EGR on combustion and emissions characteristics, including ignition delay, combustion rate, brake thermal efficiency, combustion stability, NOx and UHC emissions when the engine operates at medium loads (i.e., 11 bar BMEP @ 1620 RPM).

The investigation consisted of increasing the EGR content from 0% to 15% in increments of 5% while maintaining engine load and combustion phasing (i.e., CA50) constant by controlling the pilot SOI and intake boost pressure. The engine was operated at a constant pilot injection pressure of 1000 bar, constant intake air temperature of 35°C, constant pilot injection quantity of 3.3mg/inj., and constant EQR of 1.0. The EGR percentage is calculated as the ratio of intake and exhaust CO_2.

Figure C-1 shows the in-cylinder pressure and heat release rate. As shown in Figure C-1 (a), as EGR increases, the peak cylinder pressure reduces, resulting in a reduction in load output. In order to maintain the load constant, the pilot SOI had to be advanced, and at 15% EGR, the intake manifold boost pressure had to be increased from 116 kPa to 135kPa. Figure C-1 (b), shows the heat release rate and the diesel pilot injection timing for each EGR case. As expected, the operating condition with no EGR shows a 56% shorter combustion duration with a 27% higher heat release rate peak compared to the case with 15% EGR. Moreover, as the EGR% increases, a smaller secondary peak is observed.

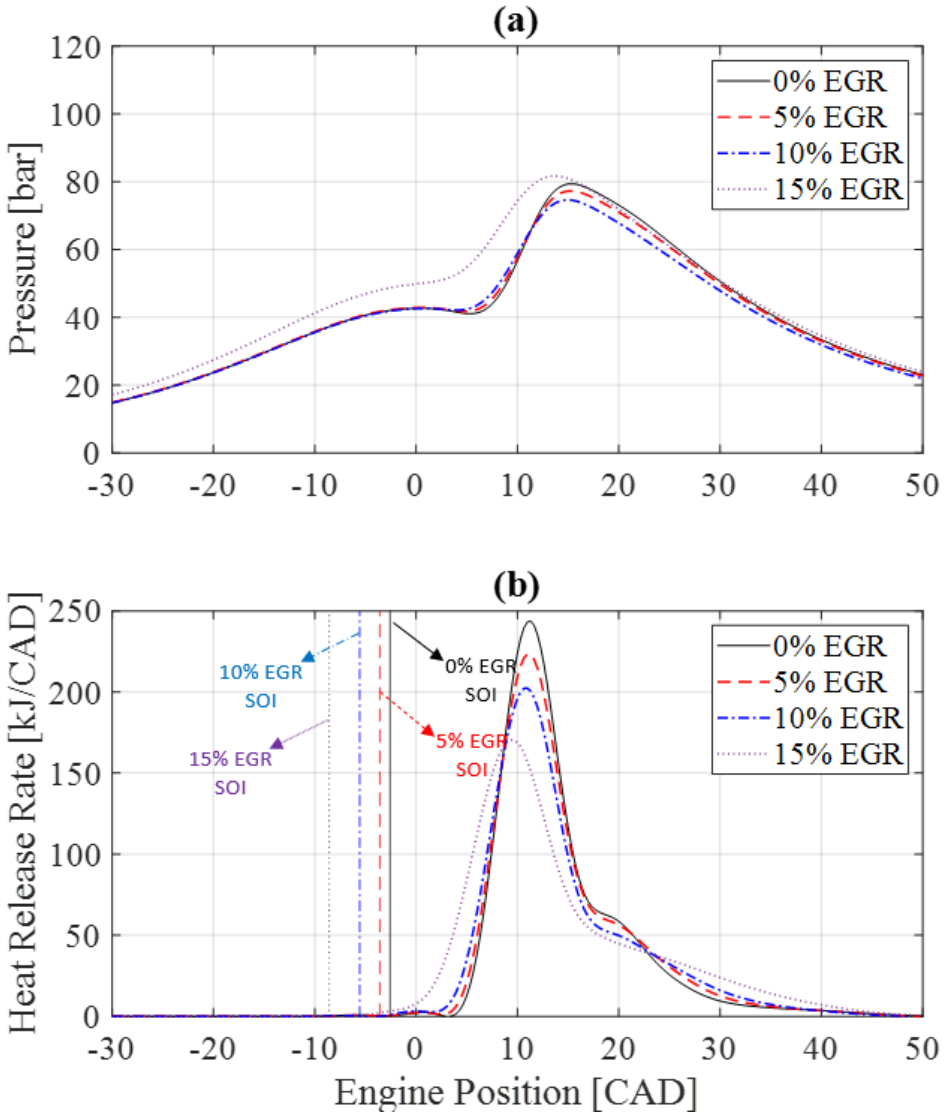

Figure C-1. (a) In-Cylinder pressure; (b) Heat release rate and hydraulic pilot SOI. Engine operating conditions: 0%EGR: 116 kPa MAP, 5.5°bTDC Pilot SOI; 5%EGR: 116 kPa MAP, 6.5°bTDC Pilot SOI; 10%EGR: 116 kPa MAP, 8.5°bTDC Pilot SOI; 15%EGR: 135 kPa MAP, 11.5°bTDC Pilot SOI; Constant in all conditions: 35 °C IMAT; pilot quantity of 3.3 mg/inj. at 1000 bar inj. pressure; 1600 RPM; EQR 1. Vertical lines represent the pilot injection timing for each condition.

Figure 2 shows the cycle-to-cycle ignition delay in (a) and the combustion duration in (b). In this study, the ignition delay is calculated from the start of hydraulic injection timing to

the crank angle at which 10% of the total energy release has occurred. Combustion duration is calculated using the integrated heat release rate and is defined as the number of degrees between the crank angle at which 10% and 90% of the total energy release has occurred (CA10-90).

Figure C-2 (a) shows that the addition of EGR increases the ignition delay of the diesel pilot as it increases the specific heat of the in-cylinder charge, resulting in lower in-cylinder temperature; In this study, the ignition delay increased by 31%, with a cycle-to-cycle variation of less than 1% for all levels of EGR. This indicates that, at these levels of EGR, it does not affect the ignition delay's cyclic variability.

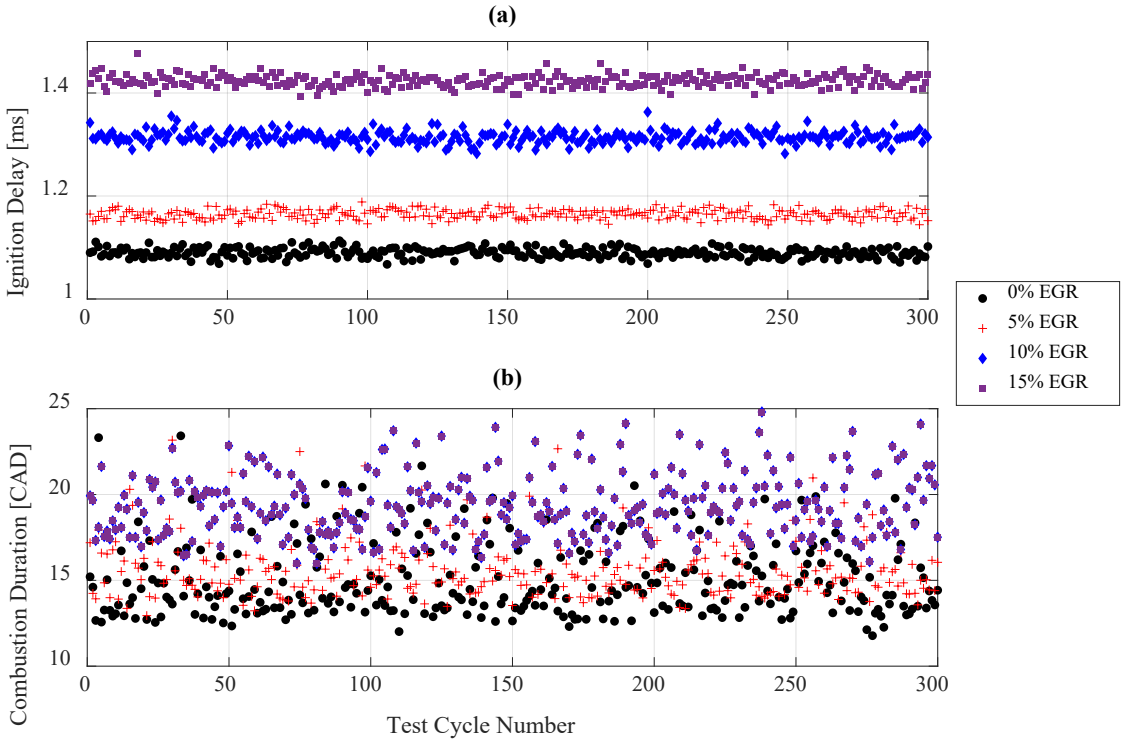

Figure C-2. Cycle-to-Cycle Ignition Delay. Engine operating conditions: 0%EGR: 116 kPa MAP, 5.5°bTDC Pilot SOI; 5%EGR: 116 kPa MAP, 6.5°bTDC Pilot SOI; 10%EGR: 116 kPa MAP, 8.5°bTDC Pilot SOI; 15%EGR: 135 kPa MAP, 11.5°bTDC Pilot SOI; Constant in all conditions: 35 °C IMAT; pilot quantity of 3.3 mg/inj. at 1000 bar inj. pressure; 1600 RPM; EQR 1.

Figure C-2 (b) shows the cycle-to-cycle combustion duration (i.e., CA10-90). As EGR increases from 0% to 15%, a 56% longer combustion duration was observed, with an average cycle-to-cycle variation of 10% for all EGR cases. Indicating that, at these levels of EGR, the combustion duration cyclic variability is not affected. It is important to note that the COV_{IMEP} for all operating conditions investigated was below 1%. Additional investigation is required to assess the dilution tolerance and what is the maximum EGR that can be achieved with stable combustion at medium loads.

Figure C-3 shows the EGR study's engine-out NOx and UHC emissions results at medium loads.

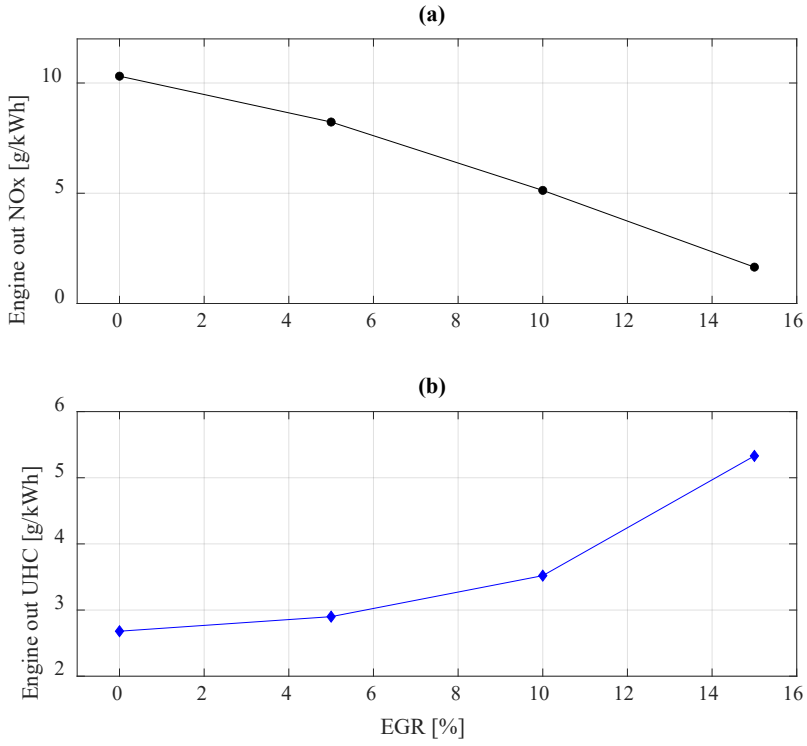

Figure C-3. (a) Engine out NOx vs. EGR; (b) Engine Out UHC vs. EGR. Engine operating conditions: 0%EGR: 116 kPa MAP, 5.5°bTDC Pilot SOI; 5%EGR: 116 kPa MAP, 6.5°bTDC Pilot SOI; 10%EGR: 116 kPa MAP, 8.5°bTDC Pilot SOI; 15%EGR: 135 kPa MAP, 11.5°bTDC Pilot SOI; Constant in all conditions: 35 °C IMAT; pilot quantity of 3.3 mg/inj. at 1000 bar inj. pressure; 1600 RPM; EQR 1.

Figure C-3 (a) shows that as EGR is increased from 0% to 15%, the NOx significantly reduces by 84%. This is expected as EGR reduces the in-cylinder temperature; conversely, UHC is observed double, negatively affecting combustion efficiency. These results agree with the literature and the recent studies reviewed in Chapter 2.

D MICRO-PILOT ENGINE HARDWARE MODIFICATION / INSTRUMENTATION

Sub-systems	**Part**	**Units**	**Supplier**
Engine Controls			
ECM-0564-128	Prototype ECU	1	New Eagle
ASM-CON-003-00	Connector Kit for ECU	1	New Eagle
ASM-NIRA (Quoted but not purchased)	Injector Driver	1	New Eagle
ASM-CON-NiRA (Quoted but not purchased)	Connector Kit for NiRA	1	New Eagle
	Diesel Injector Driver	-	Custom made
Engine Performance System			
	Cummins ISB 6.7L Engine	1	Previously Owned
	Stock Pistons	6	Cummins
	Piston Machining for CR Reduction	1	MTU Machine Shop

C11-HB	Turbonetics Wastegate Turbocharger	1	Provided by Westport
Engine mounting			
	Mount Isolators	4	Carquest
	Engine Foot ACME Thread	1	McMaster
	Aluminum catch tray	1	GLSV or in house
	Engine isolator framework	1	Universal MetalWorks
	Powdercoating	1	Local
	Misc. Bolts	1	
Engine Instrumentation			
AVL-GH15D	In-Cylinder Pressure Transducer	3	AVL
	Turbocharger Speed Sensor Kit	1	Bosch
H25D-SS-360-ABZC-28V/V-SM18-S	Encoder 360x1	1	BEI
K33 ICB 30% CO2	CO2 Sensor for Intake CO2 Measurement	1	CO2Meter

	CO2 Sensor Development & Pump Kit	1	CO2Meter
	High Temp Thermocouples 'K'	13	Temprel
	Thermocouple Jacks 'K'	25	Temprel
	Thermocouple 1/8 X 4" 'K'	3	Temprel
	Thermocouple 1/8 X 6" 'K'	5	Temprel
	Plastic 1/4" line clamps	3	McMaster
	Exhaust Pressure Tap Tube (6')	2	McMaster
	GP50 Transducer Holding Clamp	3	McMaster
	Omega Transducer Hold Clamp	3	McMaster
	1/4" Pressure Tap Nylon Tubing	50	McMaster
	1/8 YorLok Sleeve-SS	21	McMaster
	1/4 YorLok Sleeve-Brass	17	McMaster
	1/4 YorLok Sleeve-SS	6	McMaster
	DIN Rail, DIN 3 size	2	McMaster
	DIN Rail Terminal Block	16	McMaster

	DIN Rail Terminal Block End Cover	8	McMaster
	DIN Rail End Stop	4	McMaster
	DIN Rail Terminal Block Jumper	3	McMaster
MMA050V5P4D1T3A5CE / MMA250V5P4D1T3A5CE	Omega Abs. Pressure Trans;0-5V;0-100psia	2	Omega
MMG030V5P4D1T3A5CE	Omega Gage Pressure Trans	1	Omega
	Braided ground strap	2	McMaster
	Shielded twisted 2 wire Data cable	40	McMaster
	Loop Clamp	5	McMaster
	Expandable Wire Sleeve	1	McMaster
	Blade-style fuses 5,15,20A	3	McMaster
Lambda Sensor Controller	LC-2 controller and bosch sensor	1	Innovate Motorsports
Lambda Sensor	Bosch LSU 4.9 O2 sensor	2	Innovate Motorsports
	Oil pressure tap	1	McMaster
	Male std hose plugs for air	7	McMaster

	Female std hose sockets for air	8	McMaster
	1/4 tube-1/4NPT swage lok	19	McMaster
	1/8 tube-1/4NPT swage lok	21	McMaster
	1/4 tube-1/4 tube swage lok	2	McMaster
	Misc. Bolts / Mounts	1	
Engine Cooling			
	Dyno Cooling Hose Cam-Lock Coupling	2	McMaster
	2" Threaded pipe nipple	2	McMaster
	2 X 1.5 - 90° Reducing Elbow	2	McMaster
	1.5"NPT X 1.25" hose barb	2	Carquest
	3/4" coolant hose	20	McMaster
	1.25" coolant hose	25	McMaster
	hose clamps	1	Carquest
	5/8" or 3/4" hose nipple	2	Carquest
	Coolant	6	McMaster
	t handle ball valve 3/4	1	McMaster

	brass 3/4 T	1	McMaster
Fuel Delivery			
	CNG Fuel Injector Rail	-	Custom Design (WPT)
	Air/Fuel/EGR Mixer	-	Custom Design (WPT)
Westport AEC 8 g/s	CNG Injector	6	Provided by Westport
IMP-HPR3600-5/8A	CNG Fuel Pressure Regulator	1	Century Fuel Products
REGO-3125L	Relief Valve	1	
	24VDC Proportional Valve	1	belimo
	3/8 fuel hose	20	McMaster
	Fuel hose coupling (male)	2	McMaster
	Brass through-wall coupling	2	McMaster
	3/8NPT cross	1	McMaster
	3/8" NPT X 3/8" hose barb	1	McMaster
	3/8 X 1/8 hex bushing	2	McMaster
	3/8NPT fuel filter	2	McMaster

	5/8 loop clamp	1	McMaster
	3/8 hose clamp	1	McMaster
	fuel hose adapter to stock system	1	Carquest
Torque Delivery			
	Flywheel machining	1	Royale Inc.
	Driveshaft	1	Local
Air Intake Plenum			
68027034AB	Throttle Valve	1	Cummins
#1394	Pololu JrK WSB Motor Controller with Fdbck	1	Pololu
#2303	LACT2P-12V Linear Actuator for EGR Valve	1	Pololu
	Intercooler 3"X3" I/O	1	Frozenboost
	Misc. Silicon Intake Pieces	1	Frozenboost
	Dyno I/O Intercooler Coupling	2	ALSCO
	Int cooler coupling hex bushing	2	McMaster
	3/4" plumbing nipple	4	McMaster

	3/4" hose clamps	1	McMaster
	3/4" coolant hose	20	Carquest
	3" t-bolt clamps	6	Frozenboost
For Charge Air Cooler Control	24VDC Proportional Valve	1	belimo
	Prop valve harness connector	1	McMaster
	Mounting steel	1	Universal MetalWorks
Exhaust Collection			
	Exhaust Elbows	1	Carquest
	Turbo Outlet Reducer	1	Jegs
	Turbo/Exhaust Flange Fabrication	2	Universal MetalWorks
	Gaskets	6	GLSV
	High Temp Gasket material	1	Summit
	Marmon Flanges	2	Frozenboost
	Band Clamps	2	Frozenboost
	Exhaust Wrap	1	Summit
	Heat Wrap Sleeve for wiring	1	Summit

	1/4npt weld bung (cut in half for 2)	6	mcmaster
	O2 sensor bungs	2	Summit

E RESEARCH PUBLICATIONS

Papers that are part of the dissertation:

1. Bonfochi Vinhaes, V., Yang, X., McTaggart-Cowan, G., Munshi, S., Naber, J.D., Shahbakhti, M., “Development of a Medium-Duty Stoichiometric Diesel Micro-Pilot Natural Gas Engine.”, International Journal of Engine Research, 2022

2. Bonfochi Vinhaes, V., Yang, X., McTaggart-Cowan, G., Eggart, B., Munshi, S., Naber, J.D., Shahbakhti, M."Multi-Variable Sensitivity Analysis and Ranking of Control Factors Impact in a Stoichiometric Micro-Pilot Natural Gas Engine at Medium Loads". SAE Technical Paper 2022-01-0463

3. Bonfochi Vinhaes, V.; McTaggart-Cowan, G.; Munshi, S.; Shahbakhti, M.; Naber, J.D. “Experimental Studies of Low-Load Limit in a Stoichiometric Micro-Pilot Diesel Natural Gas Engine.”, Energies, 2022, 15, 728

Papers published that are not part of the dissertation:

4. Yang, X., Bonfochi Vinhaes, V., Turcios, M., Huang, J., McTaggart-Cowan, G., Naber, J.D., Shahbakhti, M., “Effect of Pilot Injection Pressure on Ignition Characteristics of a Micro-pilot Ignition Natural Gas Combustion”. Manuscript is being prepared for submission to the journal Fuel.

5. Tuma, N., Bonfochi Vinhaes, V., Eggart, B., Barros, S., Naber, J.D., “Performance and Emissions Improvements of a Natural Gas Diesel Dual Fuel Engine with Indirect Water Injection”. Manuscript is being prepared for submission to the journal Fuel.

6. Reddy CR, Bonfochi Vinhaes V, Naber JD, Robinett RD, Shahbakhti M., “Model Predictive Control of a Dual Fuel Engine Integrated With Waste Heat Recovery Used for Electric Power in Buildings.” Optim Control Appl Meth. 2022;1-20.

7. Reddy, C.R., Vinhaes, V.B., Robinett, R.D., Naber, J.D. and Shahbakhti, M., “Model Predictive Control of a Waste Heat Recovery System Integrated with a Dual Fuel Natural Gas-Diesel Engine”. In 2021 American Control Conference (ACC) (pp. 1842-1847). IEEE.

8. Yang, X., Bonfochi Vinhaes, V., Turcios, M., McTaggart-Cowan, G., Huang, J., Naber, J., Shahbakhti, M., Schmidt, H. and Atkinson, W., ”Process for Study of Micro-pilot Diesel-NG Dual Fuel Combustion in a Constant Volume Combustion Vessel Utilizing the Premixed Pre-burn Procedure.” SAE2019-01-1160

9. Yang, Z., Miganakallu, N., Miller, T., Vinhaes, V.B., Worm, J., Naber, J. and Roth, D.,” Investigation of High Load Operation of Spark-Ignited Over-Expanded Atkinson Cycle Engine.”, Applied Energy, 262, p.114519.

F COPYRIGHT DOCUMENTATION

Bonfochi Vinhaes V, Yang X, McTaggart-Cowan G, Munshi S, Shahbakhti M, Naber JD. "Development of a medium-duty stoichiometric diesel micro-pilot natural gas engine". International Journal of Engine Research. April 2022. doi: https://doi.org/10.1177/14680874221087954

SAGE's Author Archiving and Re-Use Guidelines

These guidelines should be followed by authors of Contributions published in a SAGE subscription journal, including authors whose Contributions were published under a previous version of the author guidelines. For a list of exceptions to these guidelines, please see below.

Three versions of the Contribution are referenced in these guidelines:

- **Original Submission:** the version submitted by the author before peer review
- **Accepted Manuscript:** version updated to include the author's revisions after peer review, prior to any typesetting for the journal. This is often the version accepted by the editor
- **Final Published PDF:** copy-edited and typeset Publisher's PDF, the same version published on the journal's website

Green Open Access: SAGE's Archiving and Sharing Policy

You may share the **Original Submission** or **Accepted Manuscript** at any time after your paper is accepted and in any format. Your sharing of the **Original Submission** or **Accepted Manuscript** may include posting a downloadable copy on any website, saving a copy in any repository or network, sharing a copy through any social media channel, and distributing print or electronic copies. Please note some journals will not consider papers that have been posted as preprints prior to submission and you may check a journal's policy regarding considering previously-posted papers by referring to the journal's submission guidelines.

For information on use of Institutional Repository (IR) copies by authors and IR users, see Posting to an Institutional Repository - Green Open Access.

You may use the **Final Published PDF** (or **Original Submission** or **Accepted Manuscript**, if preferred) in the following ways:

- in relation to your own teaching, provided that any electronic distribution maintains restricted access
- to share on an individual basis with research colleagues, provided that such sharing is not for commercial purposes
- in your dissertation or thesis, including where the dissertation or thesis will be posted in any electronic Institutional Repository or database
- in a book authored or edited by you, at any time after the Contribution's publication in the journal.

Provided that:

- Access to the Original Submission and Accepted Manuscript is provided at no charge.
- Any re-use terms for users of websites and repositories (where your **Original Submission** or **Accepted Manuscript** are posted) are restricted to non-commercial and no derivative uses.
- You may not post the **Final Published PDF** on any unrestricted website or repository without permission from SAGE.
- You may not republish or translate any version of your Contribution in another journal without prior permission from SAGE.
- The journal as the original publication of your Contribution is appropriately credited by including the full citation information each time your Contribution, or excerpts, are further distributed or re-used:
    - After your Contribution has been accepted for publication and until it is assigned a DOI, please include a statement that your Contribution has been accepted for publication in the journal.
    - Once full citation information for your Contribution is available, please include this with your posted Contribution, in a format similar to the following:
      Author(s), Contribution Title, Journal Title (Journal Volume Number and Issue Number) pp. xx-xx. Copyright © [year] (Copyright Holder). DOI: [DOI number].

Bonfochi Vinhaes, V., Yang, X., McTaggart-Cowan, G., Eggart, B., Munshi, S., Naber, J.D., Shahbakhti, M. “Multi-Variable Sensitivity Analysis and Ranking of Control Factors Impact in a Stoichiometric Micro-Pilot Natural Gas Engine at Medium Loads". SAE Technical Paper 2022-01-0463, 2022, https://doi.org/10.4271/2022-01-0463.

Vinicius Bonfochi Vinhaes <vbvinhae@mtu.edu>

Request for Permission to Republish Technical Paper in my PhD Thesis

copyright <copyright@sae.org> Tue, Apr 5, 2022 at 11:41 AM
To: Vinicius Bonfochi Vinhaes <vbvinhae@mtu.edu>

Dear Vinicius,

This is your interim permission until you can obtain a license through Copyright Clearance Center (copyright.com) once we have uploaded the paper details into the CCC system.

Author: Vinicius Bonfochi Vinhaes

SAE Publication: SAE Technical Paper 2022-01-0463 " Multi-Variable Sensitivity Analysis and Ranking of Control Factors Impact in a Stoichiometric Micro-Pilot Natural Gas Engine at Medium Loads"

Author's Thesis: "COMBUSTION DEVELOPMENT OF A HIGH LOAD HIGH-EFFICIENCY MICRO-PILOT DIESEL NATURAL GAS ENGINE" submitted to
Michigan Technological University

Permission is granted for the author to include the SAE publication above in the
Michigan Technological University thesis as outlined above. Any reproduction must include a full reference to the original published source, as well as the copyright notice for the published paper. Any further use requires
written permission from SAE International.

Bonfochi Vinhaes, V.; McTaggart-Cowan, G.; Munshi, S.; Shahbakhti, M.; Naber, J.D. "Experimental Studies of Low-Load Limit in a Stoichiometric Micro-Pilot Diesel Natural Gas Engine.", Energies, 2022, 15, 728. https://doi.org/10.3390/en15030728.

This article was published in the Energies Journal under the MPDI Open Access Policy (https://www.mdpi.com/openaccess):

MDPI Open Access Information and Policy

All articles published by MDPI are made immediately available worldwide under an open access license. This means:

- everyone has free and unlimited access to the full-text of *all* articles published in MDPI journals;
- everyone is free to re-use the published material if proper accreditation/citation of the original publication is given;
- open access publication is supported by the authors' institutes or research funding agencies by payment of a comparatively low **Article Processing Charge (APC)** for accepted articles.

Permissions

No special permission is required to reuse all or part of article published by MDPI, including figures and tables. For articles published under an open access Creative Common CC BY license, any part of the article may be reused without permission provided that the original article is clearly cited. Reuse of an article does not imply endorsement by the authors or MDPI.